Dissertation zur Erlangung des Doktorgrades
der Fakultät für Chemie und Pharmazie
der Ludwig-Maximilians-Universität München

Mitochondrial adaptations to dietary lipids in liver steatosis prevent hepatotoxicity but sensitize to secondary liver insults

Claudia Einer
aus
Bad Schlema, Deutschland
2016

Erklärung

Diese Dissertation wurde im Sinne von § 7 der Promotionsordnung vom 28. November 2011 von Herrn **PD Dr. Hans Zischka** (Institut für molekulare Toxikologie und Pharmakologie, Helmholtz-Zentrum München) betreut und von Frau **Prof. Dr. Angelika M. Vollmar** von der Fakultät für Chemie und Pharmazie vertreten.

Eidesstattliche Versicherung

Diese Dissertation wurde eigenständig und ohne unerlaubte Hilfe erarbeitet.

München, den 19.12.2016.....

_____

Claudia Einer

Dissertation eingereicht am:	19.12.2016
1. Gutachterin:	Prof. Dr. Angelika M. Vollmar
2. Gutachter:	PD Dr. Hans Zischka
Mündliche Prüfung am:	15.02.2017

Contents

1. Introduction

1.1 Prevalence and pathogenesis of non-alcoholic fatty liver disease

Non-alcoholic fatty liver disease (NAFLD) is the most common liver disease in industrialized countries with a prevalence of 20–46% [1-5]. NAFLD is characterized by an excessive hepatic fat accumulation termed steatosis and is defined by the presence of fat accumulation in > 5% of hepatocytes [6]. NAFLD represents a spectrum of liver diseases that ranges from simple steatosis to non-alcoholic steatohepatitis (NASH, chronic liver inflammation) or end-stage liver diseases such as cirrhosis and hepatocellular carcinoma (HCC) [6]. The diagnosis of NAFLD requires the exclusion of alcohol intake (> 20-30 g/d), drugs (e.g. tamoxifen, steroids, estrogens) or genetic diseases, e.g. Wilson disease [6]. NAFLD is the liver component of the metabolic syndrome, since obesity, insulin resistance, type II diabetes and dyslipidemia are associated with NAFLD [7]. Especially in western society, the prevalence of NAFLD reaches up to 70–90% in patients with diabetes or obesity [5].

The underlying molecular mechanisms of a progression from steatosis to more severe liver disease stages, e.g. NASH and cirrhosis, remain unclear. However, the so called “two-hit” model is widely accepted to explain how steatosis progresses towards NASH. In this model, the first hit is an excessive fat accumulation in the liver, caused by an increased fat supply, rise in lipolysis [8] of the adipose tissue or *de novo* lipogenesis [9-11] as well as an modified fatty acid oxidation [12]. As a second hit, elevated oxidative stress, dysfunctional mitochondria [13-15], an altered intestinal microbiome and enhanced intestinal permeability leading to inflammation [16-18] have been demonstrated to be associated with NAFLD to NASH progression. Therefore, lipid-caused cell death (lipotoxicity), mitochondrial dysfunctions and chronic inflammation seem to be of special importance as hits in NAFLD progression.

1.2 Toxic effects of free fatty acid overload in NAFLD

The increase in lipolysis and *de novo* lipogenesis leads to elevated levels of free non-esterified fatty acids (NEFA) in the liver and the serum of patients with steatosis and NASH [19, 20]. However, whether enhanced NEFA levels are cell-toxic seem to depend on specific fatty acid species to be increased. Saturated fatty acids (SFAs), such as C16:0 (palmitic acid), induce endoplasmic reticulum (ER)-stress [21], lysosomal disruption [22, 23], the mitochondrial membrane permeability transition (MPT) [22, 24, 25], cytochrome c release from mitochondria and apoptosis [24-28] in hepatocytes. In contrast, the monounsaturated fatty acid (MUFA) C18:1 (oleic acid) displays no cell-toxic effect but rather enhances lipid accumulating properties [25-27] and rescues C16:0-induced toxicity [25, 28-30]. The essential polyunsaturated fatty acid (PUFA) C18:2 (linoleic acid) is metabolized in mammalians to C20:4 (arachidonic acid) [31]. C20:4 is a precursor of the pro-inflammatory prostaglandins as well as leucotrienes and C18:2 is therefore assumed to enhance inflammation. Controversially, an immune-suppressive effect has been described for C18:2 as well [32-34]. Additionally, fatty acids have been suggested to function as uncoupling agents in mitochondria, shuttling protons from the inter membrane space (IMS) into the mitochondrial matrix and force membrane potential (MMP) depolarization [35].

Therefore, lipotoxicity may cause mitochondrial dysfunction. However, almost all of these indicated effects have been determined in cell culture (*in vitro*) or via fatty acid supply upon isolated mitochondria. *In vivo*, the influence of free fatty acid overload upon mitochondrial behavior is less understood.

1.3 The mitochondrion as central target in NAFLD

1.3.1 Mitochondrial structure and function

Mitochondria produce the main body of cellular energy (ATP) via oxidative phosphorylation [36], regulate programmed cell death (apoptosis) [37-39] and cellular calcium homeostasis [40, 41]. Mitochondria are an important source of reactive oxygen species (ROS) within mammalian cells [39]. Furthermore, mitochondria are the key organelles in lipid metabolization as fatty acid ß-oxidation takes place within the mitochondrial matrix (Fig. 1). Mitochondria contain an outer

membrane (OM), intermembrane space (IMS), inner membrane (IM) and the mitochondrial matrix (Fig. 1).

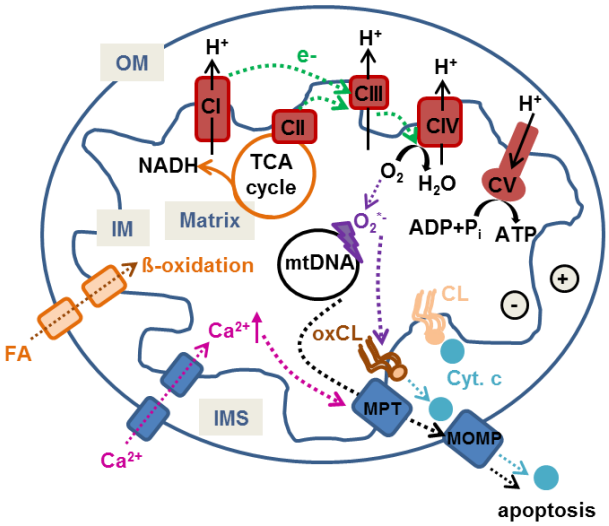

Fig. 1: Schematic illustration of mitochondrial compartmentalization and main functions
Catabolism of fatty acids (FAs) and carbohydrates takes place in the mitochondrial matrix via ß-oxidation or TCA cycle, supplying reduction equivalents for the electron transport chain (CI-CIV). During electron transport, protons (H^+) are pumped via CI, CIII or CIV into the intermembrane space (IMS) creating a proton gradient and a negative charge inside the mitochondrion. The protons flow back into the matrix across CV, which produces ATP from ADP+P_i. Upon electron leakage superoxide anion (O_2^{*-}) is formed leading to oxidative damage of mitochondrial proteins, DNA (mtDNA) or lipids, e.g. cardiolipin (CL). This results, together with high intra-mitochondrial calcium levels, in an elevated permeabilization (MPT) of the inner membrane (IM) followed by increased permebilization of the outer membrane (MOMP) and the release of IMS proteins, e.g. cytochrome c (Cyt. c) as well as the induction of cell death (apoptosis).

The OM delimitates the mitochondrion from the cytosol and is permeable for molecules with a size up to 5 kDa [42, 43]. The OM of liver mitochondria consist of 280–600 µg phospholipids/mg protein as well as 20–60 µg sterols [44]. The main phospholipid in the OM of liver mitochondria is phosphatidylcholine (PC) containing about 22% C16:0, 25% C18:0 (stearic acid) and 30% C20:4, followed by phosphatidylethanolamine (PE) with approximately 12%, 31%, 31% C16:0, C18:0, C20:4, respectively [44-46].

The inner mitochondrial membrane (IM) is folded into cristae (Fig. 1), contains almost no sterols, 40% PC, 35% PE and around 21% cardiolipin (CL) [44-46]. CL is unique for IM and liver mitochondrial CL consist of > 70% C18:2 [47]. The IM is only permeable for gases such as O_2 and NH_3. To maintain a mitochondrial

membrane potential (MMP) of approximately -180 mV, metabolites as well as ions have to be transported by channels across the IM [48] (Fig. 1). Massively increased calcium-influx may disturb the MMP leading to the membrane permeability transition (MPT), followed by increased influx of ions and water into the matrix (swelling) [49] and the rupture of the OM (MOMP, Fig. 1).

An intact IM is especially necessary for mitochondrial energy production. Electrons from the reduction equivalents NADH or $FADH_2$ produced by the tricarboxylic acid (TCA) cycle are entered into complex I or II and are transported via ubiquinone, complex III and Cyt. c to complex IV, consuming oxygen (Fig. 1). During electron transport, protons are pumped in the IMS by complex I, III and IV, establishing a negative charge inside the mitochondrion (Fig. 1). This gradient is used by the ATP synthase (complex V) as protons re-enter the matrix and force the formation of ATP from ADP and P_i (Fig. 1). Consequently, due to this coupling of the electron transport chain (ETC) with the ATP production, loss of IM-tightness results in proton leakage, termed as uncoupling, and lower ATP production. Moreover, electron leakage may promote mitochondrial ROS production, lipid peroxidation and mitochondrial DNA (mtDNA) damage that may cause increased apoptosis (Fig. 1).

1.3.2 Mitochondrial alterations in NAFLD

Diverse structural and functional impairments of mitochondria have been described in NAFLD and NASH. Swollen mega-mitochondria, circular cristae and crystalline inclusions have been reported in humans [14, 50-54] as well as in animal models [55, 56] with NAFLD. As functional impairments, a reduced ATP production capacity [57, 58], an altered respiration [59-61], increased lipid peroxidation [13, 14] and augmented ROS production [15, 62, 63] have been reported in liver mitochondria from humans and rodents with NAFLD or NASH. Despite these results, it is still a matter of debate whether mitochondrial alterations are steatosis or NASH-dependent, and if such modifications restore or aggravate disease progression. A main reason for this insufficient understanding is caused by conflicting results dependent on the diversity of NAFLD animal and feeding models. Several of them do not or only partially reflect the human situation and therefore complicate the interpretation of these studies.

1.4 Animal models to study mitochondrial impairments in NAFLD

Choline-deficient nutrition is frequently used to investigate the molecular mechanisms in steatosis and NASH since early liver damage and liver inflammation occur upon short term feeding. Choline deficiency induces liver steatosis because the choline derivative, phosphatidylcholine (PC), is a main constituent of very low density lipoprotein (VLDL) and is required for fat export from the liver [64]. However, choline deficiency fails to produce insulin resistance and metabolic syndrome, which are important features of human NAFLD [65]. Wolf *et al*. established a choline-deficient high fat diet (CD-HFD) model to combine early NAFLD to NASH progression with metabolic changes [56]. In a collaborative effort, we studied whether CD-HFD causes mitochondrial impairments in mouse livers. Of note, CD-HFD feeding induced steatosis, liver damage and similar mitochondrial alterations as observed in humans (ballooned cristae, lower ATP production, Fig. 3) [56]. However, if these mitochondrial impairments are caused by choline deficiency or by high fat intake or if they are a consequence of liver damage, has not been evaluated in this feeding model. More importantly, choline deficiency does not mirror human dietary habits and the early and frequent NASH development is non-conform to the human situation.

For these reasons, the human-like “American Lifestyle-induced Obesity Syndrome” (ALiOS) model also termed “western diet” (WD) model has been chosen in the current thesis to unravel the role of mitochondria upon malnutrition. This feeding model was established by Tetri *et al.* including high concentrations of saturated fatty acids (SFAs) in the diet and fructose supplementation in drinking water [66]. Thus, the WD model resembles the eating habits in western society. Feeding mice this WD demonstrated a phenotype of NAFLD after 16 weeks [66], revealed first signs of NASH after 24 weeks and displayed more advanced NASH after 48 weeks of feeding [67]. Consequently, the WD feeding animal model reflects human NAFLD pathogenesis as a slowly progressive disease.

With respect to the concept that two or multiple hits are necessary to promote steatosis to NASH progression, WD feeding is applied in the present study to LPP rats (Wilson disease animal model). Wilson disease is an autosomal recessively inherited disorder with *loss-of-function* mutations in the copper transporter

ATP7B [68]. LPP rats contain the same genetic defect in *Atp7b*. Homozygous *Atp7b*$^{-/-}$ rats, but not heterozygous *Atp7b*$^{+/-}$ rats, develop mitochondrial copper overload, mitochondrial dysfunction and acute liver failure [69, 70]. Additionally, patients with Wilson disease often display liver steatosis, chronic liver inflammation as well as fibrosis [71] and thus become frequently misdiagnosed as NAFLD [72]. Since steatosis as well as Wilson disease target mitochondria, it is analyzed whether steatosis-related and copper-related mitochondrial dysfunctions are additive and it is examined if WD promotes Wilson disease progression.

1.5 The activated immune system in NAFLD

In case of obesity and NASH, it has been reported that hepatic macrophages (Kupffer cells) and recruited macrophages [73] are activated via damage-associated molecular pattern (DAMP) such as soluble ATP, oxidative stress or disrupted mitochondria, leading to the induction of the NLRP3 inflammasome in the liver [74-76] (Fig. 2). The NOD-like pyrin domain containing receptor 3 (NLRP3) inflammasome is a multiprotein complex (~700 kDa), which consist of NLRP3, ASC adaptor protein (apoptosis-associated speck-like protein containing caspase activation and recruitment domain) and pro-caspase-1 [77] (Fig. 2). Following inflammasome activation, conformal changes occur and pro-caspase-1 is auto-activated. The active caspase-1 processes pro-IL-1ß and pro-IL-18 to their biological active forms (Fig. 2). These pro-inflammatory cytokines are further released into the circulation and induce, among others, the activation of NFκB (nuclear factor kappa-light-chain-enhancer of activated B cells), which elevates pro-IL-1 and pro-IL-18 transcription [78] (Fig. 2).

Moreover, during obesity and NASH, the adaptive immune system is activated as well via infiltration of pro-inflammatory $CD4^+$T cells, $CD8^+$T cells and B cells [79-81] into the adipose tissue paralleled by $CD8^+$T cell infiltration into the liver [56]. T lymphocytes are activated by antigen-presenting cells (e.g. dendritic cells, DC) and differentiate into $CD4^+$T or $CD8^+$T cells that secrete immune-regulatory cytokines or cytotoxic proteins, respectively (Fig. 2). $CD4^+$T cells further activate B cells to differentiate into antibody-producing plasma cells and therefore elevate the efficiency of the immune response (Fig. 2). In agreement, increased levels of pathogenic IgG antibodies are present in obese mice [79].

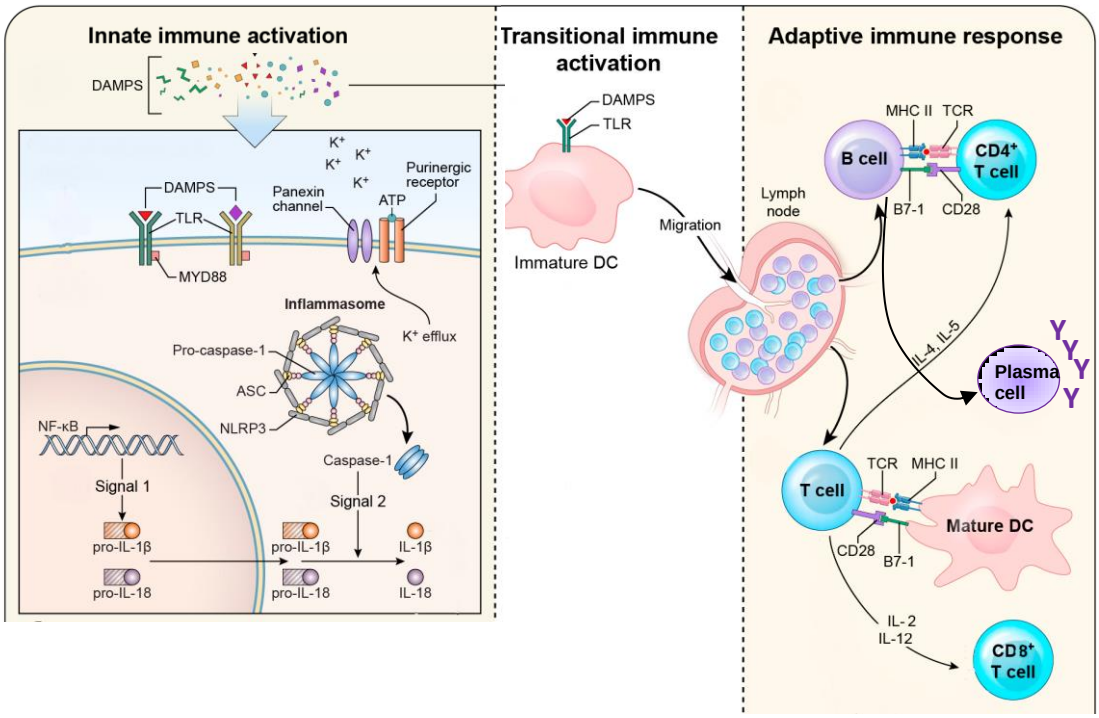

Fig. 2: Schematic overview of the interplay between innate and adaptive immunity during damage recognition

Damage-associated molecular patterns (DAMPs) are recognized via Toll-like receptors (TLRs) upon dendritic cells (DCs) of the innate immune system and activate in combination with K^+-efflux or soluble ATP the NLRP3 inflammasome, leading to caspase-1 activation and the processing of mature IL-1ß and IL-18. At this, NFκB regulates the transcription of pro-IL-1ß and pro-IL-18. In the lymph node, DCs present MHCII-bound DAMPs to T cells, following T cell differentiation into $CD4^+$T cells and $CD8^+$T cells as well as B cell activation into antibody-producing plasma cells. (Adapted from: Famakin *et al*. 2014 [82])

In a collaborative effort, we have studied the impact of B and T lymphocytes in NAFLD progression by feeding a CD-HFD to *Rag1*$^{-/-}$ mice [56]. *Rag1*$^{-/-}$ mice are deficient in mature B and T cells [83]. CD-HFD fed *Rag1*$^{-/-}$ mice did not develop any signs of steatosis, liver damage, NASH or liver cancer compared to wildtype controls [56]. Furthermore, we revealed that CD-HFD-related mitochondrial structural changes (ballooned cristae) and functional impairments, such as decreased ATP production and elevated susceptibility to calcium, are absent in *Rag1*$^{-/-}$ mice in contrast to wildtype mice (Fig. 3, unpublished data). Because of the observed protective effect, depleting components of the adaptive immune system in mitochondrial functionality, the present work addresses the issue if a depletion

of innate immune system components (NLRP3$^{-/-}$, IL-18R$^{-/-}$, IL-1R$^{-/-}$) avoids mitochondrial impairments as well.

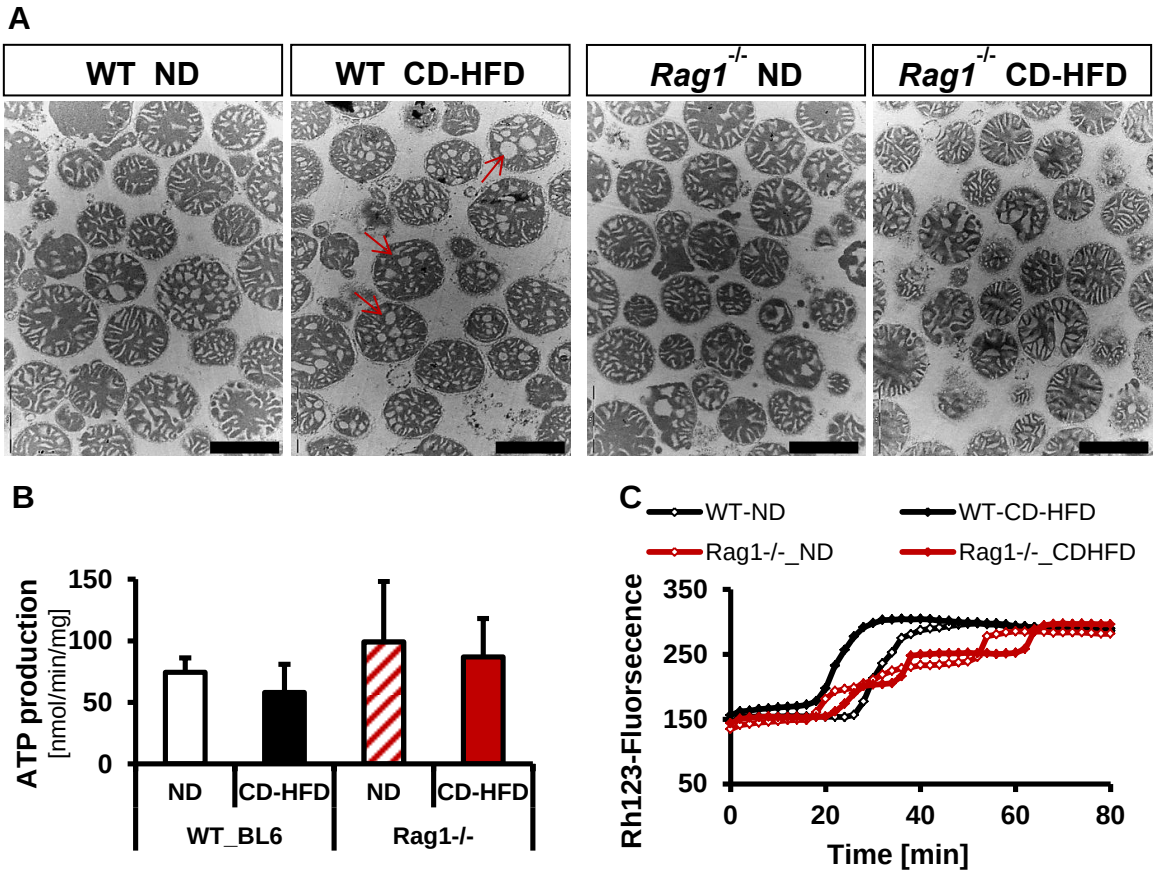

Fig. 3: CD-HFD-induced mitochondrial changes are not present in *Rag1*$^{-/-}$ mice

(A) Representative electron micrographs reveal high quota of rounded and widened cristae (arrow) in CD-HFD wildtype mitochondria those are not present in CD-HFD mitochondria isolated from *Rag1*$^{-/-}$ mice (scale bar: 1 µm). (B) Mitochondrial ATP production decreases upon CD-HFD and is re-established in *Rag1*$^{-/-}$ mice. (C) Earlier depolarization of the MMP occurs in wildtype CD-HFD mitochondria treated with 100 µM calcium and this is delayed in *Rag1*$^{-/-}$ mitochondria.

1.6 Aim of the study

The prevalence of NAFLD is steadily rising in industrialized countries over the last decades. The molecular mechanisms that cause steatosis to NASH progression remain incompletely understood and therapeutic strategies are mostly lacking. Consequently, NASH-related cirrhosis is the third most common cause of liver transplantation worldwide [6]. Lipid overflow, mitochondrial dysfunction and low-grade chronic inflammation are important hallmarks of NASH but whether and how they influence the NAFLD to NASH progression is still a matter of debate.

Therefore, the present thesis addresses the issues whether mitochondrial impairments are steatosis-related or appear as consequence of liver damage in NASH. Thus, C57BL/6 mice were fed a western diet (WD) for 6 to 48 weeks. The molecular mechanisms that cause the mitochondrial changes are characterized and it is studied if the depletion of the NLRP3 inflammasome (NLRP3$^{-/-}$, IL-18R$^{-/-}$, IL-1R$^{-/-}$) prevent mitochondrial dysfunction.

Since steatosis and mitochondrial impairments occur in Wilson disease, the impact of WD in Wilson disease progression is analyzed to examine if steatosis- and Wilson disease-related mitochondrial deficits are additive and aggravate disease progression.

Finally, the impact of single fatty acids on hepatocyte viability and mitochondrial functionality is investigated to unravel the molecular mechanisms that cause steatosis and mitochondrial impairments upon WD nutrition.

2. Material and Methods

2.1 Reagents and technical equipment

Tab. 1: Chemicals, dyes and cell culture reagents

Name	Producer
37 component FAME mix	Supelco, Sigma-Aldrich, Taufkirchen, Germany
Acetone	Merck, Darmstadt, Germany
ADP (adenosine-5'-diphosphate)	Sigma-Aldrich, Taufkirchen, Germany
Albumin Fraction V, (BSA, fatty acid free)	Carl Roth, Karlsruhe, Germany
6-Aminocabronic acid	Carl Roth, Karlsruhe, Germany
Amplex™ Red	Molecular Probes, Invitrogen, Karlsruhe, Germany
Antibiotic-antimycotic solution	Life Technologies, Darmstadt, Germany
Antimycin A	Sigma-Aldrich, Taufkirchen, Germany
Arachidonic aicd (C20:4)	Sigma-Aldrich, Taufkirchen, Germany
ATP (adenosine-5'-triphosphate disodium salt)	Roche Diagnostics, Mannheim, Germany
ATP Bioluminescence Assay Kit (luciferase reagent, ATP standard, cell lysis reagent, dilution buffer)	Roche Diagnostics, Mannheim, Germany
$CaCl_2$ (calcium chloride)	Carl Roth, Karlsruhe, Germany
CAY-10566 (SCD1 inhibitor)	Cayman Chemical Company, Ann Arbor, MI, USA
CCCP (Carbonyl cyanide m-chloro-phenyl-hydrazone)	Sigma-Aldrich, Taufkirchen, Germany
Chloroform	Sigma-Aldrich, Taufkirchen, Germany
Coomassie® Brilliant Blue G-250	Serva Electrophoresis GmbH, Heidelberg, Germany
$CuCl_2$*$2H_2O$ (copper (II) chloride-dihydrate)	Sigma-Aldrich, Taufkirchen, Germany
Cyclosporine A (CysA)	Fluka, Sigma-Aldrich, Taufkirchen, Germany
Derivatization reagent	Supelco, Sigma-Aldrich, Taufkirchen, Germany
Digitonin (high purity)	Calbiochem, Sigma-Aldrich, Taufkirchen, Germany
DiOC6 (3,3'-dihexyloxacarbocyanine iodide)	Molecular Probes, Invitrogen, Karlsruhe, Germany
DMSO (dimethylsulfoxide)	Sigma-Aldrich, Taufkirchen, Germany
DPBS (Dulbecco's phosphate buffered saline)	Biochrom AG, Berlin, Germany
DPH (1,6-diphenyl-1,3,5-hexatriene)	Sigma-Aldrich, Taufkirchen, Germany

Name	Producer
DTNB (5'5-dithiobis-2-nitrobenzoic acid)	Sigma-Aldrich, Taufkirchen, Germany
EGTA (ethylene glycol-bis(2-amino-ethylether)-tetraacetic acid)	Fluka, Sigma-Aldrich, Taufkirchen, Germany
Ethanol	Merck, Darmstadt, Germany
FCCP (Carbonyl cyanide-p-trifluoromethoxy-phenylhydrazone)	Sigma-Aldrich, Taufkirchen, Germany
FCS (fetal calf serum)	Biochrom AG, Berlin, Germany
Glucose	Sigma-Aldrich, Taufkirchen, Germany
Glutamate (monohydrate)	Fluka, Sigma-Aldrich, Taufkirchen, Germany
Glycerin	Sigma-Aldrich, Taufkirchen, Germany
Glycine	Sigma-Aldrich, Taufkirchen, Germany
HEPES (4-(2-hydroxyethyl)piperazine-1-ethanesulfonic acid)	Sigma-Aldrich, Taufkirchen, Germany
Hexane	Merck, Darmstadt, Germany
Hoechst 33342	Life Technologies, Darmstadt, Germany
Imidazole	Carl Roth, Karlsruhe, Germany
KCl (potassium chloride)	Merck, Darmstadt, Germany
KCN (potassium ferrocyanide * $3H_2O$)	Sigma-Aldrich, Taufkirchen, Germany
KOH (potassium hydroxide)	Merck, Darmstadt, Germany
Linoleic acid (C18:2)	Sigma-Aldrich, Taufkirchen, Germany
20x LumiGLO® reagent and 20x peroxide	Cell Signaling Technology, Frankfurt a.M., Germany
$MgCl_2$ (magnesium chloride)	Sigma-Aldrich, Taufkirchen, Germany
Methanol	Fluka, Sigma-Aldrich, Taufkirchen, Germany
3-MA (3-methyladenine)	Sigma-Aldrich, Taufkirchen, Germany
Malate (disodium salt)	Merck, Darmstadt, Germany
Mitosox™ Red	Molecular Probes, Invitrogen, Karlsruhe, Germany
MOPS (4-morpholinepropanesulfonic acid)	Fluka, Sigma-Aldrich, Taufkirchen, Germany
NaCl (sodium chloride)	Sigma-Aldrich, Taufkirchen, Germany
NaOH (sodium hydroxide solution)	Fluka, Sigma-Aldrich, Taufkirchen, Germany
NEAA (non-essential amino acids)	Life Technologies, Darmstadt, Germany
Neutral red	Sigma-Aldrich, Taufkirchen, Germany
Nile Red	Sigma-Aldrich, Taufkirchen, Germany
NP40 (Tergitol-type nonyl phenoxypolyethoxyl-ethanol)	Sigma-Aldrich, Taufkirchen, Germany
Oleic acid (C18:1)	Sigma-Aldrich, Taufkirchen, Germany
Oligomycin	Sigma-Aldrich, Taufkirchen, Germany

Name	Producer
Palmitic acid (C16:0)	Sigma-Aldrich, Taufkirchen, Germany
Palmitoylcarnitine-DL-chloride	Sigma-Aldrich, Taufkirchen, Germany
Percoll®	GE Healthcare, Munich, Germany
Phosphoric acid (H_3PO_4)	Sigma-Aldrich, Taufkirchen, Germany
Rh123 (Rhodamine 123)	Invitrogen, Karlsruhe, Germany
Rotenone	Sigma-Aldrich, Taufkirchen, Germany
SDS (sodium salt)	Serva Electrophoresis GmbH, Heidelberg, Germany
Sodium pyruvate	Life Technologies, Darmstadt, Germany
Stearic acid (C18:0)	Sigma-Aldrich, Taufkirchen, Germany
Succinate Na_2-salt * $6H_2O$	Sigma-Aldrich, Taufkirchen, Germany
Sucrose	Fluka, Sigma-Aldrich, Taufkirchen, Germany
THF (tetrahydrofurane)	Carl Roth, Karlsruhe, Germany
TMA-DPH (Trimethylamine-diphenylhexatriene)	Sigma-Aldrich, Taufkirchen, Germany
Tricine	Carl Roth, Karlsruhe, Germany
TRIS	VWR International GmbH, Ismaning, Germany
Triton X-100	Sigma-Aldrich, Taufkirchen, Germany
Trizma® base	Sigma-Aldrich, Taufkirchen, Germany

Tab. 2: Technical Equipment

Name	Application	Producer
BD LSRII flow cytometer	DiOC6 and Mitosox staining	BD Bioscience, Heidelberg, Germany
Centro LB 960 luminometer	Luminescence measurement (ATP assays)	Berthold Technologies GmbH & Co. KG, Bad Wildbad, Germany
ChemoCam Imager 3.2	Immunoblotting	INTAS Science Imaging Instruments GmbH, Göttingen, Germany
Clario-Star plate reader	Fluorescence measurement (Hoechst staining)	BMG Labtech, Ortenberg, Germany
Evos FL Fluorescence Microscope	Microscopy (Nile Red staining)	Life Technologies, Darmstadt, Germany
Gas chromatograph	Analyses of mitochondrial fatty acid composition	Carlo ERBA instruments HRGC 5300, Egelsbach, Germany
BPX70 GC capillary column	Separation of fatty acid methyl-esters (FAME)	SGE Analytical Science, Milton Keynes, United Kingdom

Name	Application	Producer
Oxygraph-2k	Respiration measurements	Oroboros Instruments GmbH, Innsbruck, Austria
Respons® 910	Serum transaminases and triglyceride measurements	Diasys Greiner GmbH, Flacht, Germany
Synergy 2 plate reader	Fluorescence, anisotropy and absorbance measurements	BioTek Instruments, Inc., Bad Friedrichshall, Germany
96-well plates (white, flat bottom)	ATP assays	Thermo Fisher Scientific GmbH, Dreieich, Germany
96-well plates (black, clear flat bottom)	mitochondrial membrane potential, swelling, anisotropy, H_2O_2 production	Greiner Bio-One GmbH, Frickenhausen, Germany
96-well plates (clear, flat bottom)	Neutral red, Nile Red, Hoechst staining, F_1F_O-activity	Falcon, VWR, Ismaning, Germany

2.2 Animal studies

Male C57BL/6 wildtype, IL-1R$^{-/-}$ and IL-18R$^{-/-}$ mice were from Charles River (Sulzfeld, Germany) and NLRP3$^{-/-}$ mice were kindly provided by the group of Prof. M. Schnurr (Department of Clinical Pharmacology, LMU Munich). Mice were housed according to the guidelines for the care and use of laboratory animals at the University Hospital Munich. Mice had free access to water and food and the feeding study started at the age of eight weeks. Standard rodent diet (ND) was from Ssniff (Spezialdiäten GmbH, Germany, V1535-0) and western diet (WD) was from Altromin (Spezialfutter GmbH & Co. KG, Seelenkamp, Germany). The WD was composed of 45% calories from fat and was supplemented with fructose-rich water (23.1 g/l fructose, 18.9 g/l glucose-monohydrate) according to the “American Lifestyle-induced Obesity Syndrome” (ALiOS) model [66].

To study Wilson disease progression upon high caloric nutrition, LPP rats [84] (*Atp7b*$^{-/-}$ or *Atp7b*$^{+/-}$) were fed with either WD and fructose-rich water or normal diet (Altromin Spezialfutter GmbH & Co. KG, Germany, 1314) and tap water ad libitum. The feeding period took 3-5 weeks starting at the age of 46 days and fructose-rich water was additionally supplemented with 8.32 mg/l $CuCl_2$*$2H_2O$ to adapt nutritional copper content to normal diet (13 mg/kg). Rats were maintained under the guidelines for the care and use of laboratory animals of the Helmholtz Center

Munich. The animal experiments were approved by the government authorities of the “Regierung von Oberbayern” (Munich, Germany).

2.3 Serum-, triglyceride- and liver histology analyses

The serum transaminases (ALT, AST) were analyzed with Respons® 910 according to the manufactural guideline. R. Wimmer (Department of Medicine II, LMU, Munich) did the quantification of liver triglycerides (TGs). 100 mg/ml liver tissue was sonicated in 5% NP40 solution, heated for 5 min at 96 °C and cooled down on ice. Subsequently, the homogenate was centrifuged for 2 min at 20,000 g, the supernatant was diluted 1:10 in 5% NP40 solution and analyzed with Respons® 910. Histological analyses of hematoxylin and eosin (HE)-stained mouse liver samples were done by Prof. D. Mayr (Institute of Pathology, LMU, Munich).

2.4 Cell culture experiments

2.4.1 HepG2 cell cultivation and fatty acid treatment

HepG2 cells (ATCC, Wesel, Germany) were maintained in 5% CO_2 atmosphere at 37 °C and cultured in minimum essential medium (MEM), containing 1.9 mM GlutaMAX™, 5.5 mM glucose, 10% FCS, 1% non-essential amino acids (NEAA), 1% sodium pyruvate and 1% antibiotic-antimycotic solution.

For fatty acid (FA) treatment, cells were cultured 24 h or 48 h with the indicated FAs (C16:0, C18:0, C18:1, C18:2, C20:4) or FA-mixtures (SLFC: standard liver fatty acid composition, HFLC: high fat liver composition (Fig. 21), containing 1% bovine serum albumin (BSA, FA-free) as vehicle and diluted in medium with 2% FCS. The FAs stock solutions (10 mM) were prepared by saponification with 25 mM KOH at 70 °C. Subsequently, the FAs were complexed (1:1) for 10 min at 50 °C with BSA (20% dissolved in DPBS), cooled to room temperature (RT) and added to HepG2 cells 24 h after seeding.

2.4.2 Determination of intracellular lipid accumulation

Nile Red staining was done as described earlier [85], with slight adaptions. Per well of a clear bottom 96-well plate, $2x10^4$ HepG2 cells were seeded and 24 h after seeding, the cells were incubated with FAs for 24 h or 48 h. Nile Red was freshly diluted 1:200 in DPBS from stock solution (0.5 mg/ml dissolved in acetone) and 100 µl were added to each well. After 2 h incubation in the dark at 37 °C, Nile Red was removed and cells were washed twice with DPBS. The fat content per well was quantified by fluorescence measurements ($\lambda_{Ex.}$ 520/25 nm, $\lambda_{Em.}$ 620/40 nm) in a plate reader (Synergy 2) or pictured via Evos FL fluorescence microscope. To exclude a lower lipid accumulation because of potential cell death, the fluorescence intensity of Nile Red staining was normalized to the fluorescence intensity of Hoechst staining (nuclear staining, equivalent to cell density). For cell density measurement, a 10 mg/ml stock solution of Hoechst dye was diluted 1:10,000 in DPBS and 100 µl were added to each well. After 50 min incubation in the dark at 37 °C, each well was washed twice with DPBS and fluorescence was determined with Clario-Star Reader ($\lambda_{Ex.}$ 355/20 nm, $\lambda_{Em.}$ 455/30 nm).

2.4.3 Cell viability assay

For analyzing cell viability, $2x10^4$ HepG2 cells were seeded per well of a clear bottom 96-well plate and 24 h after seeding, the cells were incubated with FAs for 24 h or 48 h. To block SCD1, the cells were incubated with 15 µM CAY-10566 and inhibition of autophagy was done by adding 89.3 µM 3-methyladenine (3-MA). Neutral red cell toxicity assay was done as described elsewhere [86]. Neutral red fluorescence was analyzed after washing and cell de-staining in a plate reader (Synergy 2, $\lambda_{Ex.}$ 520/25 nm, $\lambda_{Em.}$ 620/40 nm).

2.4.4 Cellular ATP content

The ATP content of HepG2 cells was measured with the ATP Bioluminescence Assay Kit according to the manufactural guidelines. In detail, $1x10^5$ cells were pelleted at 400 g for 5 min, dissolved in 100 µl dilution buffer and lysed by adding 100 µl lysis buffer for 5–10 min at RT. Subsequently, cell lysates were heated for 5 min at 95 °C, centrifuged for 2 min at 16,000 rcf and the supernatants were

diluted 1:5 in dilution buffer. Per well of a 96-well plate (white, flat bottom), 50 µl diluted supernatant as well as 50 µl luciferase reagent were added and chemiluminescence signals were detected in a luminometer (Centro LB 960). The quantification of the ATP content was done via ATP standard curves (0, 0.165, 1.65, 16.5, 165, 1650 nM; stock: 16.5 mM).

2.4.5 Oxygen consumption measurements in HepG2 cells

High-resolution respirometry (HRR) was done in a Oxygraph-2k instrument in accordance to an earlier report [87]. Per chamber, $2x10^6$ HepG2 cells were supplied in cell culture media containing 2% FCS and oxygen consumption rates were measured without any additions (= routine respiration, Fig. 4). To analyze the leak respiration, 2.5 mM oligomycin was added (final 2.5 µM). Oligomycin blocks the ATP synthase. Therefore, mitochondrial O_2 consumption is minimal and is equivalent to the unspecific proton leakage across the inner mitochondrial membrane (Fig. 4).

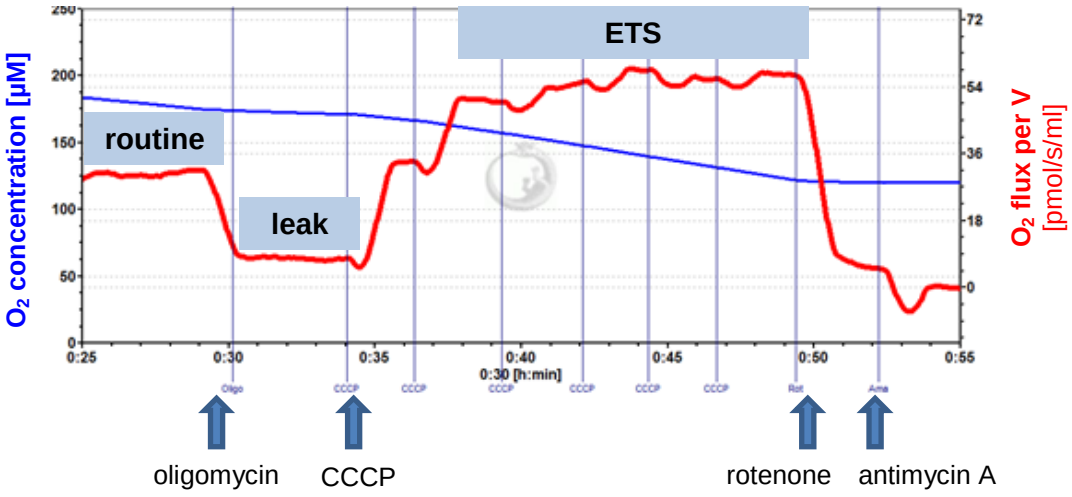

Fig. 4: Schematic overview of a high resolution respirometry measurement

The O_2 flux of intact cells per volt (red line) decreases upon oligomycin addition (leak state), appears maximal after CCCP application (ETS) and drops down if the respiratory chain complexes I+III are blocked via rotenone or antimycin A, respectively. Therefore, the O_2 concentration in the chamber (blue line) decreases at routine state and much more pronounced during ETS but displays almost no reduction at leak state or if CI and CIII are blocked.

Subsequently, the protonophore CCCP was added (1-2 µl steps from a 1 mM stock solution) to induce maximal O_2 consumption (ETS, electron transfer system

capacity, Fig. 4). The oxygen flux was baseline-corrected for non-mitochondrial O_2 consumption with 0.5 µM rotenone (inhibitor of complex I) and 2.5 µM antimycin A (inhibitor of complex III, Fig. 4).

2.4.6 Flow cytometry

Mitochondrial membrane potential (MMP) of HepG2 cells was determined by DiOC6 staining and mitochondrial superoxide production was investigated via Mitosox™ Red staining according to manufactural guidelines. HepG2 cells ($2x10^6$) were incubated for 15–20 min at 37 °C with 100 µl buffer, containing 10 mM HEPES, 140 mM NaCl, 5 mM $CaCl_2$ and 20 nM DiOC6 or 5 µM Mitosox, respectively. After the addition of 100 µl buffer, the stained cells were analyzed by flow cytometry (BD LSRII) at $\lambda_{Em.}$ 530 nm or $\lambda_{Em.}$ 585 nm, respectively. As MMP-dissipating control, 500 µM CCCP was added. The quantitative evaluations of DiOC6-positive cells as well as the amount of HepG2 cells with strong Mitosox accumulation were done with FlowJo 7.6.5 software (Tree Star).

2.5 Mitochondrial analyses

2.5.1 Mitochondrial isolation procedure and adaptation for fatty acid treated cells

Mitochondria were freshly prepared from mouse livers as described elsewhere [88-91]. The mitochondria were pelleted by a differential centrifugation and purified using Percoll™ density gradient.

For fatty acid treated HepG2 cells (48 h), the mitochondrial isolation procedure was adapted based on protocols reported for cell culture [90, 92] and for white adipose tissue [93]. $7–10x10^6$ cells/ml were homogenized via PCC pumping [92] with a constant rate of 1400 µl/min. Subsequently, the homogenates from control treated cells were cleared through 800 g centrifugation (10 min, 4 °C) and mitochondria were pelleted via a 9,000 g centrifugation step (10 min, 4 °C). Mitochondria from fatty acid treated cells (48 h) had a lower specific weight and did not pellet with the standard isolation procedure. Therefore, homogenates were

cleared by 2,000 g centrifugation (10 min, 4 °C) and mitochondria were pelleted by 20,000 g (10 min, 4 °C).

2.5.2 Mitochondrial swelling and membrane potential measurements

Mitochondrial swelling (± 50–100 µM calcium) was analyzed in a black 96-well plate (clear flat bottom) by light scattering at 540 nm (plate reader Synergy 2). In parallel, the mitochondrial membrane potential (MMP) was measured by Rhodamine123 (Rh123) fluorescence quenching at $\lambda_{Ex.}$ 485/20 nm and $\lambda_{Em.}$ 528/20 nm as described elsewhere [88]. The ratio of ± FCCP addition (1 µM), was considered as indicative of an intact inner mitochondrial membrane. The characterization of the MMP depolarization process was done with MATLAB software (CurveAnalyst) as described by Schulz *et al.* [88] and start, end, maximum as well as the duration of the depolarization process (in min) were calculated.

2.5.3 ATP production of isolated mitochondria

The ATP production was measured with the ATP Bioluminescence Assay Kit according to the manufactural guideline. Isolated mitochondria (10 µg) were incubated with 160 µM ADP and 5 mM succinate for 30 min at RT in a buffer containing 0.2 M sucrose, 10 mM MOPS-Tris, 1 mM Pi, 10 µM EGTA, 5 mM succinate, 2 µM rotenone. As background control, 2 mM KCN was added that blocks respiratory chain (complex IV) and mitochondrial ATP production was calculated in pmol/min/mg protein based on background-corrected luminescence signals and the ATP standard curves (0, 0.165, 1.65, 16.5, 165, 1650 nM; stock: 16.5 mM).

2.5.4 F_1F_O-activity assay

F_1F_O-activity (ATP synthase activity) was performed as described before [94, 95]. Briefly, 20 µg mitochondria were incubated in buffer containing either 50 mM TRIS (pH 8.0) or additional 3 µM oligomycin (F_1F_o inhibitor, negative control) for 5 min at 37 °C in a plate reader (Synergy 2). To start the reaction, a mixture of finally

0.5 mM ATP, 3 µM CCCP, 1 mg/ml BSA, 1 µM antimycin A, 10 mM KCl, 4 mM $MgCl_2$, 0.2 mM NADH, 2 mM phosphoenolpyruvate (PEP), 4 units of lactate dehydrogenase (LDH) and pyruvate kinase (PK) were added (Tab. 3).

Tab. 3: Enzymes and substrates for F_1F_O-activity measurements

Enzymes	**Provider**	**dissolved in**	**final concentration**
LDH (lactate dehydrogenase)	Roche	50 mM TRIS (pH 8)	4 units/well
NADH (nicotinamide adenine dinucleotide)	Roche	50 mM TRIS (pH 8)	0.2 mM
PEP (phosphoenolpyruvate)	Roche	50 mM TRIS (pH 8)	2 mM
PK (pyruvate kinase)	Roche	50 mM TRIS (pH 8)	4 units/well

The F_1F_O-activity was determined in the reverse direction following ATP hydrolysis and NADH oxidation in parallel to the conversion of pyruvate to lactate (Fig. 5). The decrease in NADH absorbance at 340 nm is proportional to the ATPase activity and was calculated in nmol/min/mg using the formula: $(\Delta A * V)/(\varepsilon * h * m)*1000$ (ΔA: changes in absorbance; V: volume per well; ε: molar extinction coefficient of NADH; h: layer thickness, m: content of mitochondria). The F_1F_O-activity was normalized to the activity of the housekeeping enzyme citrate synthase. For analyzing the citrate synthase activity, 20 µg mitochondria were used and the increase in absorbance of 5-thio-2-nitrobenzoate anion (TNB^{2-}) was followed at 412 nm according to the protocols described elsewhere [90, 96].

$$ATP \xrightarrow{\textbf{ATPase}} ADP + P_i$$
$$ADP + P_i + PEP \xrightarrow{PK} ATP + pyruvate$$
$$pyruvate + NADH + H^+ \xrightarrow{LDH} lactate + NAD^+$$

Fig. 5: Reaction scheme of the F_1F_O-activity assay

F_1F_O-activity is determined in reverse direction by ATP hydrolysis (ATPase). The reaction is coupled with the conversion of phosphoenolpyruvate (PEP) to pyruvate by pyruvate kinase (PK) and the conversion of pyruvate and $NADH+H^+$ to lactate and NAD^+ by lactate dehydrogenase (LDH). The decrease in NADH is followed spectrophotometrically and is proportional to the F_1F_O-activity.

2.5.5 Mitochondrial H_2O_2 production

According to earlier reports [97], mitochondrial H_2O_2 production was analyzed following Resorufin fluorescence (converted from Amplex^{TM} Red) at $\lambda_{Ex.}$ 540/20 nm and $\lambda_{Em.}$ 620/40 nm. Substrates were either 10 mM succinate and 2 µM rotenone or 5 mM glutamate and 5 mM malate or 10 µM palmitoylcarnitine-DL-chloride and 2 mM malate in the presence or absence of 3.2 mM ADP.

2.5.6 Fluorescence anisotropy measurements

Fluorescence anisotropy was determined in DPH- and TMA-DPH-dyed mitochondria [98, 99]. Mitochondria (3 µg/µl) were incubated in the dark for 30 min at 37 °C with DPH (50 µM dissolved in THF) or TMA-DPH (20 µM dissolved in DMSO). Subsequently, 75 µg stained mitochondria were added into a 96-well plate (black, clear flat bottom) containing 175 µl buffer (0.2 M sucrose, 10 mM MOPS-Tris, 1 mM Pi, 10 µM EGTA, 5 mM succinate, 2 µM rotenone). Parallel ($I_{\parallel}$) and perpendicular ($I_{\perp}$) fluorescence was assessed (Synergy 2, $\lambda_{Ex.}$ 366 nm, $\lambda_{Em.}$ 425 nm) and fluorescence anisotropy was calculated by Gen5 software (BioTek Instruments) using the formula:

$A = (I_{\parallel} - G * I_{\perp})/(I_{\parallel} + 2*G * I_{\perp})$; G = 0.89 [100].

2.5.7 Structural analysis of isolated mitochondria

Mitochondrial structure was analyzed via electron microscopy by Dr. B. Popper (Biomedical Center, Department of Anatomy and Cell Biology, LMU, Munich) and the sample preparation was done by C. Eberhagen and C. Leitzinger (Institute of Molecular Toxicology and Pharmacology, Helmholtz Center Munich) as described elsewhere [101]. For structural analysis, mitochondria were grouped into “normal structured” of the so called “condensed type mitochondria” [102] or in “altered” mitochondria with widened cristae and massive matrix condensations. For each feeding time point, about 500-700 mitochondria (150-180 mitochondria per animal) were included into this analysis.

2.5.8 Proteome data analysis

The analysis of the mitochondrial proteome was done on isolated mitochondria from 6–24 weeks fed C57BL/6 mice. Sample digestion and mass spectrometry was done by Dr. C. von Törne (Research Unit Protein Science, Helmholtz Center Munich) as described elsewhere [103-105]. Data analysis was performed comparing ND and WD peptides in an age-matched manner and set as enriched or decreased if the mean raw abundance as well as the normalized abundance was ≥ 1.5 or ≤ 0.67 in WD compared to ND mitochondrial fractions, respectively. Additionally, peptides were set as regulated if the mean differs significantly ($p < 0.05$) between ND and WD and if the coefficient of variation was < 33% (Supplementary Table). Using the protein and pathway databases UniProt [106], KEGG (Kanehisa Laboratories, Japanese) [107] and PANTHER [108], the identified proteins were grouped based to their cellular localization and metabolic pathway affiliation. A cluster analysis with Scaffold 4 software (Proteome Software, Inc, Portland, OR, USA) revealed a highly comparable proteome with an overlap of about 400 proteins (Fig. 6A) and the identified proteins displayed mainly mitochondrial origin (Fig. 6B).

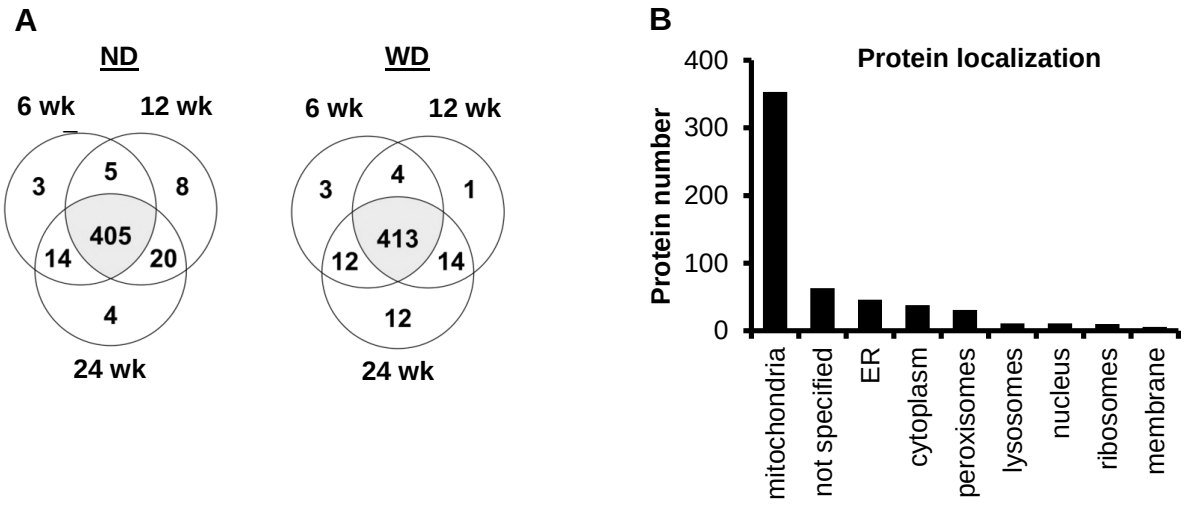

Fig. 6: Quality control of the proteome analysis

(A) ND and WD mitochondria from mice at different feeding times appear with highly comparable proteomes. (B) The isolated fractions mainly contain proteins that are localized in mitochondria.

2.5.9 Mitochondrial copper content

The determination of mitochondrial copper was done by P. Grill (Research Unit Analytical BioGeoChemistry, Helmholtz Center Munich) via ICP-OES (Ciros Vision, SPECTRO Analytical Instruments GmbH) after wet ashing of samples with 65% nitric acid [70].

2.6 Blue Native Page and Immunoblotting

2.6.1 Blue Native Page

Mitochondrial protein quantification was done by the Bradford assay [109] and the Blue Native Page was performed according to Wittig *et al.* [110] and Diaz *et al.* [111]. Briefly, 70 µg mitochondrial protein was solubilized in 70 µl buffer (50 mM NaCl, 50 mM imidazole, 2 mM 6-aminocabronic acid, 1 mM EDTA, pH 7.0), containing digitonin (protein/digitonin ratio 1:6), for 10 min on ice and centrifuged at 20,000 g for 20 min. The supernatant was collected and glycerin (final 5%) as well as Coomassie® Brilliant Blue G-250 solution (digitonin/dye ratio 1:8; dissolved in Bis-Tris buffer, pH 7.0 and 500 mM 6-aminocapronic acid) were added. 15 µg protein was loaded on a 3-12% Bis-Tris gel (Invitrogen, Karlsruhe, Germany). Blue native gel electrophoresis was done in anode buffer (25 mM imidazole, pH 7.0) and blue cathode buffer (50 mM tricine, 7.5 mM imidazole, 0.02% Coomassie) for 1 h at 150 V and 4 °C. After the exchange of the blue cathode buffer with 1:10 diluted blue cathode buffer, separation was continued for 1 h at 250 V. For protein transfer, gels were de-stained via 30–40 min shaking in transfer buffer (20 mM Trizma® base, 150 mM glycine, 20% methanol, 0.05% SDS).

2.6.2 Immunoblotting

For immunoblotting, separated proteins were transferred from the de-stained Bis-Tris gel or SDS-PAGE to an activated PVDF membrane (Bio-Rad, Munich, Germany) according to earlier reports [111, 112]. Subsequently, the membranes were probed with primary antibodies at 4 °C (overnight) and secondary antibodies at 4 °C for 1–2 h (Tab. 4). The detection of specific proteins was achieved by using

the 20x LumiGLO® and 20x peroxide reagents. The quantification of the chemiluminescence signals was done with ImageJ software [113].

Tab. 4: Primary and secondary antibodies used for immunoblotting

Primary antibodies			Secondary antibodies		
Antigen	**Provider**	**Dilution**	**Name**	**Provider**	**Dilution**
CS	Novus Biologicals	1:1000	goat anti-rabbit IgG HRP	Cell Signaling Technology	1:1000
COXIV	Cell Signaling Technology	1:1000	goat anti-rabbit IgG HRP	Cell Signaling Technology	1:1000
NDUFB8	Abcam	1:2000	goat anti-mouse IgG HRP	Cell Signaling Technology	1:1000
SCD1	Cell Signaling Technology	1:1000	goat anti-rabbit IgG HRP	Cell Signaling Technology	1:1000
SDHA	Abcam	1:2000	goat anti-rabbit IgG HRP	Cell Signaling Technology	1:1000
UQCRC2	Abcam	1:500	goat anti-rabbit IgG HRP	Cell Signaling Technology	1:1000

2.7 Quantitative fatty acid analysis by gas chromatography

Fatty acids (FAs) were extracted from isolated liver mitochondria according to the method from Folch with chloroform/methanol (2:1 v/v) [114]. For FA extraction, 250 µg purified mitochondria were mixed with 4 ml chloroform/methanol. Subsequently, the extract was separated from protein debris by centrifugation (15 min, 3,500 g) and was washed once with NaCl (0.9%, 0.2-fold volume) and twice with methanol/water (1:1 v/v). Afterwards the organic phase was evaporated via N_2, esterified with derivatization reagent and re-solved in n-hexane (hexane/water, 1:1). Fatty acid methyl esters (FAME) were separated by capillary gas chromatography at an oven temperature of 120–210°C (steadily increase of 2 °C/min) and H_2 as carrier gas. The detection was done via flame ionization and FAMEs were identified by comparison of their retention time relative to those of the standard mixture (37 component FAME mix). The quantification was done using C15:0 as internal standard by Clarity Lite software (DataApex). Analyzing the fatty acid composition of ND and WD chow was done by R. Artmann (Department of Medicine II, LMU, Munich).

2.8 Statistics

Data are presented as mean and standard deviation (SD). Statistical analysis was performed using Student's t test and data were tested unpaired and tow-tailed. For multiple comparisons, one-way ANOVA and Tukey test was done for parametric data or Kruskal-Wallis test for non-parametric data with GraphPad Prism 7 (GraphPad Software). Differences were considered statistically significant if * $p < 0.05$, ** $p < 0.01$, *** $p < 0.001$.

3. Results

3.1 Western diet causes liver steatosis and mitochondrial impairments in mice

3.1.1 Western diet promotes obesity and steatosis

Nutrition in western society is characterized by an elevated uptake of fat and fructose-rich soft drinks, leading to a massive rise of NAFLD-affected persons. In order to mirror eating habits, male C57BL/6 mice were fed for 6, 12 and 24 weeks with western diet (WD) as well as fructose-containing water and indicators of obesity, steatosis and liver damage were determined. Obesity was analyzed by the elevation of body weight (Fig. 7A), liver weight (Fig. 7B) and visceral fat mass (Fig. 7C). Steatosis was demonstrated by liver triglyceride (TG) accumulation (Fig. 7D).

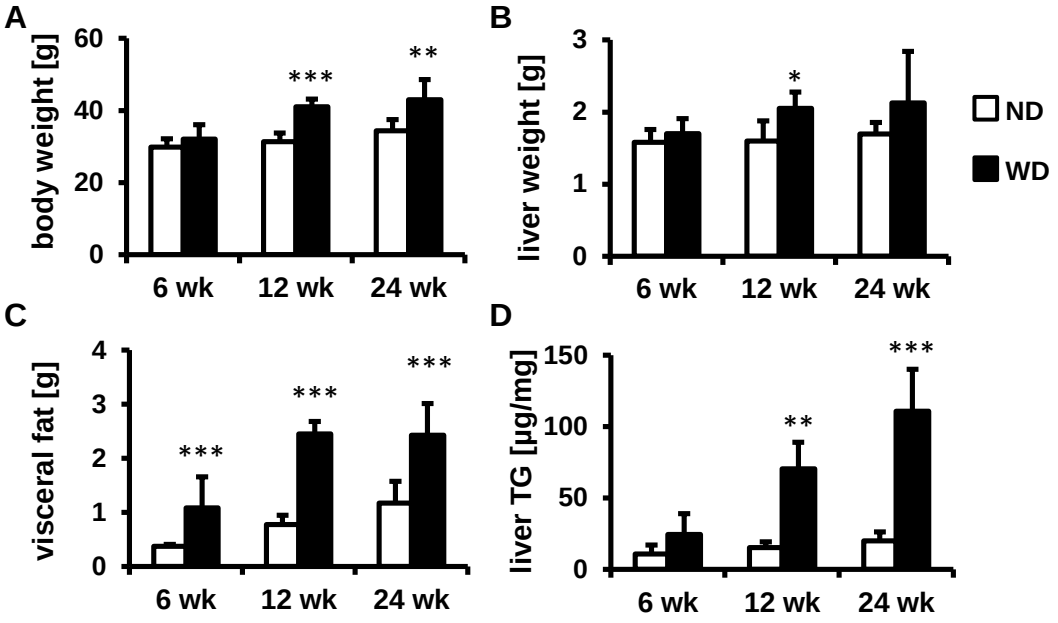

Fig. 7: Western diet induces obesity and liver steatosis

(A-D) Body weight (A), liver weight (B), mass of visceral fat (C) and liver TG content (D) of 6, 12 and 24 weeks fed male C57BL/6 mice are increased in WD compared to ND control (A-C: 6 wk: n=8, 12 wk: n=7, 24 wk n=8; D n=4). *Significant to age-matched control.

Histological analyses of the livers demonstrated that WD nutrition induced macrosteatosis starting at 12 weeks of feeding, which was more pronounced after 24 weeks of feeding (Fig. 8). However, signs of liver damage such as apoptosis,

necrosis or infiltration of inflammatory cells were not detectable in WD livers (Fig. 8). Nevertheless, the liver damage marker ALT was slightly increased in serum of 24 weeks fed WD mice (Fig. 14). Thus, WD nutrition caused steatosis without establishing NASH in 24 weeks fed mice, which is in parallel with the observation in humans that steatosis only slowly aggravates in a minority of NAFLD patients.

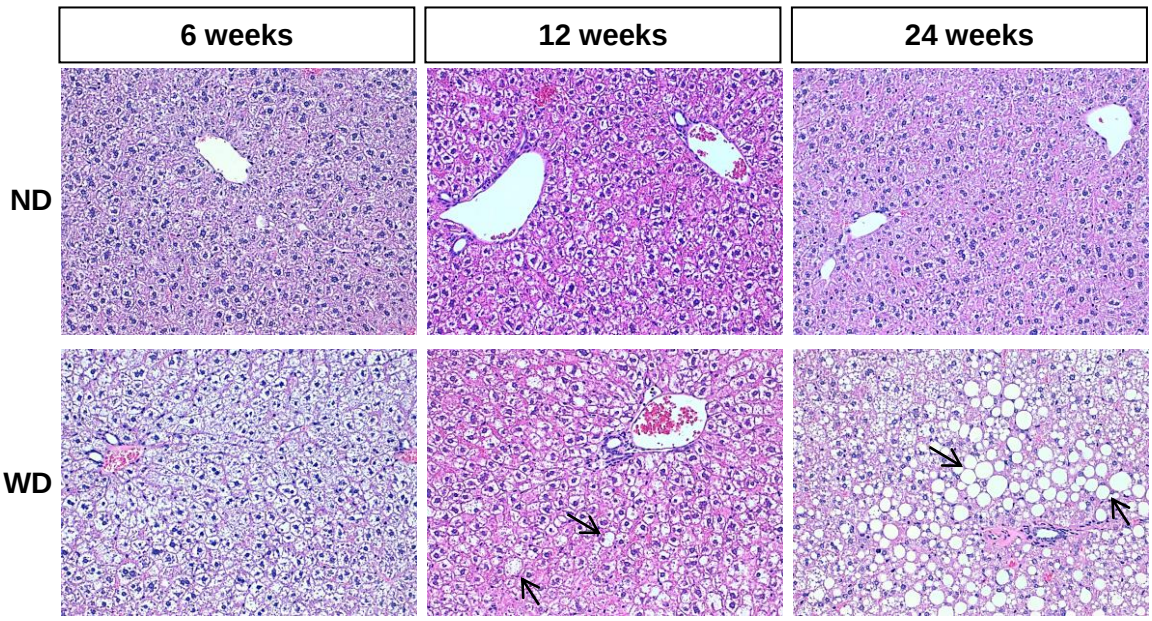

Fig. 8: Liver histology reveals macrosteatosis after 24 weeks of WD feeding
Hematoxylin/Eosin staining (HE, magnification: 200) of ND and WD mouse liver tissues demonstrate macrosteatosis (arrow) after 12 and 24 weeks of WD feeding.

3.1.2 Western diet induces structural alterations in mitochondria

In human NAFLD and NASH, mitochondrial structural changes have been frequently reported [14, 50-54]. However, at which disease stage these mitochondrial alterations occur and their role in steatosis progression are still a matter of debate. Therefore, liver mitochondria were isolated after 6, 12 and 24 weeks of feeding and ND as well as WD mitochondrial structures were compared by electron microscopy. Structural changes such as rounded and ballooned or tubular cristae appeared early after 6 weeks of feeding in WD compared to ND mitochondria (Fig. 9A). A quantitative analysis revealed a significant higher quota of mitochondria with altered cristae structures after 6 weeks of feeding in WD (24%) compared to ND (14%) mitochondria (Fig. 9B).

The amount of altered mitochondria progressively rose with prolonged feeding time and was higher in WD (34%, 39%) than in ND (18%, 29%) mitochondria (Fig. 9B). Thus, WD induced similar circular and rounded cristae alterations as observed in human NASH [14, 52]. These alterations appeared in parallel to steatosis and not as a result of liver damage.

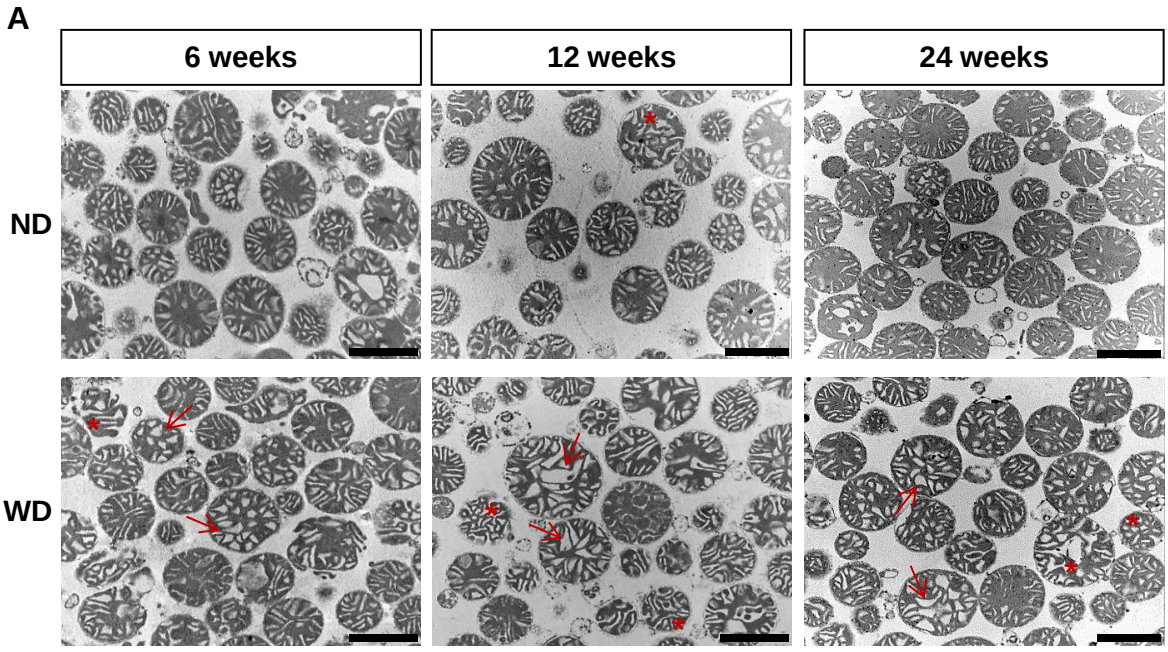

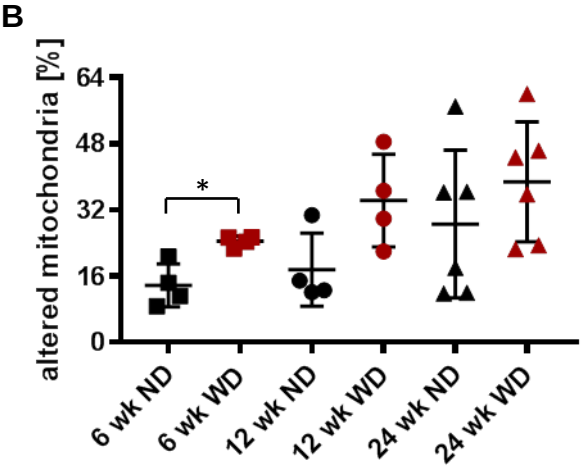

Fig. 9: Western diet impairs mitochondrial structure

(A) Representative electron micrographs demonstrate WD-induced increase in mitochondria with rounded and ballooned (arrow) or tubular (asterisk) cristae (scale bar: 1 µm).

(B) Quantification of altered mitochondria with widened and tubular cristae (6/12 wk: n=4; 24 wk: n=6, 150-180 mitochondria per animal).

3.1.3 Western diet induces minor proteome changes

The proteome of WD mitochondrial fractions were compared to age-matched ND mitochondrial fractions. Only 2–6% (11-37 proteins) of all identified proteins (569) were either enriched (≥ 1.5-fold) or reduced (≤ 0.67-fold) in WD compared to ND

mitochondrial fractions (Tab. 5). The most consistent alterations were changes in lipid metabolism (Tab. 5, Supplementary Table). In detail, proteins involved in lipid degradation, ß-oxidation, lipid transport and lipid synthesis were upregulated in WD mitochondria. Furthermore, a reduction of lysosomal degradation proteins and an elevation of proteins involved in translation processes occurred over time. Proteins that are involved in ER stress were increased after 6 weeks of feeding.
Unexpectedly, proteins that cause lipid synthesis were enriched in WD compared to ND mitochondria. Therefore, these proteins underwent a more detailed investigation. The FA-modifying enzymes TECR (Trans-2,3-enoyl-CoA reductase), ELOVL2 (elongation of very long chain fatty acids) and SCD1 (Stearoyl-CoA desaturase 1) were increased in WD mitochondria (Tab. 5). TECR and ELOVL2 elongate FAs and SCD1 incorporates a double bound at position *delta-9*. SCD1 mainly processes palmitic acid (C16:0) and stearic acid (C18:0) towards their monounsaturated counterparts palmitoleic aicd (C16:1n9) and oleic acid (C18:1n9), respectively. The upregulation of SCD1 was confirmed by immunoblotting and displayed a significant elevation after 6 weeks of feeding (Fig. 10).

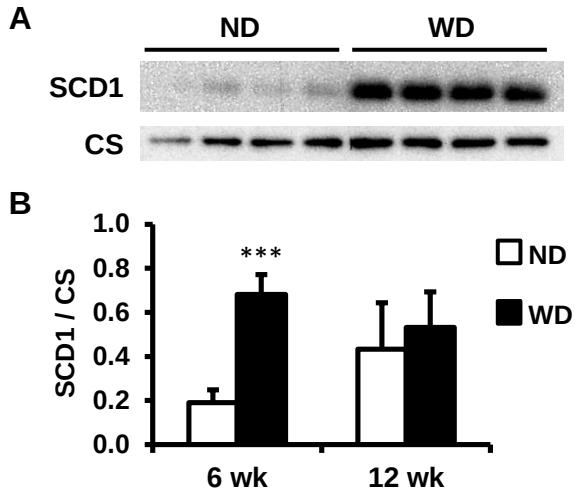

Fig. 10: Immunoblot analysis of Stearoyl-CoA desaturase 1 (SCD1)

(A) Immunoblots from mitochondria isolated after 6 weeks feeding reveal upregulation of SCD1 in WD. (B) Quantitative evaluation of SCD1 expression normalized to citrate synthase (CS, n=4). *Significant to age-matched control.

Tab. 5: Comparative proteomic analysis of WD versus ND mitochondrial fractions

Proteins that are enriched (≥ 1.5-fold) or reduced (≤ 0.67-fold) in WD compared to ND mitochondrial fractions are termed as up- or downregulated, respectively. These regulated proteins are grouped regarding their biological function and represent 2–6% of all identified proteins. Protein description and localization are shown in "Supplementary Table" (page XI).

WD vs. ND	fold enrichment	6 wk	12 wk	24 wk
oxidative phosphorylation	> 1.5	ATP5D	MT-CO3	MT-ND5, NDUFA11
	< 0.67		MT-ND4, UQCR11	
lipid degradation (ß-oxidation)	> 1.5	ACOT13, HADHB	ECHS1, ECI2	ACOT2, CYP2D9, EHHADH, HADHA
	< 0.67	ACOX2, LIPA, PHYH		LIPA, PHYH
lipid transport	> 1.5	MTTP, SLC27A5	MCAT	SCP2
lipid synthesis	> 1.5	ELOVL2, HMGCS2, TECR		ECHDC2,ELOVL2, HMGCS2, SCD1
ER stress	> 1.5	CALR, CANX, HSP90B1, HSPA5, P4HB, PDIA6		
lysosomal-/ protein degradation	> 1.5	OTUB1	CTSB, GAA, GM2A, SCPEP1	PMPCA, CTSB, GAA, LIPA, FBXO16, SCPEP1
	< 0.67	CTSB, LGMN, LIPA, TPP1		
autophagy/ apoptosis	> 1.5	PGRMC1, PEX14	DAP3	NIT1
	< 0.67	CREG1, NIT1	BNIP3, CREG1, PEX14	
antioxidative	> 1.5	SOD1		P4HB
	< 0.67	GPX1	GSTA3, GSTM1, GSTZ1	
steroid metabolism	> 1.5	CYP2A12		CYP2D9, UGT2B36
	< 0.67	DHRS1	CYP3A16, DHRS1	ALDH1B1, CYP3A16
translation	> 1.5	EEF1A1, GM10036, GM5619, MRPL10, MRPL43, MRPS23, RPLP0, RPLP2, RPS3	RPL26, RPL9	GM10036, MRPS30, RPL9
	< 0.67		MRRF, RNASET2B	
retinol metabolism	> 1.5			UGT2B36, STRA6
	< 0.67	STRA6	CYP2A5, STRA6, TTR, CYP3A17	CYP2A5, CYP3A16
amino acid metabolism	> 1.5	BHMT, FMO5, HADHB		AMT, EHHADH, HADHA
	< 0.67	ETHE1, NAGS	FMO1, GNMT, NAGS, QDPR	ETHE1, GNMT, SARDH
miscellaneous	> 1.5	ALDOB, METTL7A1, RPN2, SURF4, TMEM205, UGT1A1, VKORC1	FMC1, H2-Q10, HSPE1, SELO	ATL2, BDH1, MCU, MTHFS, NNT, SURF4, SSR4
	< 0.67	MCU	ATL2, ISCU, PTGES2, TMEM256	MUP10, OCT
identified proteins (569)	up	37 (6.5%)	11 (1.9%)	26 (4.6%)
	down	15 (2.6%)	28 (4.9%)	15 (2.6%)

3.1.4 Western diet causes membrane-lipid alterations

The upregulation of FA-modifying enzymes indicated changes in the FA composition of the mitochondrial membranes as a possible reason for WD-related cristae modifications (3.1.3). Therefore, the fatty acid profile of mitochondria was determined by gas chromatography.

The gas chromatographic analysis of FAs from isolated mitochondria revealed no change in the saturated fatty acid (SFA) content but demonstrated a significant rise of monounsaturated fatty acids (MUFAs) in WD compared to ND mitochondria. For instance, C16:1 and C18:1 were elevated after 12 and 24 weeks of feeding (Tab. 7). Furthermore, the amount of polyunsaturated fatty acids (PUFAs) significantly decreased in WD mitochondria (Tab. 7). Although, the ratio of unsaturated to saturated FA did not differ between ND and WD mitochondria, a significant upregulation of the proportion of C18:1 was detectable upon WD feeding (Tab. 7). To figure out whether alterations in mitochondrial FA composition are triggered by differences in chow FA composition or if they are mainly caused by FA metabolization via e.g. SCD1, the FA composition of ND and WD chow was analyzed (Tab. 6). The WD chow displayed, in comparison to ND chow, a 5-fold higher FA concentration and contained high rates of SFAs such as C12:0, C14:0, C16:0 and C18:0 (Tab. 6). In contrast, ND chow revealed C18:2 (PUFA) as major component and contained almost no SFAs. However, the amount of C18:1 was similar in ND and WD chow (Tab. 6). Thus, FA changes in WD mitochondria were not caused by the altered FA composition in the diet but due to metabolic adaptions, possibly by upregulation of SCD1.

Tab. 6: Fatty acid composition of WD and ND chow

Fatty acid content is displayed in mg FA per g chow (n=3). *Significant to age-matched control.

	C10:0	C12:0	C14:0	C16:0	C16:1n9	C16:1n7	C17:0	C18:0	C18:1n9t	C18:1n9c	C18:1n7	C18:2n6c	C18:3n3	C20:0	C20:1n9	C20:3n3	total
Sniff (ND) [mg/g]	n.d.	n.d.	**0.17** ± 0.14	**6.02** ± 1.88	**0.22** ± 0.10	**0.12** ± 0.11	**0.10** ± 0.04	**1.18** ± 0.45	n.d.	**7.09** ± 1.17	**0.55** ± 0.22	**16.97** ± 0.57	**1.94** ± 0.09	**0.12** ± 0.03	**0.20** ± 0.03	n.d.	**34.62** ± 4.13
Altromin (WD) [mg/g]	**1.44** ± 0.54	**68.66** ± 4.67	**31.66** ± 0.90 ***	**18.08** ± 0.19 **	**0.04** ± 0.01	**0.04** ± 0.00	**0.13** ± 0.13	**13.89** ± 0.80 ***	**0.16** ± 0.02	**8.49** ± 1.66	**0.24** ± 0.03	**6.22** ± 1.09 ***	**0.60** ± 0.01 **	**0.28** ± 0.06 *	**0.09** ± 0.02 *	**0.20** ± 0.00	**150.10** ± 3.72 ***

Tab. 7: Fatty acid composition of mitochondria after 6, 12 and 24 weeks feeding

FA content is displayed in µg fatty acid methyl ester (FAME) per mg mitochondrial protein (n=4). The distribution of FA classes is presented in percent. n.d. not detected, *Significant changes to age-matched controls (bold).

	6 weeks		12 weeks		24 weeks	
	ND [µg/mg]	**WD** [µg/mg]	**ND** [µg/mg]	**WD** [µg/mg]	**ND** [µg/mg]	**WD** [µg/mg]
C16:0	23.3 ± 2.5	24.4 ± 1.5	30.3 ± 9.9	28.0 ± 2.8	21.1 ± 3.0	22.24 ± 1.1
C16:1n7c	2.6 ± 1.3	2.5 ± 1.0	2.5 ± 0.7	3.5 ± 2.0	1.5 ± 0.2	**3.0 ±0.2*** **
C18:0	21.5 ± 2.4	23.9 ± 3.9	27.0 ± 9.4	23.9 ± 1.9	20.2 ± 6.7	19.7 ± 1.4
C18:1n9c	8.5 ± 2.9	8.3 ± 2.1	10.1 ± 3.1	**15.5 ± 3.1***	6.4 ± 1.0	**11.7 ± 1.8****
C18:1n7c	3.3 ± 1.4	3.4 ± 1.1	3.6 ± 1.1	**6.3 ± 1.0***	2.5 ± 0.4	**5.6 ±0.6*** **
C18:2n6c	16.0 ± 2.3	18.5 ± 2.8	23.7 ± 7.7	14.3 ± 1.2	15.7 ± 3.1	11.0 ± 0.6
C20:2n6c	n.d.	n.d.	n.d.	2.0 ± 0.6	n.d.	0.97 ± 0.2
C20:3n6c	1.2 ± 0.9	1.4 ± 0.4	2.3 ± 0.8	2.8 ± 0.6	2.9 ± 0.8	3.7 ± 0.5
C20:4n6c	13.8 ± 1.8	15.6 ± 1.8	20.1 ± 7.3	18.4 ± 2.6	14.1 ± 2.6	14.7 ± 1.4
C24:0	n.d.	n.d.	n.d.	0.9 ± 0.1	n.d.	0.95 ± 0.3
C22:6n3c	4.2 ± 0.6	5.0 ± 0.7	6.6 ± 2.6	5.3 ± 0.8	5.5 ± 1.0	4.7 ± 0.7
total	94.5 ± 12.0	103 ± 10.7	126 ± 41.6	121 ± 13.3	90.5 ± 8.4	99.8 ± 5.4
SFA [%]	47.5 ± 2.4	46.9 ± 0.6	45.4 ± 2.2	43.5 ± 3.6	45.8 ± 8.5	43.6 ± 1.2
MUFA [%]	15.0 ± 4.3	13.7 ± 3.1	13.0 ± 1.4	**20.9 ± 3.0****	11.6 ± 1.9	**21.0 ±1.1*** **
PUFA [%]	37.4 ± 4.1	39.5 ± 3.6	41.5 ± 3.0	**35.6 ± 1.6***	42.6 ± 7.1	35.4 ± 0.2
Ratio:						
unsat./sat.	1.11 ± 0.1	1.13 ± 0.0	1.21 ± 0.1	1.29 ± 0.2	1.23 ± 0.4	1.29 ± 0.1
16:1/16:0	0.11 ± 0.1	0.10 ± 0.0	0.08 ± 0.0	0.12 ± 0.1	0.07 ± 0.0	**0.14 ±0.0*** **
18:1/18:0	0.40 ± 0.1	0.35 ± 0.1	0.38 ± 0.0	**0.65 ± 0.2***	0.34 ± 0.1	**0.59 ± 0.1***
18:1/18:2	0.77 ± 0.4	0.65 ± 0.3	0.59 ± 0.1	**1.51 ± 0.2*** **	0.58 ± 0.1	**1.57 ± 0.3****

In order to investigate whether WD-induced changes in the mitochondrial FA composition influence the mitochondrial membrane properties, fluorescence anisotropy measurements were performed using DPH or TMA-DPH staining. The fluorescence dye DPH incorporates into the inner-lipid phase, while TMA-DPH attaches to the lipid-water interphase (Fig. 11A). Depending on the motility of the respective membrane phase, the fluorescence dyes rotate and scatter light more strongly, indicating higher membrane fluidity. At 24 weeks WD feeding, differences

in DPH but not in TMA-DPH anisotropy were present compared to ND controls (Fig. 11B-D). Thus, fluidity changes occurred especially in the inner lipid phase, supporting the idea that mitochondria adapt upon lipid supply with incorporation of FAs into mitochondrial membranes and possibly cause structural modifications of mitochondria in NAFLD. Whether these WD-induced molecular alterations influence mitochondrial function as well is addressed below.

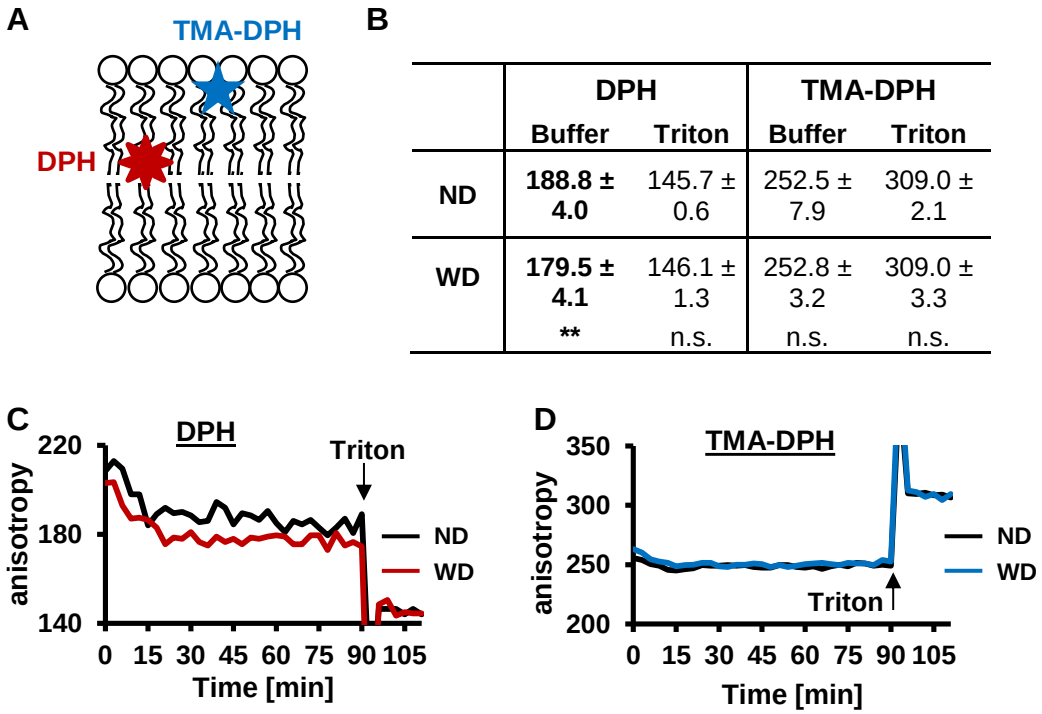

	DPH		TMA-DPH	
	Buffer	Triton	Buffer	Triton
ND	**188.8 ± 4.0**	145.7 ± 0.6	252.5 ± 7.9	309.0 ± 2.1
WD	**179.5 ± 4.1**	146.1 ± 1.3	252.8 ± 3.2	309.0 ± 3.3
	**	n.s.	n.s.	n.s.

Fig. 11: Fluorescence anisotropy measurements of mitochondria after 24 weeks feeding
(A) Schematic overview of DPH and TMA-DPH incorporation into phospholipid bilayers (adapted from: Grebowski *et al.* 2013 [115]). (B) Quantification of anisotropy values demonstrates changes in DPH but not in TMA-DPH fluorescence as well as equal values after detergent (Triton) addition in WD compared to ND membranes (biological replicates N=2, technical replicates n=6). (C, D) Average anisotropy curves are shown for DPH and TMA-DPH measures. *Significant changes to age-matched control (bold).

3.1.5 Western diet is associated with energetic deficits but not with elevated ROS production

As the WD nutrition caused mitochondrial membrane modifications (3.1.4), the functional integrity of the inner mitochondrial membrane (IM) was studied by measuring the time-dependent stability of the mitochondrial membrane potential

(MMP), following Rh123 fluorescence. The positively charged fluorescence dye Rh123 is quenched during accumulation in mitochondria (inside negatively charged) with an intact IM, resulting in low RFU (relative fluorescence units). After dissipating the MMP with the protonophore FCCP, the dye is released, leading to an increase of RFU (Fig. 12A). Calculating the ratio before and after FCCP addition (+/- FCCP) allows a statement according to the mitochondrial MMP stability. Neither 6, 12 nor 24 weeks of WD feeding affected the MMP stability (Fig. 12B). The stable membrane potential was in line with an unaffected mitochondrial H_2O_2 production at 6 and 24 weeks of WD feeding (Fig. 12C). In contrast, mitochondrial ATP production capacity was significantly reduced in WD mitochondria, isolated from 12 weeks fed mice (Fig. 12D).

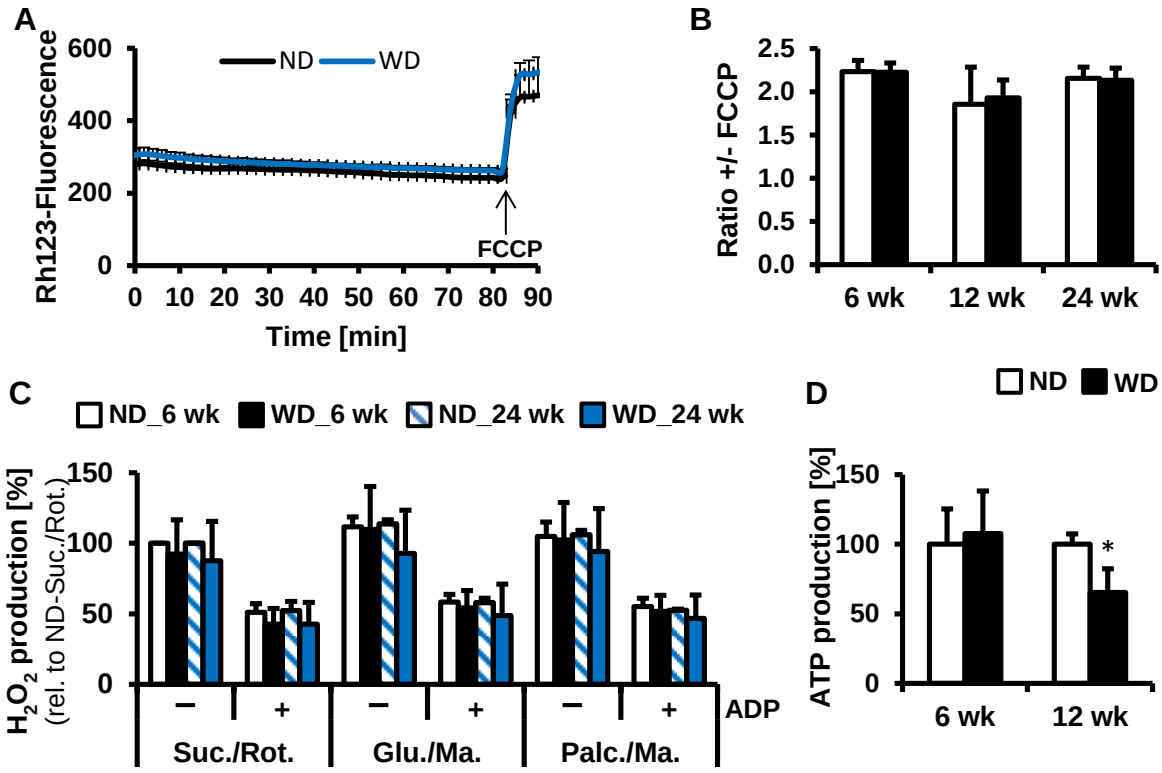

Fig. 12: Mitochondrial functional analyses upon western diet feeding

(A) Isolated mitochondria present a time-stable membrane potential (MMP) as representatively shown for the 12 weeks feed. (B) Quantitative evaluation of MMP stability determined by the ratio +/- FCCP addition reveals no changes upon WD feeding (6 wk: n=8, 12 wk: n=7, 24 wk: n=5). (C) H_2O_2 production does not differ between ND and WD liver mitochondria at 6 (n=7) and 24 weeks feeding (n=4). Substrates are succinate/rotenone (Suc./Rot.), glutamate/malate (Glu./Ma.) or palmitoylcarnitine/malate (Palc./Ma.) either in the presence or in absence of ADP. (D) Mitochondrial ATP production decreases upon WD compared to ND control (6 wk: n=8, 12 wk: n=4). *Significant to age-matched control.

Since membrane lipid alterations affect the structural organization of the oxidative phosphorylation complexes into mitochondrial supercomplexes (SC) [116] and might therefore cause the observed energetic deficits, the mitochondrial SC-formation was determined by blue native gel electrophoresis (Fig. 13). Modified SC assembly appeared in WD compared to ND mitochondria but displayed inhomogeneous changes (Fig. 13B). In detail, WD compared to ND mitochondria demonstrated decreased SC-CI expression from 6 to 24 weeks feeding. SC-CIII and SC-CIV expression was reduced after 6 weeks and was elevated after 24 weeks of feeding (Fig. 13B).

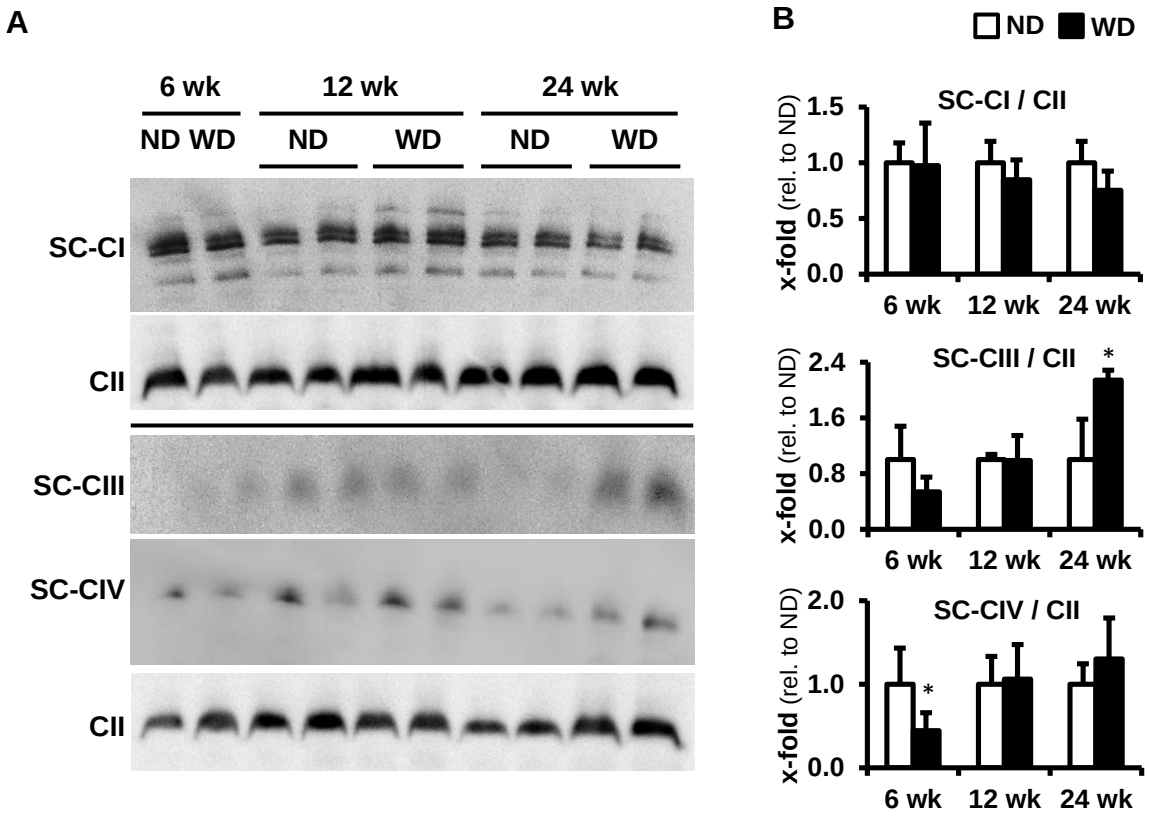

Fig. 13: Western diet influences mitochondrial supercomplex assembly

(A) Representative immunoblots of supercomplexes (SC) containing complex I, III and IV are pictured together with complex II expression after blue native gel electrophoresis. (B) Quantification of SC-CI, SC-CIII and SC-CIV levels relative to complex II demonstrate distinct regulation upon WD compared to ND control (6+12 wk: n=5; 24 wk: n=4). *Significant to age-matched control.

3.2 Western diet-related mitochondrial adaptions occur upstream of NLRP3 inflammasome activation

3.2.1 Western diet-related mitochondrial changes after 24 weeks of feeding

Upon 24 weeks of WD feeding, a similar rise in body weight (Fig. 14A), visceral fat mass (Fig. 14B) and liver TG accumulation (Fig. 14C) occurred in NLRP3$^{-/-}$ and IL-18R$^{-/-}$ mice compared to C57BL/6 wildtype mice. While NLRP3$^{-/-}$ mice revealed a slight increase in the hepatocyte death marker ALT, similar to wildtype mice, this effect was not present in IL-18R$^{-/-}$ mice (Fig. 14D).

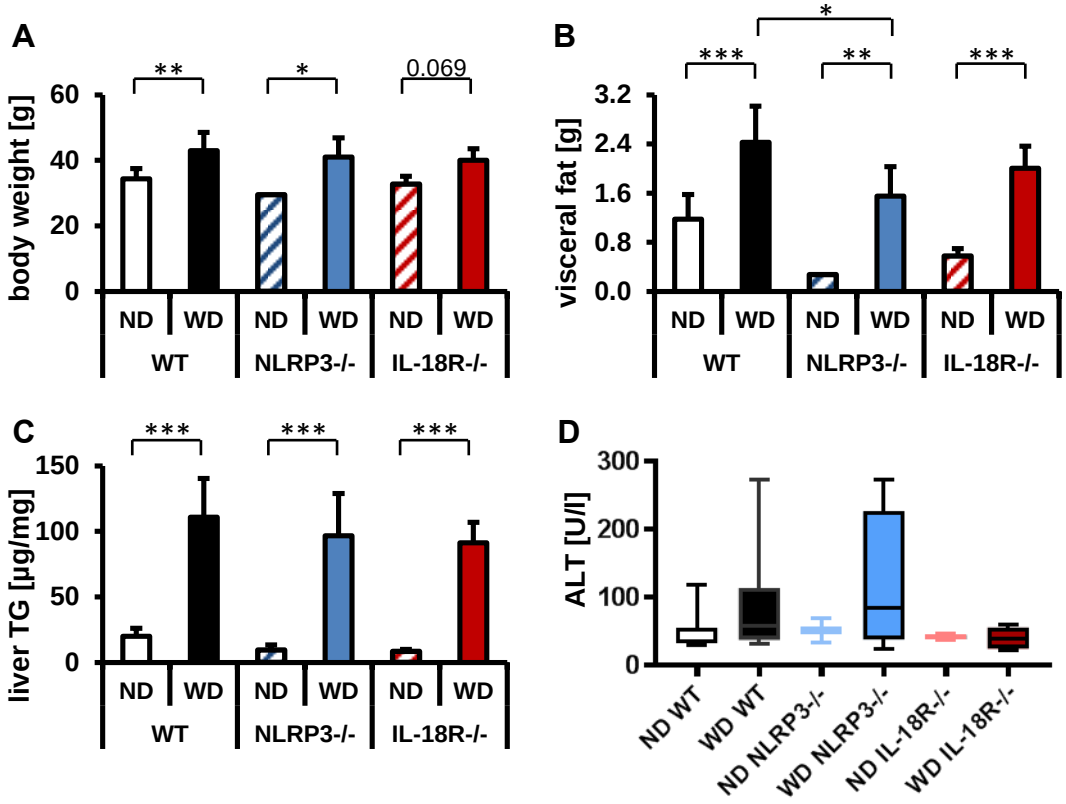

Fig. 14: NLRP3 inflammasome-deficient mice likewise present obesity and liver steatosis but a different shape of liver damage

(A-C) Western diet induces rise in body weight (A), visceral fat mass (B) and liver TG content (C, ND: n=4, WD: n=3) in NLRP3$^{-/-}$ and IL-18R$^{-/-}$ mice equally to wildtype (WT) mice. (D) Serum ALT levels are elevated in WT and NLRP3$^{-/-}$ but not in IL-18R$^{-/-}$ mice upon 24 weeks of WD feeding (WT: n=8; NLRP3$^{-/-}$ ND: n=2, WD: n=4; IL-18R$^{-/-}$: n=4).

Despite the differently displayed hepatocyte toxicity, identical mitochondrial structure modifications appeared in NLRP3$^{-/-}$ as well as in IL-18R$^{-/-}$ mice compared to wildtypes (Fig. 15). WD feeding induced widened and rounded cristae

(Fig. 15A). As in wildtype mice, these mitochondrial structural alterations correlated in NLRP3$^{-/-}$ mice with significantly increased membrane fluidity in the inner lipid phase (DPH) but not in the lipid-water interphase (TMA-DPH, Fig. 15B) of isolated mitochondria. Moreover, the mitochondrial energy production was declined in WD-fed IL-18-R$^{-/-}$ mice compared to ND-fed controls (Fig. 15C).

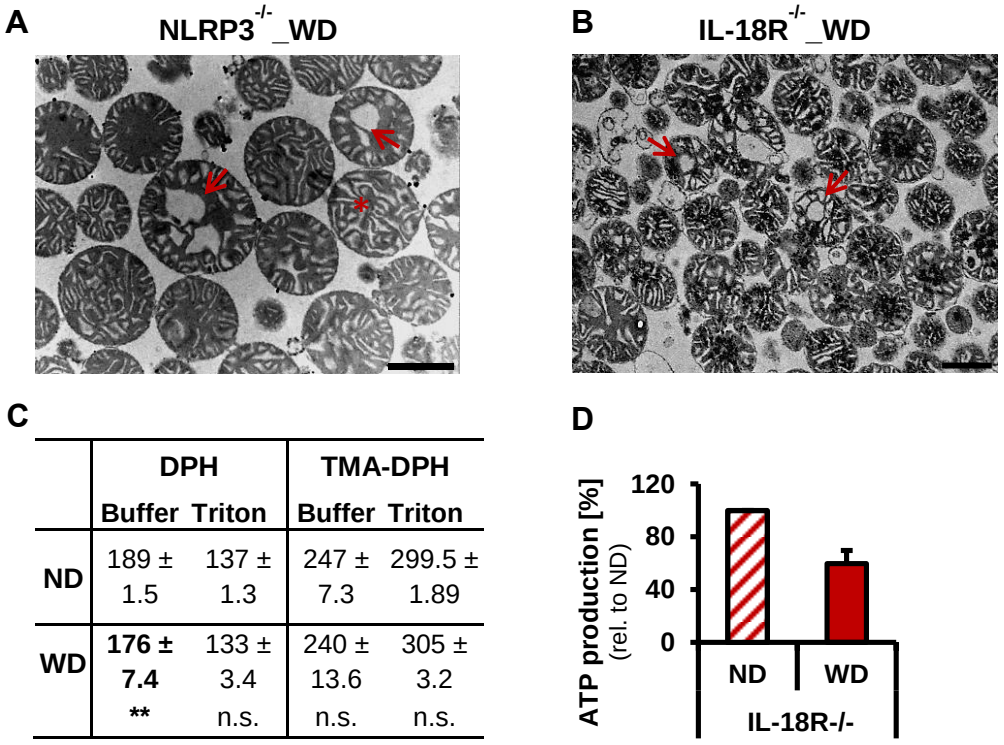

	DPH		TMA-DPH	
	Buffer	Triton	Buffer	Triton
ND	189 ± 1.5	137 ± 1.3	247 ± 7.3	299.5 ± 1.89
WD	**176 ± 7.4** **	133 ± 3.4 n.s.	240 ± 13.6 n.s.	305 ± 3.2 n.s.

Fig. 15: NLRP3 inflammasome-deficient mice displays similar mitochondrial modifications as wildtype mice

(A, B) Representative electron micrographs demonstrate ballooned and widened cristae (arrow) in NLRP3$^{-/-}$ (A) and IL-18R$^{-/-}$ mice (B, scale bar: 1 µm). (C) DPH- and TMA-DPH fluorescence anisotropy of NLRP3$^{-/-}$ ND and WD mitochondria (ND: N=2, n=4; WD: N=4, n=8; N biological replicates, n technical replicates). (D) ATP production capacity of IL-18R$^{-/-}$ mitochondria is presented relative to ND control (n=3). *Significant changes to ND control (bold).

3.2.2 Western diet-related mitochondrial changes after 48 weeks of feeding

Upon 48 weeks of WD feeding, wildtype, NLRP3$^{-/-}$ and IL-1R$^{-/-}$ mice demonstrated elevated body (Fig. 16A) as well as liver weight (Fig. 16B) and increased visceral fat mass (Fig. 16C) compared to ND-fed mice. The liver damage marker ALT was strongly elevated in serum of WD-fed wildtype, NLRP3$^{-/-}$ and IL-1R$^{-/-}$ mice, therefore indicating steatosis progression to NASH.

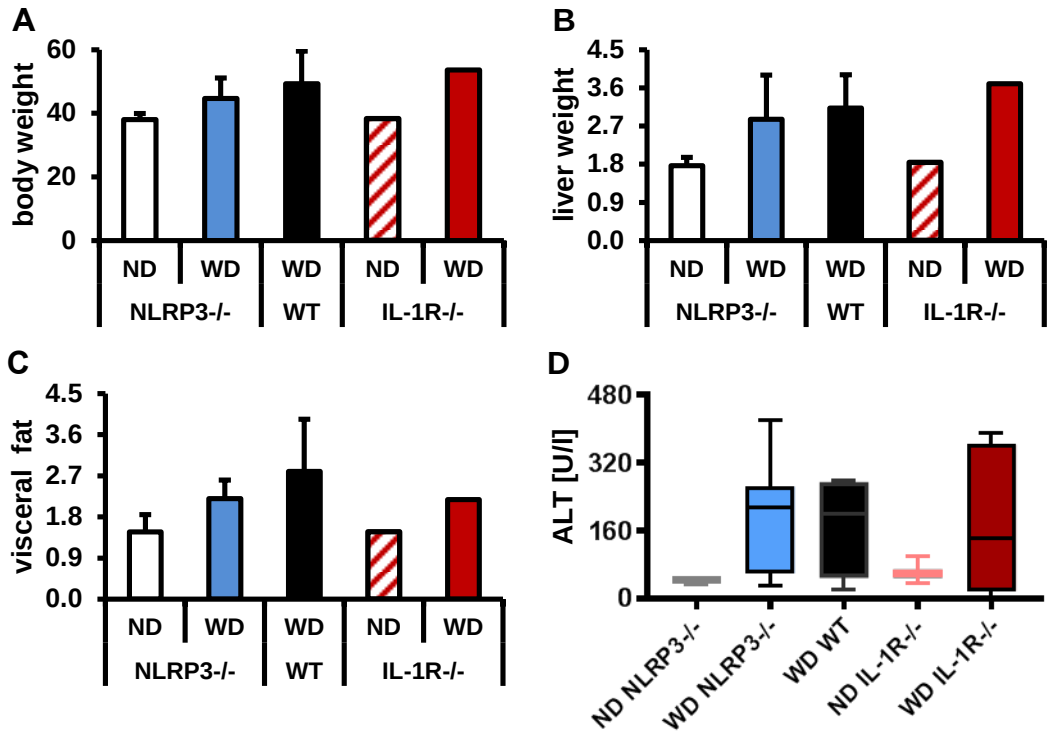

Fig. 16: Forty-eight weeks of western diet induces hepatocyte damage

(A-C) Western diet raises the body weight (A), liver weight (B) and mass of visceral fat (C) in NLRP3$^{-/-}$ and IL-1R$^{-/-}$ mice equally compared to wildtype (WT) mice. (D) Serum ALT levels are elevated upon 48 weeks of WD feeding. (NLRP3$^{-/-}$ ND: n=3, WD: n=7; WT WD: n=4; IL-1R$^{-/-}$: n=2; ALT IL-1R$^{-/-}$ ND: n=9, WD: n=7).

At mitochondrial level, WD NLRP3$^{-/-}$ and IL-1R$^{-/-}$ mitochondria demonstrated higher membrane fluidity (lower DPH anisotropy, Fig. 17A, B) and less stable MMP (Fig. 17C). Forty-eight weeks of WD slightly raised the mitochondrial H_2O_2 production in wildtype, NLRP3$^{-/-}$ and IL-1R$^{-/-}$ mice, especially with palmitoyl-carnitine as substrate (Fig. 17D).

Thus, steatosis-related mitochondrial adaptions, which are equally present in NLRP3 inflammasome-deficient and wildtype mice, are upstream of NLRP3 inflammasome activation. Furthermore, as they appeared likewise in immune-compromised mice with slightly or no liver damage (Fig. 14D), they are insufficient to cause pronounced hepatocyte death. On the contrary, since mitochondrial dysfunction such as reduced MMP stability and elevated ROS production were present together with elevated ALT level after 48 weeks of feeding, these alterations seem to be late occurring mitochondrial impairments that are associated with liver damage.

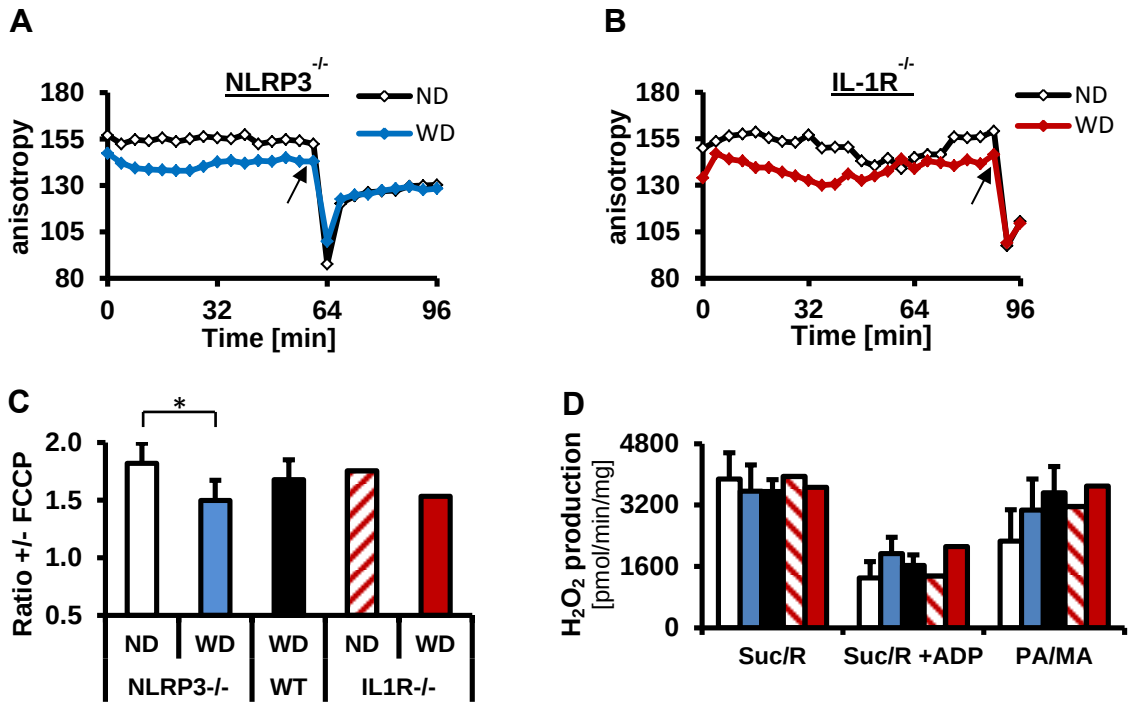

Fig. 17: Mitochondrial modifications after 48 weeks of western diet feeding

(A, B) DPH fluorescence anisotropy is lowered in NLRP3$^{-/-}$ (A, n=3) and IL-1R$^{-/-}$ (B, n=2) WD compared to ND mitochondria (arrow, triton addition). (C) The ratios +/- FCCP addition display less stable MMP in NLRP3$^{-/-}$ mitochondria upon WD feeding (NLRP3$^{-/-}$ ND: n=4, WD: n=7; WT WD: n=4; IL-1R$^{-/-}$: n=2). (D) Mitochondrial H_2O_2 production is elevated in WD mitochondria with succinate+ADP (Suc/R+ADP) or palmitoylcarnitine/malate (PA/MA) but not with succinate/rotenone (Suc/R) as substrate (NLRP3$^{-/-}$ ND: n=3, WD: n=6; WT WD: n=3; IL-1R$^{-/-}$: n=2).

3.3 Western diet mitochondria display an increased sensitivity to calcium

An altered mitochondrial membrane lipid composition influences calcium flux across mitochondrial membranes [117, 118] and elevated calcium levels have been reported in NASH-related inflammation [119, 120]. Therefore, it was analyzed whether WD influences mitochondrial calcium susceptibility. Isolated mitochondria from C57BL/6 mice were treated with 50 µM calcium and membrane potential (MMP)-loss as well as mitochondrial membrane permeability transition (MPT) were measured (Fig. 18). WD mitochondria revealed an earlier disruption of MMP and MPT upon calcium treatment most prominently after 12 weeks of feeding (Fig. 18). The time of start, end, duration and the time point of maximal depolarization (max slope) were calculated (Tab. 8) to compare and quantify

mitochondrial MMP-loss between ND and WD nutrition. In particular, after 6 and 12 weeks feeding, WD mitochondria displayed significant earlier start, end or max depolarization (Tab. 8). Thus, WD nutrition increased the sensitivity of mitochondria to elevated calcium levels.

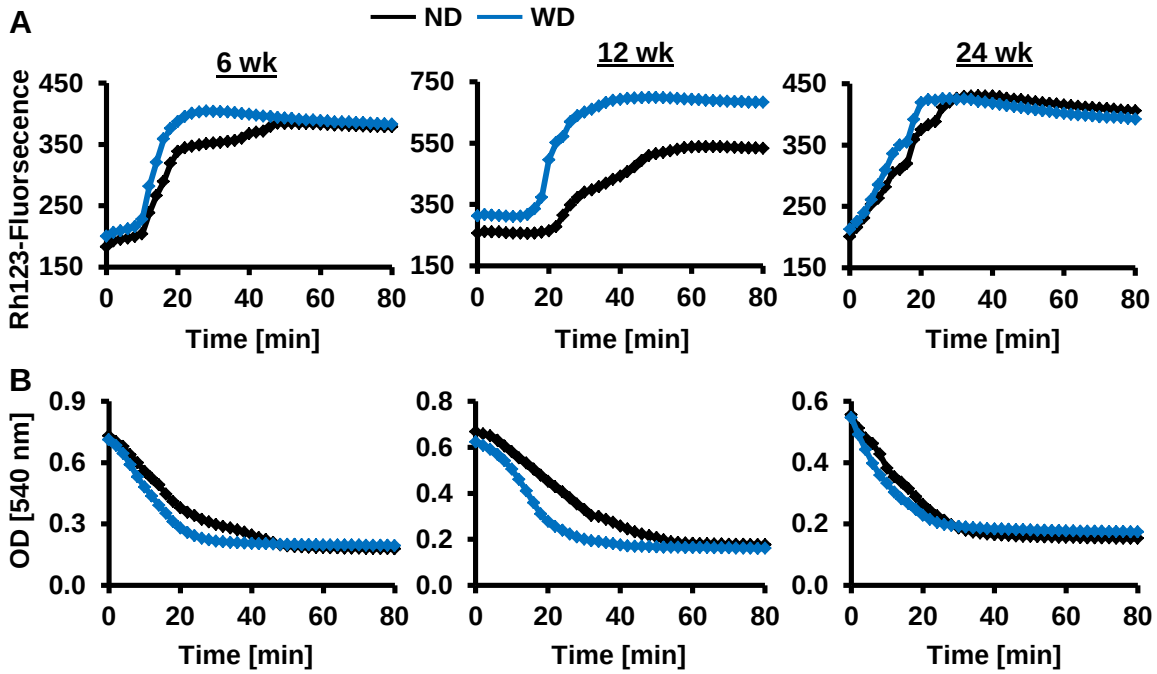

Fig. 18: Earlier destruction of mitochondrial MMP and MPT upon calcium treatment

(A, B) Isolated WD mitochondria treated with 50 µM Ca^{2+} present earlier MMP-loss (A, 6 wk: n=8, 12 wk: n=3, 24 wk: n=5) and MPT (B, 6 wk: n=4, 12 wk: n=3, 24 wk: n=5) than ND mitochondria.

Tab. 8: Characterization of mitochondrial depolarization

Time calculation [min] of start, end, max and duration of depolarization upon 50 µM calcium treatment (n: number of animals, square bracket: technical replicates). *Significant to age-matched control (bold).

Depolarization period [min]		Start	Max	End	Duration
6 wk (n=8), [10]	**ND**	11.3 ± 14.3	31.3 ± 13.2	40.1 ± 14.5	28.8 ± 5.7
	WD	3.1 ± 4.2	**17.9 ± 4.2***	**27.5 ± 5.5***	24.4 ± 4.5
12 wk (n=6), [8]	**ND**	12.8 ± 14.0	30.5 ± 12.0	45.8 ± 15.6	33.0 ± 5.8
	WD	6.3 ± 7.3	**20.0 ± 4.6***	32.3 ± 7.5	**26.0 ± 3.2***
24 wk (n=5), [5]	**ND**	5.5 ± 6.6	15.5 ± 8.3	26.7 ± 12.3	21.2 ± 8.7
	WD	2.3 ± 3.6	11.2 ± 6.0	19.7 ± 9.0	19.2 ± 7.8

3.4 Western diet aggravates mitochondrial impairments in an animal model for Wilson disease

As WD nutrition caused mitochondrial impairments (3.1) and elevated the sensitivity to calcium (3.3), it was studied whether mitochondrial dysfunctions promote the development of liver damage. WD feeding may target mitochondria as copper overload in Wilson disease does. Therefore, the effect of WD nutrition on Wilson disease progression was determined. Wilson disease is a copper storage disease, caused by mutations in the copper transporter *ATP7B*. A*tp7b*$^{-/-}$ LPP rats were used as animal model for Wilson disease since they develop hepatic copper accumulation, liver inflammation and mitochondrial impairments similar to Wilson patients [69-71]. Heterozygous A*tp7*$^{+/-}$ LPP rats do not develop a Wilson phenotype and function as controls.

Similar to C57BL/6 mice, WD-fed LPP rats demonstrated enhanced triglyceride (Fig. 19A) and visceral fat (Fig. 19B) accumulations. Moreover, WD induced liver damage (raised AST, Fig. 19C) and mitochondrial copper accumulation in *Atp7b*$^{-/-}$ rats (Fig. 19D). Interestingly, mitochondrial copper was slightly elevated in WD-fed *Atp7b*$^{+/-}$ rats as well (Fig. 19D).

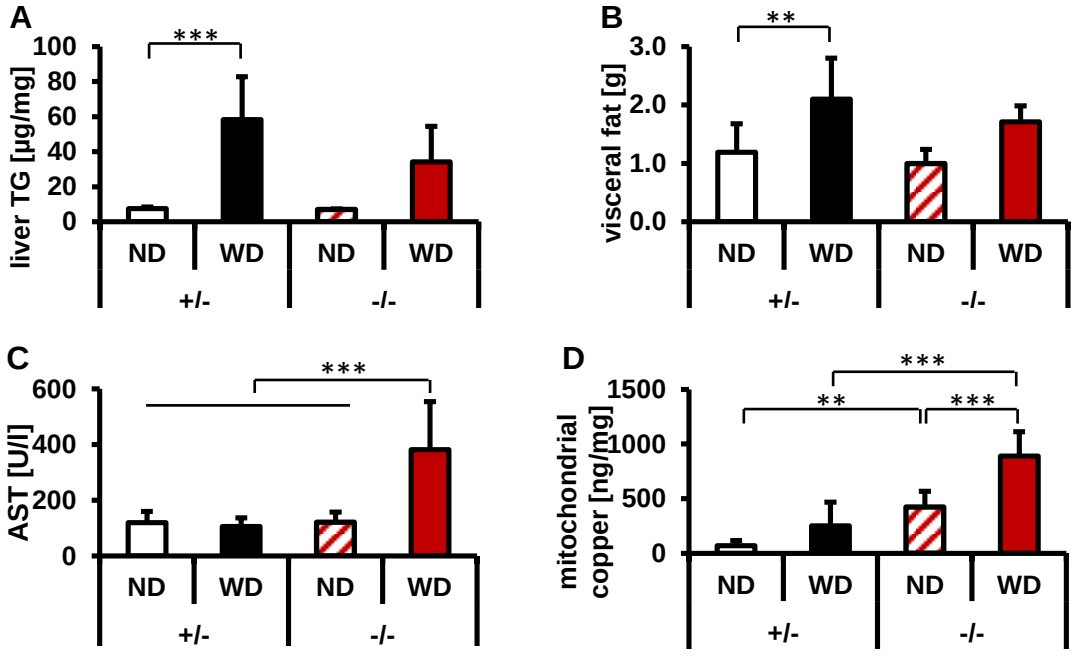

Fig. 19: Western diet induces steatosis, liver damage and mitochondrial copper accumulation in LPP rats

(A, B) WD causes liver triglyceride (A, n=5) and visceral fat mass accumulation (B, n=6) in *Atp7b*$^{+/-}$ and *Atp7b*$^{-/-}$ rats. (C) AST is elusively enhanced in WD fed *Atp7b*$^{-/-}$ rats (ND: n=8; WD: n=6). (D) Mitochondrial copper load increases due to WD feeding (n=6).

The mitochondrial membrane fluidity, measured by DPH fluorescence, was not or slightly reduced in *Atp7b*$^{+/-}$ or *Atp7b*$^{-/-}$ rats, respectively (Fig. 20A, B). WD feeding impaired the ability to inhibit calcium-induced MPT by cyclosporine A. Thus, calcium supplementation caused earlier MPT induction in WD mitochondria from *Atp7b*$^{+/-}$ rats compared to ND mitochondria and this was further shortened in WD *Atp7b*$^{-/-}$ mitochondria (Fig. 20C).

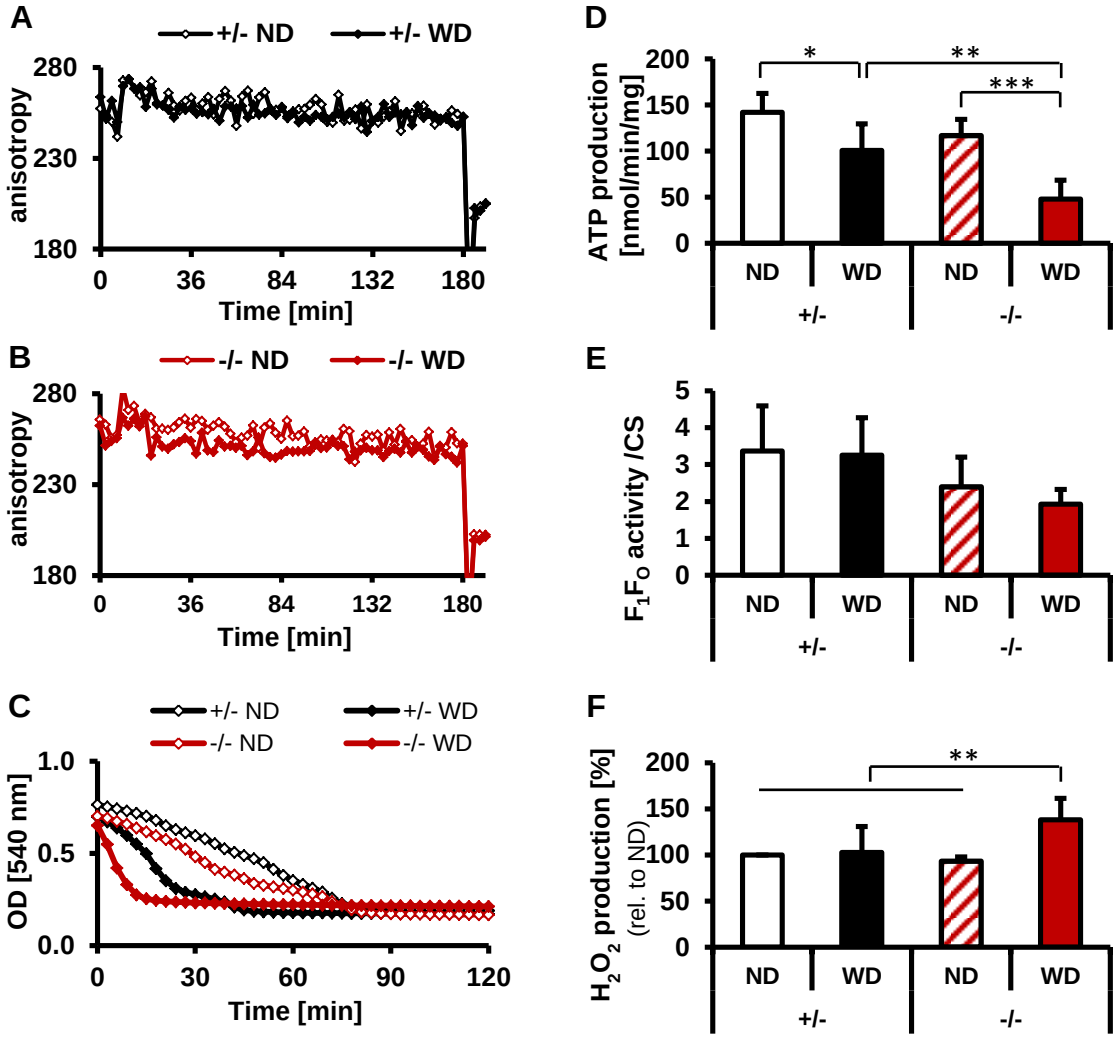

Fig. 20: Western diet promotes mitochondrial deficits in *Atp7b*$^{-/-}$ rats

(A, B) The average DPH fluorescence does not differ between ND and WD mitochondria in *Atp7b*$^{+/-}$ rats (A, n=5) but displays a slight reduction in *Atp7b*$^{-/-}$ rats (B, n=5). (C) WD impairs calcium-induced MPT inhibition by cyclosporine A (CysA: 5 µM, Ca^{2+}: 100 µM, n=5). (D) WD decreases ATP production capacity in *Atp7b*$^{+/-}$ rats and more pronounced in *Atp7b*$^{-/-}$ rats (n=5). (E) The F_1F_O-activity normalized to citrate synthase (CS) declines in *Atp7b*$^{-/-}$ mitochondria upon WD feeding (n=5). (F) Mitochondrial H_2O_2 production (substrates: succinate, ADP) increases in WD *Atp7b*$^{-/-}$ rats (n=5).

Comparable to WD-fed mice, a significant decrease in ATP production capacity occurred in WD mitochondria from *Atp7b*$^{+/-}$ rats and this was further reduced in mitochondria from WD-fed *Atp7b*$^{-/-}$ rats (Fig. 20D). This reduction in energy production of *Atp7b*$^{-/-}$ rats was associated with lower ATP-synthase (F_1F_O) activity (Fig. 20E) normalized to the activity of the mitochondrial housekeeping enzyme citrate synthase (CS). As observed in mice, WD was insufficient to cause mitochondrial ROS production in *Atp7b*$^{+/-}$ rats, but appeared in *Atp7b*$^{-/-}$ rats (Fig. 20F) that are associated with mitochondrial copper accumulation and liver damage (Fig. 19C, D). Thus, WD aggravated mitochondrial copper accumulation, amplified mitochondrial deficits and promoted liver damage in Wilson disease.

3.5 The Western diet-related steatosis cell culture model highlights C18:1 as protective contributor in NAFLD

To unravel the underlying mechanisms that trigger WD-related mitochondrial dysfunction and to understand why such nutrition is stable without developing liver damage, a steatosis cell culture model was established based on the fatty acid composition of mouse livers from 24 weeks fed mice (Fig. 21). Standard liver fatty acid composition (SLFC) and high fat liver composition (HFLC) were compared regarding to their fattening potential, hepatocyte toxicity and influence on mitochondrial functionality.

	SLFC	HFLC
C16:0	31.57 %	39.29 %
C18:0	18.70 %	5.42 %
C18:1	23.10 %	49.75 %
C18:2	16.76 %	3.71 %
C20:4	9.99 %	1.84 %

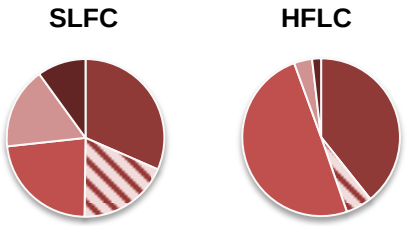

Fig. 21: Standard liver fatty acid composition (SLFC) and high fat liver composition (HFLC) determined from mouse livers after 24 weeks of feeding.

3.5.1 Elevated C18:1 levels in cell culture media cause intracellular lipid accumulation

HepG2 cells were treated with SLFC or HFLC for 48 h and fat accumulation was determined by Nile Red staining. Both fatty acid mixtures induced progressive fat accumulation in HepG2 cells compared to vehicle control albumin, displayed as increased fluorescence signal as well as enhanced granularity in transmitted light micrographs (Fig. 22). The quantification of the fluorescence signal revealed a higher quota of fat accumulation in HFLC compared to SLFC particularly at doses of 125 µM or 250 µM, respectively (Fig. 23A).

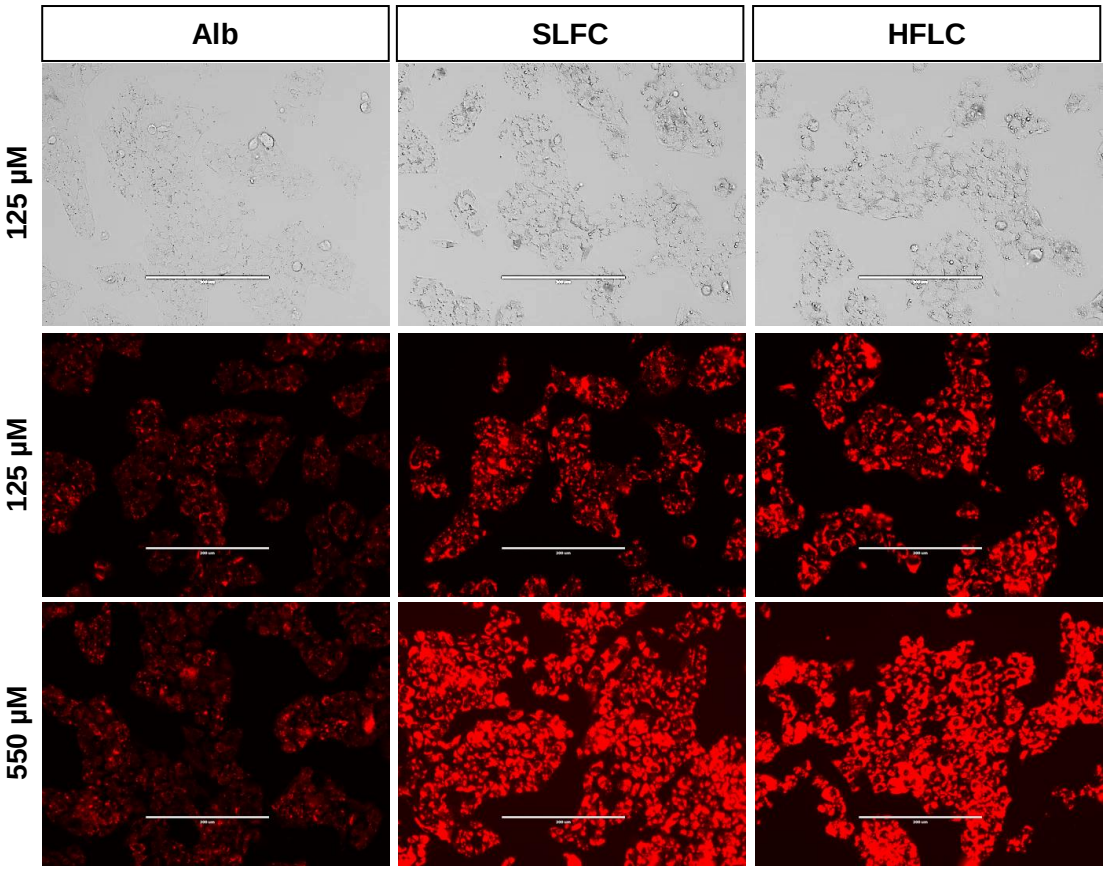

Fig. 22: Fat accumulation in HepG2 cells through SLFC and HFLC supplementation
Representative transmitted light micrographs (upper lane) demonstrate an enhanced granularity in HepG2 cells treated for 48 h with 125 µM SLFC or HFLC compared to albumin. Nile Red fluorescence is shown for 125 µM (middle lane) and 550 µM (lower lane) FA treatment. Scale bar: 200 µm.

To determine which FA of the SLFC or HFLC mixture promotes this difference in fat accumulation, HepG2 cells were treated with each fatty acid alone and the fattening potential of HFLC compared to SLFC was calculated. In detail, the difference of the relative amount between HFLC vs. SLFC of each FA was calculated first. Then, the measured fat increase (Fig. 23B) was multiplied, resulting in the fattening potential of the indicated FAs (Fig. 23C). This calculation presented C18:1 as the major determinant (94%) for fat accumulation in HFLC. The overall fattening potential of HFLC was calculated to be ~15% higher than the fattening potential of SFLC (Fig. 23C). This theoretical value was in conformity to the mean fat increase, analyzed by Nile Red stain (125 µM: 16%, 250 µM: 19% higher in HFLC compared to SLFC, Fig. 23A). Thus, the elevated fattening potential of HFLC, which reflects the FA composition of WD liver, is mainly caused by high concentrations of C18:1.

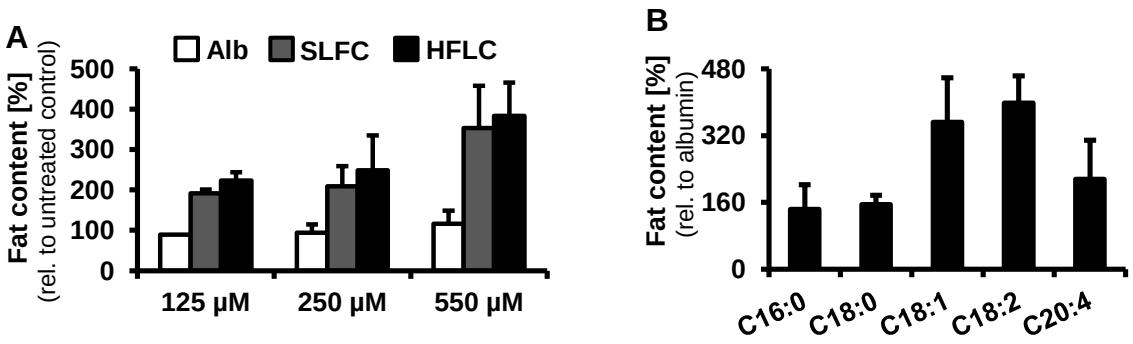

C

HFLC vs. SLFC	difference [%]	fat increase	fattening potential [%]
C16:0	+ 7.70	1.43	+ 11.0
C18:0	- 13.30	1.55	- 20.6
C18:1	+ 26.70	3.53	+ 94.3
C18:2	- 13.05	3.98	- 51.9
C20:4	- 8.15	2.16	- 17.6
		Balance:	**+ 15.2**

Fig. 23: Quantitative analysis of fat accumulation and calculation of the fattening potential

(A) Quantification of Nile Red fluorescence of HepG2 cells, treating for 48 h with SLFC (125 µM: n=6, 250 µM: n=3, 550 µM: n=7), HFLC (125 µM: n=5, 250 µM: n=5, 550 µM: n=11) or albumin (125 µM: n=2, 250 µM: n=5, 550 µM: n=8). (B) Cell fat content upon 24 h incubation with 250 µM of the indicated fatty acids normalized to albumin (n=5). (C) Calculation of the fattening potential of HFLC compared to SLFC medium.

3.5.2 Elevated C18:1 levels in cell culture media avoids toxicity of saturated fatty acids

Each FA of the SLFC and HFLC mix was individually applied for 24 h (250 µM) to HepG2 cells, measuring their toxic potential. The FAs C16:0 and C20:4 decreased the cell viability compared to albumin, whereas C18:0, C18:1 and C18:2 displayed no cell-toxic effects (Fig. 24A).

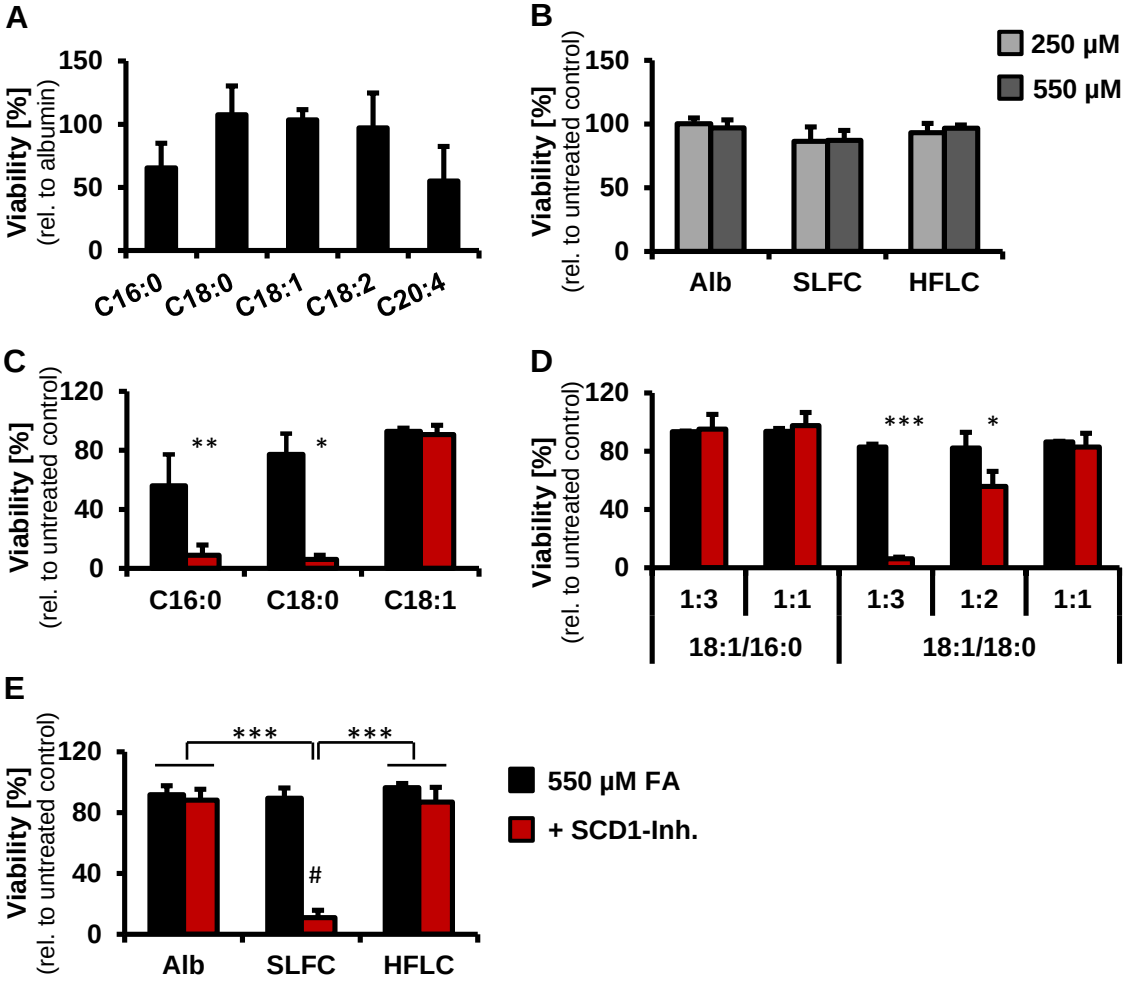

Fig. 24: HFLC maintains HepG2 cell viability because of high rates of C18:1

(A) HepG2 cell viability decreases upon C16:0 and C20:4 supplementation but not upon C18:0, C18.1 or C18:2 addition (250 µM, 24 h, n=3). (B) Forty-eight hour treatment of HepG2 cells with albumin (Alb, 250 µM: n=5, 550 µM: n=11), SLFC (250 µM: n=2, 550 µM: n=5) or HFLC (250 µM: n=3, 550 µM: n=5) presents no hepatocyte toxicity. (C-E) Inhibition of SCD1 (CAY-10566, 15 µM, 48 h) induces HepG2 cell death in C16:0 and C18:0 but not in C18:1 cultivated cells (C, 550 µM, n=3). C18:1 addition to C16:0 and C18:0 treated cells restores HepG2 cell viability (D, 550 µM, 48 h, n=3). SCD1 inhibition decreases HepG2 cell viability in SLFC but not in albumin or HFLC cultivated cells (E, 550 µM, 48 h, n=4; # significant to 275 µM SLFC $p<0.001$). *Significant to non-inhibited control.

HFLC and SLFC consist of approximately 41% C16:0 and C20:4 (Fig. 21) but these FA mixtures did not induce any hepatocyte death if they were applied for 48 h to HepG2 cells (Fig. 24B). Therefore, the other non-toxic FAs in HFLC and SLFC possibly counteract this lipotoxicity. Prior reports have demonstrated that C18:1 rescues C16:0-induced hepatocyte death [25, 28-30]. Therefore, different proportions of C18:1 and SFAs, e.g. C16:0 and C18:0, were tested for cellular toxicity. Additionally, the SFA-transforming enzyme, SCD1, was blocked with CAY10566 [121] to analyze whether an active SCD1 desaturase protect against SFA toxicity.

SCD1 inhibition strongly decreased the viability of cells treated with SFAs (C16:0, C18:0) but did not cause any cell death if C18:1 was applied to the medium (Fig. 24C). In the presence and absence of CAY10566, the addition of C18:1 to C16:0 (1:3) restored HepG2 cell viability completely, while higher rates of C18:1 (50%) were necessary to rescue C18:0-induced toxicity in the presence of the SCD1 inhibitor (Fig. 24D). Thus, if C18:0 is not metabolized to C18:1 or if only low amounts of C18:1 are present, this causes elevated hepatocyte death. Consequently, SLFC compared to HFLC is highly cell toxic upon SCD1 inhibition (Fig. 24E). Therefore, the upregulation of SCD1 and synthesis of C18:1 during WD nutrition function as protective mechanisms against excessive nutritional supply of SFAs *in vivo*.

It has been reported that SFAs (especially C16:0) display an increased hepatocyte toxicity if the cellular recycling (autophagy) of lipid droplets or dysfunctional mitochondria is blocked via 3-methyladenine (3-MA) [122]. 3-MA inhibits phosphatidylinositol 3-kinases and blocks autophagosome formation [123]. Therefore, the next analysis addressed the issue whether a high content of C18:1 in HFLC compared to SLFC is beneficial in case of autophagy inhibition as well. In agreement, SLFC but not HFLC or albumin cultivated cells demonstrated hepatocyte death in the presence of 3-MA (Fig. 25).

These findings indicate that lipotoxicity depends on the FA species that are provided to hepatocytes (chow fat composition) and if an adaption (C18:1 synthesis) is possible. In this context, the C18:1-caused elevated fat accumulation seems to be accepted by hepatocytes as non-toxic side effect.

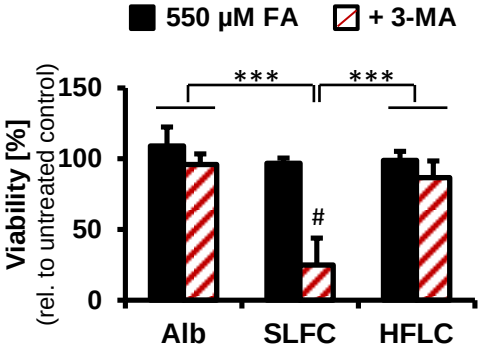

Fig. 25: Autophagy inhibition impairs HepG2 cell viability upon SLFC supplementation

Blocking autophagy via 3-methyladenine (3-MA, 89.3 µM, 24 h) leads to HepG2 cell viability loss in SLFC treated cells but not in HFLC or albumin treated cells (550 µM FA: n=4, +3-MA: n=3; # significant to 550 µM SLFC $p<0.001$).

3.5.3 Fatty acid-induced mitochondrial changes *in vitro* are similar to those in steatotic mice

FA supply during WD nutrition induced lipid membrane changes (3.1.4) and mitochondrial dysfunction in mice livers (Fig. 12). Whether these alterations likewise occur *in vitro* was further investigated. Incubating HepG2 cells for 48 h with 550 µM HFLC revealed, equally to WD feeding, an enrichment of C18:1 in mitochondrial membranes (Fig. 26A) and a declined mitochondrial ATP production capacity (Fig. 26B) relative to albumin.

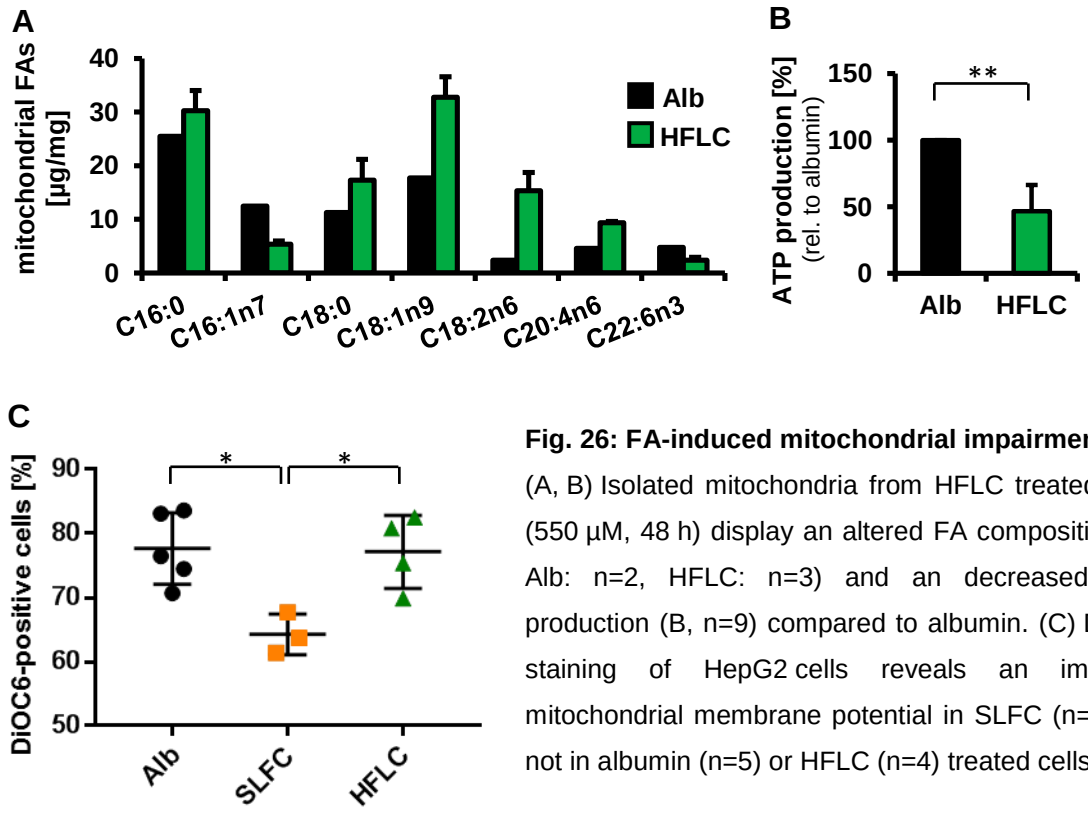

Fig. 26: FA-induced mitochondrial impairments

(A, B) Isolated mitochondria from HFLC treated cells (550 µM, 48 h) display an altered FA composition (A, Alb: n=2, HFLC: n=3) and an decreased ATP production (B, n=9) compared to albumin. (C) DiOC6 staining of HepG2 cells reveals an impaired mitochondrial membrane potential in SLFC (n=3) but not in albumin (n=5) or HFLC (n=4) treated cells.

Moreover, mitochondrial membrane potential (MMP) was not affected in HFLC treated cells (Fig. 26C) compared to albumin, which was analyzed by DiOC6 staining. DiOC6 is a positively charged fluorescence dye that accumulates in mitochondria with an intact MMP (inside negatively charged). In contrast, the addition of SLFC, which is rich in C18:0 and low in C18:1, induced a significant reduction in the amount of cells with an intact MMP (Fig. 26C). Therefore, the incorporation of C18:1 into mitochondrial membranes seems to be associated with a defective energy production independent of the disruption of the MMP.

3.6 L-carnitine supplementation increases fatty acid oxidation and avoids steatosis-related mitochondrial impairments

During steatosis, FA oxidation has been suggested to be impaired [12]. L-carnitine supplementation favors FA-uptake into mitochondria and consequently augments ß-oxidation, implicating improved liver function and decreased fat accumulation in NAFLD rodents and humans [124-127]. Thus, L-carnitine is discussed as potential therapeutic intervention in NAFLD. In the above introduced steatosis cell culture model, C18:1 and C18:2 demonstrated the highest fattening potentials of all tested FAs (Fig. 23). For these reasons, the influence of an improved fatty acid oxidation on mitochondrial function was addressed, treating HepG2 cells with C18:1 and C18:2 in the presence or absence of L-carnitine. First, the fattening capacities of C18:1 and C18:2 were reconfirmed and demonstrated a dose dependent lipid accumulation in HepG2 cells, which was more pronounced for C18:2 supplementation at the highest dose (Fig. 27A). To exclude a lower lipid accumulation because of potential cell death, the fluorescence intensity of Nile Red staining was normalized to cell density (determined by Hoechst staining) and additionally Neutral red viability assay was performed. Twenty-for hour treatment with C18:1 or C18:2 did not induce any cell-toxic effects neither with a concentration of 275 µM nor 1.1 mM (Fig. 27B). For further investigations, the concentration of 275 µM FA was chosen to study the effect of L-carnitine on lipid accumulation and mitochondrial functionality.

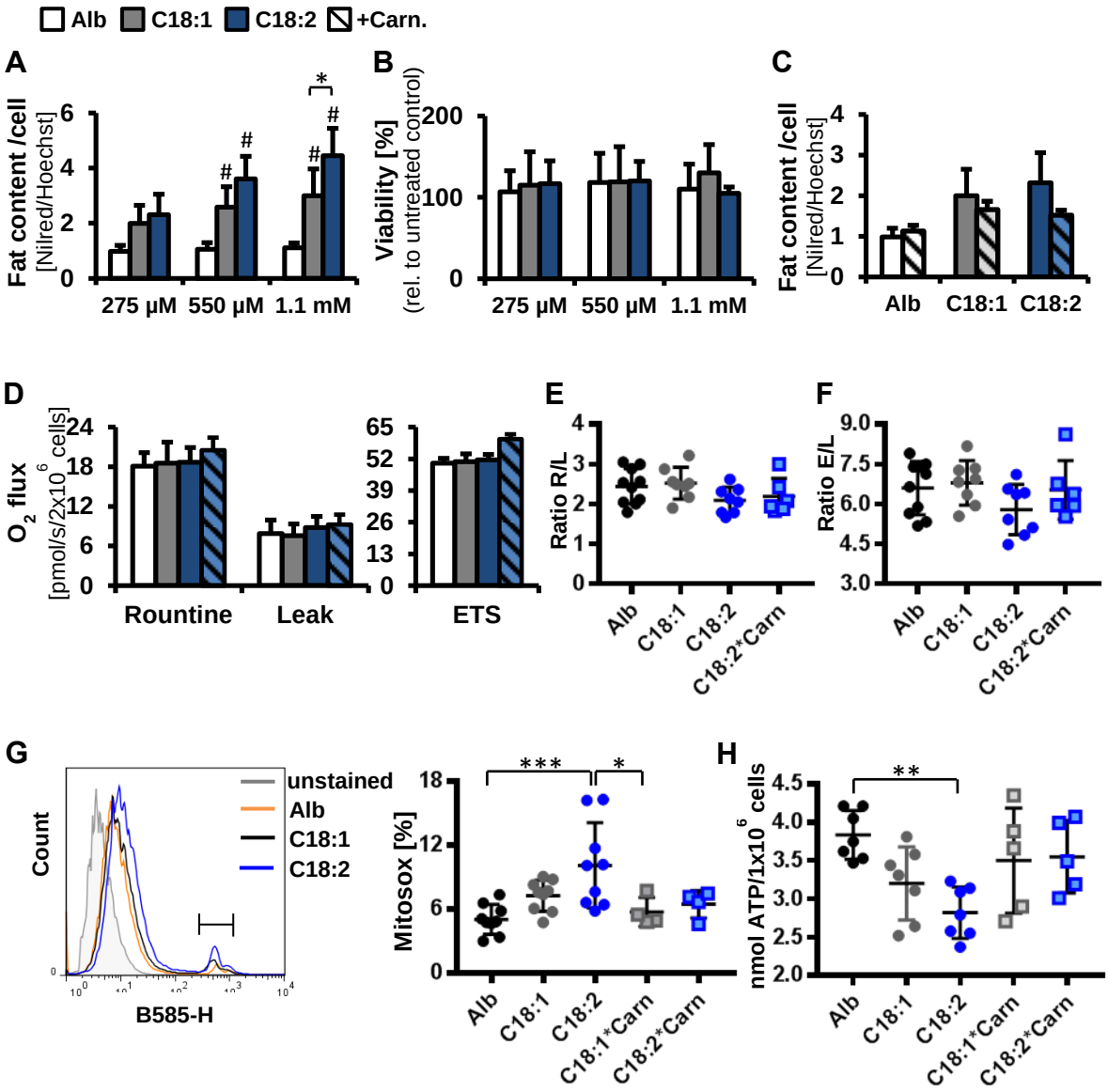

Fig. 27: L-carnitine restores mitochondrial function after fatty acid supplementation

HepG2 cells are treated for 24 h with 275 µM C18:1, C18:2 or additional 275 µM L-carnitine. (A) Both FAs cause a dose-dependent increase in cellular fat accumulation, which is more pronounced for C18:2 supplementation (n=5, # significant to albumin). (B) Cell viability is not affected up to 1.1 mM FA treatment (n=3). (C) L-carnitine addition reduces fat accumulation in HepG2 cells (n=3). (D-F) High resolution respirometry reveals elevated carnitine-induced oxygen flux (D, n=5) and lower C18:2-induced ratios of routine/leak and ETS/leak respiration (E, F Alb: n=10, FAs: n=8, Carn: n=6). (G) C18:2 treatment rises the amount of HepG2 cells with high mitochondrial ROS production that is lowered by L-carnitine addition (Alb, FAs: n=9, Carn: n=4). (H) Cellular ATP content is decreased by C18:1 and C18:2 application and is rescued through carnitine addition (Alb/FAs: n=7, Carn: n=5).

The addition of L-carnitine reduced cellular lipid accumulation, especially of C18:2 (Fig. 27C), indicating improved fatty acid oxidation. In agreement, the mitochondrial oxygen consumption rates revealed carnitine-dependent elevated basal routine and maximal respiration (ETS, Fig. 27D). Calculating the ratios of routine/leak or ETS/leak respiration demonstrated slightly lower ratios upon C18:2 treatments compared to albumin or C18:1, which were almost not improved by L-carnitine addition (Fig. 27E, F). Therefore, C18:2 but not C18:1 seem to cause elevated membrane leakage. The mitochondrial ROS production was followed by flow cytometry and Mitosox staining. Particularly, C18:2 treatment induced a significant rise of cells with high mitochondrial ROS production, which was downregulated in cells treated with L-carnitine (Fig. 27G). Moreover, L-carnitine supplementation restored FA-induced declines in cellular ATP content (Fig. 27H). These results indicate that L-carnitine treatment promotes FA oxidation, which is followed by decreased lipid accumulation, reduced ROS production and re-established cellular ATP levels.

4. Discussion

NAFLD is the most common liver disorder in western society and malnutrition-caused obesity is rising worldwide [6]. NAFLD is a slowly deteriorating disease and only a minority of NAFLD patients progress to the more severe liver disease state NASH. Nevertheless, the underlying molecular mechanisms that cause steatosis progression to NASH and cirrhosis remain incompletely understood. Consequently, therapeutic strategies are mostly lacking and NASH-related cirrhosis is the third most common cause of death worldwide [6]. Mitochondrial structure changes and functional impairment of liver mitochondria have been frequently described in NAFLD and NASH. However, at what stage of the liver disease, which mitochondrial alterations occur, and the underlying molecular mechanisms that cause these alterations are still a matter of debate. One major reason for this lack of understanding is the diversity of NAFLD animal and feeding models that only partially reflect the human situation. Therefore, a high fat and fructose-rich diet (western diet, WD), which resembles human nutrition in western society, was fed to mice for 6 to 48 weeks and isolated mitochondria were analyzed regarding their molecular composition and biochemical function.

4.1 Western diet causes steatosis and induces molecular adaptations in mitochondria due to lipidome changes

In accordance to findings in humans, WD feeding induced obesity and steatosis in mice. A progressive elevation of body weight, visceral fat mass and increased triglyceride (TG) accumulation were observed upon 6 to 24 weeks of WD feeding (Fig. 7). Enhanced serum ALT levels only occurred after nearly life-long western diet nutrition (48 weeks in mice, Fig. 16). Thus, steatosis only slowly progresses to overt liver damage in WD-fed mice and resembles the human situation in which only a minority of NAFLD patients progress to the severe liver disease state NASH. Despite this, mitochondrial molecular alterations such as lipidome changes and structural impairments appeared already after 6 and 12 weeks of feeding. As WD chow contains mainly saturated fatty acids (SFA, 90%, Tab. 6), an unexpected rise in mitochondrial monounsaturated fatty acid (MUFA) levels were

observed in WD mitochondria while the amount of SFAs was unchanged between ND and WD mitochondria. Especially oleic acid (C18:1) was enriched and linoleic acid (C18:2) was decreased upon WD feeding in mitochondrial membranes (Tab. 7). This WD-induced alteration in mitochondrial FA composition was paralleled by increased mitochondrial membrane fluidity (Fig. 11) and altered mitochondrial structures (ballooned cristae, Fig. 9). In contrast, the proteome of WD mitochondria was highly comparable to age-matched ND mitochondria. Only 2–6% of all identified proteins were enriched or depleted in WD compared to ND mitochondria (Tab. 5). Furthermore, the total protein content per mitochondrion did not differ between ND and WD mitochondria, i.e., both mitochondrial populations appeared with a protein content of approximately 0.15 pg per mitochondrion. Therefore, the present study indicates that mitochondrial structure changes in NAFLD, e.g. ballooned and widened cristae, are most probably caused by mitochondrial membrane lipid changes. These alterations occur in parallel to steatosis and are not a result of liver damage.

Moreover, it was demonstrated that especially C18:1 induces steatosis in hepatocytes (Fig. 23). These elevated C18:1 levels are not caused by dietary FA composition but rather due to the upregulation of the FA-metabolizing enzymes such as ELOVL2, TECR and SCD1. The enzymes ELOVL2 and TECR elongate FAs. The desaturase SCD1 incorporates a double bound at position *delta-9* and metabolizes C16:0 and C18:0 to their monounsaturated counterparts C16:1 or C18:1, respectively. SCD1 is located in the mitochondrial-associated membranes (MAMs) of the endoplasmic reticulum (ER) that synthesize membrane phospholipids (PLs) [128]. These PLs are transported from the MAMs to the outer mitochondrial membranes via non-vesicular intermembrane transport [129]. Therefore, the increased SCD1 activity in MAMs of WD-fed mice may cause the mitochondrial membrane lipid changes in WD mitochondria. Since similar upregulations of SCD1 and MUFAs have been described in livers of rodents [11, 29, 130] and humans [131-134] with NAFLD and/or NASH, SCD1 was blocked in the present study to figure out why MUFAs are synthesized due to WD nutrition.

4.2 An active SCD1 desaturase protects against excessive supply of saturated fatty acids

Fatty acid treatment of HepG2 cells demonstrated that C16:0 and especially C18:0 are cell toxic if SCD1 is inhibited (Fig. 24). This elevated toxicity is caused by an accumulation of SFAs in hepatocytes, since it has been reported that C16:0 induces the induction of apoptosis via elevated mitochondrial membrane permeability (MPT), the release of cytochrome c and the activation of pro-apoptotic caspases [22, 24-28]. In the present study, the lipotoxic effect of SCD1 inhibition in C16:0 and C18:0 cultivated HepG2 cells was reversible by the addition of C18:1 (Fig. 24). These findings are in line with prior reports that have demonstrated that an addition of C18:1 rescues C16:0-induced toxicity [25, 28-30]. The viability of HepG2 cells was neither decreased upon C18:1 supplementation in doses up to 1.1 mM (Fig. 27) nor in combination with SCD1 inhibition (Fig. 24). However, the intracellular lipid accumulation caused by C18:1 supplementation was twofold compared to the lipid accumulation caused by C16:0 or C18:0 addition (Fig. 23). In agreement, it has been reported that C18:1 displays no hepatocyte toxicity but rather enhances lipid accumulating properties [25-27]. Our results therefore confirm the conclusions from Flowers *et al.* [134] and Attie *et al.* [135] that SCD1 upregulation has compensatory effects against high amounts of SFAs and correlates with elevated triglyceride (TG) levels. Comparable results were shown from Li *et al.* who have demonstrated that *Scd1*$^{-/-}$ mice, fed with MCD, display increased apoptosis compared to *Scd1*$^{+/+}$ mice and that this effect is reduced by C18:1 supplementation [29]. Furthermore, these authors have demonstrated an increased C16:0-induced apoptosis in HepG2 cells due to *SCD1* silencing and inhibition [29]. In addition, Listenberger *et al.* have shown that overexpression of *SCD1* in fibroblasts protects against C16:0-induced toxicity and elevates TG accumulation [136]. Altogether, these results establish an increased SCD1 activity as protective adaptation against excessive supply of SFAs.

4.3 Mitochondrial ATP and ROS production depend on the dietary as well as the mitochondrial lipid composition

In parallel to FAs changes of the mitochondrial membrane, a reduced mitochondrial ATP production was found in WD mitochondria after 12 weeks of feeding (Fig. 12). Analyzing the assembly of the oxidative phosphorylation complexes (SC-formation) demonstrated a reduction of the complex I-containing supercomplex (SC-CI) displayed in WD compared to ND mitochondria (Fig. 13). As oxidative phosphorylation complex I is the major rate-limiting step in liver mitochondrial oxidative phosphorylation [137], this finding might possibly explain the decreased energy production of WD mitochondria. Furthermore, in the present study, it was shown that WD mimicking FA composition (HFLC) promoted elevated C18:1 concentrations in mitochondria of HepG2 cells and that these mitochondria demonstrated a lower ATP production capacity compared to albumin controls (Fig. 26). Moreover, C18:1 supplementation decreased the cellular ATP content (Fig. 27). Taken together, these results imply that the altered mitochondrial membrane FA composition in WD mitochondria lowers mitochondrial supercomplex I formation thereby possibly causing a reduced mitochondrial ATP production capacity.

Importantly, mitochondria from WD-fed mice up to 24 weeks of feeding (Fig. 12) and WD-fed LPP rats (Fig. 20) did not provoke elevated ROS production. However, controversial results exist concerning ROS production in animal models of steatosis. On the one hand, it has been reported that HFD decreased ROS production in liver mitochondria [138, 139]. On the other hand it was shown that HFD- and MCD-fed rodents displayed elevated mitochondrial ROS production [61-63, 140, 141]. Resolving these contradictories, the dietary lipid composition should be considered, since it has been suggested that the mitochondrial ROS production could be altered by changes in membrane lipid composition [139, 142, 143]. In the present study, WD nutrition caused elevated C18:1 and decreased C18:2 levels in mitochondrial membranes (Tab. 7) and the supplementation of C18:1 to HepG2 cells did not increase mitochondrial ROS production in contrast to C18:2 addition (Fig. 27). In agreement, Monteiro *et al.* have reported that a rapeseed oil diet, which is rich in MUFA such as C18:1, decreased hepatic mitochondrial H_2O_2 production [138]. Further, it was demonstrated that C18:2- but

not C18:1-rich nutrition induced elevated mitochondrial ROS production in lymphocytes causing lymphocyte death in NASH [32-34]. It therefore appears that the WD applied in this study causes mainly C18:1 increases and no ROS elevation. Consequently, the present thesis showed that the dietary as well as the mitochondrial lipid compositions are crucial determinants which mitochondrial dysfunctions occur in nutritional-induced steatosis.

4.4 Improving fatty acid oxidation avoids steatosis-related mitochondrial impairments

Liver steatosis is a reversible process and L-carnitine supplementation has been described to decrease fat accumulation in steatotic rodents and humans [124-127]. However, whether a reduction of steatosis by L-carnitine supplementation improves mitochondrial functionality is unknown. Treating HepG2 cells with C18:1 or C18:2 in the presence of equal doses of L-carnitine demonstrated a decreased intracellular lipid accumulation and elevated mitochondrial respiration compared to FA-treated cells without L-carnitine supply (Fig. 27). These results imply that L-carnitine supplementation, which favors FA uptake into mitochondria, improves FA-oxidation and therefore causes decreased fat accumulation. This reduced steatosis was paralleled by a decreased mitochondrial ROS production and restored cellular ATP levels (Fig. 27). Thus, these findings indicate that a removal of these FAs by increased ß-oxidation also avoids mitochondrial membrane alterations indicating their potential reversibility. The present study therefore highlights the flexibility of mitochondria due to dietary interventions. Thus, theses mitochondrial alterations may be rather considered as adaptations and not as dysfunctions. In accordance with this conclusion, Koliaki *et al.* have demonstrated that liver mitochondria adapt their respiration in patients with steatosis and that this flexibility was lost in patients with NASH leading to elevated oxidative stress [13].

4.5 Steatosis-related mitochondrial adaptations are independent of an activated NLRP3 inflammasome

Low-grade chronic inflammation promotes enhanced liver damage and is a hallmark of obesity and NASH. Especially, the NLRP3 inflammasome is active in these metabolic disorders [74, 75, 144, 145]. In agreement, feeding C57BL/6 mice for 24 weeks with WD increased the mRNA levels of the inflammation markers NLRP3 and MCP1 (monocyte chemoattractant protein 1) in WD livers (data not shown). It has been reported that the accumulation of dysfunctional and damaged mitochondria with, e.g. elevated membrane potential (MMP)-loss, increased membrane permeability transition (MPT) and enhanced mitochondrial ROS production induced NLRP3 inflammasome activation and liver damage [146, 147]. However, whether WD-caused mitochondrial adaptations are up- or downstream of an activated NLRP3 inflammasome is still a matter of debate. In this study, mitochondria from NLRP3$^{-/-}$, IL-18R$^{-/-}$ and IL-1R$^{-/-}$ mice appeared with identical mitochondrial alterations, e.g. ballooned cristae, elevated membrane fluidity and declined ATP production, highly similar to mitochondria from C57BL/6 wildtype mice (Fig. 15, Fig. 17). Of note, these mitochondrial changes were also present in IL-18R$^{-/-}$ mice who did not develop any liver damage after 24 weeks of feeding (Fig. 14, Fig. 15). Thus, the WD-related mitochondrial adaptations are upstream and independent of NLRP3 inflammasome activation. Furthermore, these adaptations are insufficient to cause pronounced liver damage.

4.6 Western diet-caused steatosis is a balanced but vulnerable situation

Western diet-induced steatosis caused enhanced liver damage paralleled by increased mitochondrial ROS production after nearly life-long WD nutrition (48 weeks, Fig. 17). Moreover, the metabolization from SFAs to MUFAs prevented hepatocyte death (Fig. 24). Thus, steatosis and mitochondrial alterations remain stable quite long without inducing liver damage. However, WD feeding increased the sensitivity of mitochondria to cellular stress. Incubating isolated mitochondria with calcium demonstrated an earlier MMP-loss and induction of MPT in WD compared to ND mitochondria (Fig. 18). This increased sensitivity to calcium was

present already after 6 weeks of WD feeding and appeared in NLRP3 inflammasome-deficient mice as well (data not shown). It has been reported that an elevated membrane fluidity and MUFA-rich nutrition influences calcium-induced MPT induction [117, 138]. Therefore, the altered membrane lipid composition in WD mitochondria possibly causes the increased calcium sensitivity of WD mitochondria. Taken together, these findings imply that conditions that cause increased intra- and extracellular calcium levels, e.g. bacterial or viral infections and inflammation, would affect WD mitochondria more pronounced than ND mitochondria.

4.7 Western diet amplifies mitochondrial deficits and promotes Wilson disease progression

Since steatosis as well as Wilson disease target mitochondria, it was analyzed if steatosis-related and copper-related mitochondrial dysfunctions are additive and whether this promotes Wilson disease progression. Wilson disease is a copper storage disease, caused by mutations in the copper transporter *ATP7B* [68]. LPP rats contain the same genetic defect in *Atp7b* as Wilson patients. While A*tp7*$^{+/-}$ LPP rats do not develop a Wilson phenotype and function as controls, the A*tp7b*$^{-/-}$ LPP rats display, similar to humans, a Wilson phenotype with hepatic copper accumulation, liver damage and mitochondrial impairments [69-71]. In the present study, WD-fed A*tp7b*$^{+/-}$ LPP rats displayed a decreased ATP production capacity in comparison to ND-fed rats and an elevated susceptibility to calcium (Fig. 20) similar to WD-fed C57BL/6 mice (Fig. 12, Fig. 18). These mitochondrial impairments were further aggravated in WD-fed A*tp7b*$^{-/-}$ LPP rats that demonstrated pronounced liver damage but were not present in ND-fed A*tp7b*$^{-/-}$ rats (Fig. 19, Fig. 20). Therefore, WD amplifies mitochondrial sensitivity to calcium, augments energetic deficits and promotes Wilson disease progression. Moreover, WD feeding induced mitochondrial copper accumulation in LPP rats and therefore possibly caused the pronounced mitochondrial deficits in WD-fed A*tp7b*$^{-/-}$ rats. In agreement, it has been reported that mitochondrial impairments in Wilson disease are paralleled by elevated mitochondrial copper load and that mitochondrial de-coppering restores mitochondrial function [69]. However, the underlying

molecular mechanisms how WD causes mitochondrial copper accumulation remain for further studies.

4.8 Conclusions

The present thesis demonstrated that WD causes mitochondrial molecular and functional adaptations. In mice, WD-caused steatosis was stable nearly life-long without establishing pronounced liver damage. This is highly similar to the human situation, as only a minority of NAFLD patients progress to the more severe liver disease state NASH. The present study further showed that WD-induced mitochondrial adaptations occur in parallel to steatosis and are a result of an altered mitochondrial membrane lipid composition but not a consequence of liver damage. These conclusions were substantiated by the findings that a decreased steatosis avoids fatty acid-induced mitochondrial deficits and that immune-deficient mice without any signs of liver damage presented WD-caused mitochondrial adaptations as well. Finally, this study revealed WD-caused steatosis as semi-stable situation that might lead to severe liver damage by secondary liver insults, e.g. elevated calcium levels or enhanced mitochondrial copper load.

5. Summary

In western societies, NAFLD affects 20-40% of the general population and mitochondrial impairments have been frequently reported in humans with NAFLD and NASH. However, at which stage of the liver disease mitochondrial alterations occur and the molecular mechanisms that cause these alterations are still a matter of debate. Therefore, C57BL/6 mice were fed a high fat and fructose-containing western diet (WD), resembling the eating habits in western societies, and mitochondria were isolated after 6, 12, 24 and 48 weeks of feeding. To characterize the WD-induced mitochondrial alterations, the mitochondrial structure, proteome, lipidome and mitochondrial ATP and ROS production was determined.

The underlying study demonstrates a progressive rise in obesity and liver steatosis due to prolonged WD feeding. However, cell death occurred only after 48 weeks of feeding. In contrast, mitochondrial alterations such as ballooned cristae, membrane fatty acid changes, alterations in membrane fluidity as well as decreased ATP production appeared already after 6 or 12 weeks of feeding. These fatty acid-caused mitochondrial alterations were dependent on the specific added fatty acid species. Moreover, mitochondrial impairments could be avoided by L-carnitine supplementation that decreased steatosis. These findings demonstrate that WD causes mitochondrial adaptations paralleled by steatosis, which were equally present in immune-deficient NLRP3$^{-/-}$ and IL-1R$^{-/-}$ mice and therefore are independent of NLRP3 inflammasome activation. Since these adaptations also appeared in IL-18R$^{-/-}$ mice that did not develop any liver damage, such adaptations are insufficient to cause pronounced hepatocyte death. Importantly, WD feeding sensitizes mitochondria to secondary liver insults, e.g. calcium or elevated mitochondrial copper-load in an animal model of Wilson disease. Thus, WD-caused steatosis is a semi-stable situation.

In conclusion, the present thesis reveals important mechanisms how hepatocytes deal with and protect themselves against overwhelming saturated fatty acid supply in WD nutrition and highlights the mitochondrial flexibility due to dietary interventions.

6. References

1. Bedogni, G., et al., *Prevalence of and risk factors for nonalcoholic fatty liver disease: the Dionysos nutrition and liver study.* Hepatology, 2005. **42**(1): p. 44-52.
2. Jimba, S., et al., *Prevalence of non-alcoholic fatty liver disease and its association with impaired glucose metabolism in Japanese adults.* Diabet Med, 2005. **22**(9): p. 1141-5.
3. Browning, J.D., et al., *Prevalence of hepatic steatosis in an urban population in the United States: impact of ethnicity.* Hepatology, 2004. **40**(6): p. 1387-95.
4. Neuschwander-Tetri, B.A. and S.H. Caldwell, *Nonalcoholic steatohepatitis: summary of an AASLD Single Topic Conference.* Hepatology, 2003. **37**(5): p. 1202-19.
5. Do, A. and J.K. Lim, *Epidemiology of nonalcoholic fatty liver disease: A primer.* Clinical Liver Disease, 2016. **7**(5): p. 106-108.
6. European Association for the Study of the Liver European Association for the Study of Diabetes European Association for the Study of, O., *EASL–EASD–EASO Clinical Practice Guidelines for the management of non-alcoholic fatty liver disease.* Journal of Hepatology, 2016. **64**(6): p. 1388-1402.
7. Younossi, Z.M., et al., *Global epidemiology of nonalcoholic fatty liver disease-Meta-analytic assessment of prevalence, incidence, and outcomes.* Hepatology, 2016. **64**(1): p. 73-84.
8. Fabbrini, E., et al., *Alterations in adipose tissue and hepatic lipid kinetics in obese men and women with nonalcoholic fatty liver disease.* Gastroenterology, 2008. **134**(2): p. 424-31.
9. Flannery, C., et al., *Skeletal muscle insulin resistance promotes increased hepatic de novo lipogenesis, hyperlipidemia, and hepatic steatosis in the elderly.* Diabetes, 2012. **61**(11): p. 2711-7.
10. Diraison, F., P. Moulin, and M. Beylot, *Contribution of hepatic de novo lipogenesis and reesterification of plasma non esterified fatty acids to plasma triglyceride synthesis during non-alcoholic fatty liver disease.* Diabetes Metab, 2003. **29**(5): p. 478-85.
11. Neuschwander-Tetri, B.A., et al., *Dietary trans-fatty acid induced NASH is normalized following loss of trans-fatty acids from hepatic lipid pools.* Lipids, 2012. **47**(10): p. 941-50.
12. Begriche, K., et al., *Mitochondrial adaptations and dysfunctions in nonalcoholic fatty liver disease.* Hepatology, 2013. **58**(4): p. 1497-507.
13. Koliaki, C., et al., *Adaptation of hepatic mitochondrial function in humans with non-alcoholic fatty liver is lost in steatohepatitis.* Cell Metab, 2015. **21**(5): p. 739-46.
14. Sanyal, A.J., et al., *Nonalcoholic steatohepatitis: association of insulin resistance and mitochondrial abnormalities.* Gastroenterology, 2001. **120**(5): p. 1183-92.
15. Videla, L.A., et al., *Oxidative stress and depletion of hepatic long-chain polyunsaturated fatty acids may contribute to nonalcoholic fatty liver disease.* Free Radic Biol Med, 2004. **37**(9): p. 1499-507.
16. Henao-Mejia, J., et al., *Inflammasome-mediated dysbiosis regulates progression of NAFLD and obesity.* Nature, 2012. **482**(7384): p. 179-85.
17. Zhu, L., et al., *Characterization of gut microbiomes in nonalcoholic steatohepatitis (NASH) patients: a connection between endogenous alcohol and NASH.* Hepatology, 2013. **57**(2): p. 601-9.
18. Shanab, A.A., et al., *Small intestinal bacterial overgrowth in nonalcoholic steatohepatitis: association with toll-like receptor 4 expression and plasma levels of interleukin 8.* Dig Dis Sci, 2011. **56**(5): p. 1524-34.
19. Puri, P., et al., *A lipidomic analysis of nonalcoholic fatty liver disease.* Hepatology, 2007. **46**(4): p. 1081-90.

20. Holt, H.B., et al., *Non-esterified fatty acid concentrations are independently associated with hepatic steatosis in obese subjects.* Diabetologia, 2006. **49**(1): p. 141-8.
21. Wei, Y., D. Wang, and M.J. Pagliassotti, *Saturated fatty acid-mediated endoplasmic reticulum stress and apoptosis are augmented by trans-10, cis-12-conjugated linoleic acid in liver cells.* Mol Cell Biochem, 2007. **303**(1-2): p. 105-13.
22. Li, Z., et al., *The lysosomal-mitochondrial axis in free fatty acid-induced hepatic lipotoxicity.* Hepatology, 2008. **47**(5): p. 1495-503.
23. Feldstein, A.E., et al., *Free fatty acids promote hepatic lipotoxicity by stimulating TNF-alpha expression via a lysosomal pathway.* Hepatology, 2004. **40**(1): p. 185-94.
24. Malhi, H., et al., *Free fatty acids induce JNK-dependent hepatocyte lipoapoptosis.* J Biol Chem, 2006. **281**(17): p. 12093-101.
25. Han, M.S., et al., *Lysophosphatidylcholine as a death effector in the lipoapoptosis of hepatocytes.* J Lipid Res, 2008. **49**(1): p. 84-97.
26. Pusl, T., et al., *Free fatty acids sensitize hepatocytes to bile acid-induced apoptosis.* Biochem Biophys Res Commun, 2008. **371**(3): p. 441-5.
27. Ricchi, M., et al., *Differential effect of oleic and palmitic acid on lipid accumulation and apoptosis in cultured hepatocytes.* J Gastroenterol Hepatol, 2009. **24**(5): p. 830-40.
28. Gomez-Lechon, M.J., et al., *A human hepatocellular in vitro model to investigate steatosis.* Chem Biol Interact, 2007. **165**(2): p. 106-16.
29. Li, Z.Z., et al., *Hepatic lipid partitioning and liver damage in nonalcoholic fatty liver disease: role of stearoyl-CoA desaturase.* J Biol Chem, 2009. **284**(9): p. 5637-44.
30. Sommerweiss, D., et al., *Oleate rescues INS-1E β-cells from palmitate-induced apoptosis by preventing activation of the unfolded protein response.* Biochemical and Biophysical Research Communications, 2013. **441**(4): p. 770-776.
31. Mathers, L. and M.J. Bailey, *Enzyme deletions and essential fatty acid metabolism in cultured cells.* Journal of Biological Chemistry, 1975. **250**(3): p. 1152-3.
32. Cury-Boaventura, M.F., C. Pompeia, and R. Curi, *Comparative toxicity of oleic acid and linoleic acid on Jurkat cells.* Clin Nutr, 2004. **23**(4): p. 721-32.
33. Cury-Boaventura, M.F., et al., *Comparative toxicity of oleic and linoleic acid on human lymphocytes.* Life Sci, 2006. **78**(13): p. 1448-56.
34. Ma, C., et al., *NAFLD causes selective CD4 T lymphocyte loss and promotes hepatocarcinogenesis.* Nature, 2016.
35. Wojtczak, L. and H. Zaluska, *The inhibition of translocation of adenine nucleotides through mitochondrial membranes by oleate.* Biochem Biophys Res Commun, 1967. **28**(1): p. 76-81.
36. Mootha, V.K., et al., *Integrated Analysis of Protein Composition, Tissue Diversity, and Gene Regulation in Mouse Mitochondria.* Cell, 2003. **115**(5): p. 629-640.
37. Newmeyer, D.D., D.M. Farschon, and J.C. Reed, *Cell-free apoptosis in Xenopus egg extracts: inhibition by Bcl-2 and requirement for an organelle fraction enriched in mitochondria.* Cell, 1994. **79**(2): p. 353-64.
38. Vasington, F.D., *Calcium ion uptake by fragments of rat liver mitochondria and its dependence on electron transport.* J Biol Chem, 1963. **238**: p. 1841-7.
39. Murphy, M.P., *How mitochondria produce reactive oxygen species.* Biochem J, 2009. **417**(1): p. 1-13.
40. Bernardi, P., *Mitochondrial transport of cations: channels, exchangers, and permeability transition.* Physiol Rev, 1999. **79**(4): p. 1127-55.
41. Vandecasteele, G., G. Szabadkai, and R. Rizzuto, *Mitochondrial calcium homeostasis: mechanisms and molecules.* IUBMB Life, 2001. **52**(3-5): p. 213-9.
42. Colombini, M., *A candidate for the permeability pathway of the outer mitochondrial membrane.* Nature, 1979. **279**(5714): p. 643-5.

43. Colombini, M., *Structure and mode of action of a voltage dependent anion-selective channel (VDAC) located in the outer mitochondrial membrane.* Ann N Y Acad Sci, 1980. **341**: p. 552-63.
44. Daum, G., *Lipids of mitochondria.* Biochim Biophys Acta, 1985. **822**(1): p. 1-42.
45. Biran, L.A., et al., *Studies on essential fatty acid deficiency. Effect of the deficiency on the lipids in various rat tissues and the influence of dietary supplementation with essential fatty acids on deficient rats.* Biochem J, 1964. **93**(3): p. 492-8.
46. Parkes, J.G. and W. Thompson, *The composition of phospholipids in outer and inner mitochondrial membranes from guinea-pig liver.* Biochim Biophys Acta, 1970. **196**(2): p. 162-9.
47. Schlame, M., et al., *Molecular symmetry in mitochondrial cardiolipins.* Chem Phys Lipids, 2005. **138**(1-2): p. 38-49.
48. Lemasters, J.J., *Modulation of mitochondrial membrane permeability in pathogenesis, autophagy and control of metabolism.* Journal of Gastroenterology and Hepatology, 2007. **22**: p. S31-S37.
49. Hunter, D.R., R.A. Haworth, and J.H. Southard, *Relationship between configuration, function, and permeability in calcium-treated mitochondria.* J Biol Chem, 1976. **251**(16): p. 5069-77.
50. Caldwell, S.H., et al., *Intramitochondrial crystalline inclusions in nonalcoholic steatohepatitis.* Hepatology, 2009. **49**(6): p. 1888-95.
51. Ahishali, E., et al., *Electron microscopic findings in non-alcoholic fatty liver disease: is there a difference between hepatosteatosis and steatohepatitis?* J Gastroenterol Hepatol, 2010. **25**(3): p. 619-26.
52. Pirola, C.J., et al., *Epigenetic modification of liver mitochondrial DNA is associated with histological severity of nonalcoholic fatty liver disease.* Gut, 2013. **62**(9): p. 1356-63.
53. Caldwell, S.H., et al., *Mitochondrial abnormalities in non-alcoholic steatohepatitis.* J Hepatol, 1999. **31**(3): p. 430-4.
54. Silva, G.H., et al., *Steatosis of indeterminate cause in a pediatric group: is it a primary mitochondrial hepatopathy?* Sao Paulo Med J, 2011. **129**(4): p. 217-23.
55. Schugar, R.C., et al., *Role of choline deficiency in the Fatty liver phenotype of mice fed a low protein, very low carbohydrate ketogenic diet.* PLoS One, 2013. **8**(8): p. e74806.
56. Wolf, M.J., et al., *Metabolic activation of intrahepatic CD8+ T cells and NKT cells causes nonalcoholic steatohepatitis and liver cancer via cross-talk with hepatocytes.* Cancer Cell, 2014. **26**(4): p. 549-64.
57. Cortez-Pinto, H., et al., *Alterations in liver ATP homeostasis in human nonalcoholic steatohepatitis: a pilot study.* JAMA, 1999. **282**(17): p. 1659-64.
58. Serviddio, G., et al., *Alterations of hepatic ATP homeostasis and respiratory chain during development of non-alcoholic steatohepatitis in a rodent model.* Eur J Clin Invest, 2008. **38**(4): p. 245-52.
59. Brady, L.J., et al., *Elevated hepatic mitochondrial and peroxisomal oxidative capacities in fed and starved adult obese (ob/ob) mice.* Biochem J, 1985. **231**(2): p. 439-44.
60. Mollica, M.P., et al., *3,5-diiodo-l-thyronine, by modulating mitochondrial functions, reverses hepatic fat accumulation in rats fed a high-fat diet.* J Hepatol, 2009. **51**(2): p. 363-70.
61. Crescenzo, R., et al., *Increased hepatic de novo lipogenesis and mitochondrial efficiency in a model of obesity induced by diets rich in fructose.* Eur J Nutr, 2013. **52**(2): p. 537-45.
62. Hensley, K., et al., *Dietary choline restriction causes complex I dysfunction and increased H(2)O(2) generation in liver mitochondria.* Carcinogenesis, 2000. **21**(5): p. 983-9.
63. Vial, G., et al., *Effects of a high-fat diet on energy metabolism and ROS production in rat liver.* J Hepatol, 2011. **54**(2): p. 348-56.

64. Yao, Z.M. and D.E. Vance, *The active synthesis of phosphatidylcholine is required for very low density lipoprotein secretion from rat hepatocytes.* J Biol Chem, 1988. **263**(6): p. 2998-3004.
65. Takahashi, Y., Y. Soejima, and T. Fukusato, *Animal models of nonalcoholic fatty liver disease/nonalcoholic steatohepatitis.* World J Gastroenterol, 2012. **18**(19): p. 2300-8.
66. Tetri, L.H., et al., *Severe NAFLD with hepatic necroinflammatory changes in mice fed trans fats and a high-fructose corn syrup equivalent.* Am J Physiol Gastrointest Liver Physiol, 2008. **295**(5): p. G987-95.
67. Dowman, J.K., et al., *Development of hepatocellular carcinoma in a murine model of nonalcoholic steatohepatitis induced by use of a high-fat/fructose diet and sedentary lifestyle.* Am J Pathol, 2014. **184**(5): p. 1550-61.
68. Tanzi, R.E., et al., *The Wilson disease gene is a copper transporting ATPase with homology to the Menkes disease gene.* Nat Genet, 1993. **5**(4): p. 344-50.
69. Lichtmannegger, J., et al., *Methanobactin reverses acute liver failure in a rat model of Wilson disease.* J Clin Invest, 2016. **126**(7): p. 2721-35.
70. Zischka, H., et al., *Liver mitochondrial membrane crosslinking and destruction in a rat model of Wilson disease.* J Clin Invest, 2011. **121**(4): p. 1508-18.
71. Compston, A., *Progressive lenticular degeneration: a familial nervous disease associated with cirrhosis of the liver, by S. A. Kinnier Wilson, (From the National Hospital, and the Laboratory of the National Hospital, Queen Square, London) Brain 1912: 34; 295-509.* Brain, 2009. **132**(Pt 8): p. 1997-2001.
72. Stattermayer, A.F., et al., *Hepatic steatosis in Wilson disease--Role of copper and PNPLA3 mutations.* J Hepatol, 2015. **63**(1): p. 156-63.
73. Lanthier, N., et al., *Kupffer cell depletion prevents but has no therapeutic effect on metabolic and inflammatory changes induced by a high-fat diet.* FASEB J, 2011. **25**(12): p. 4301-11.
74. Vandanmagsar, B., et al., *The NLRP3 inflammasome instigates obesity-induced inflammation and insulin resistance.* Nat Med, 2011. **17**(2): p. 179-88.
75. Csak, T., et al., *Fatty acid and endotoxin activate inflammasomes in mouse hepatocytes that release danger signals to stimulate immune cells.* Hepatology, 2011. **54**(1): p. 133-44.
76. Okamura, H., et al., *Cloning of a new cytokine that induces IFN-gamma production by T cells.* Nature, 1995. **378**(6552): p. 88-91.
77. Martinon, F., K. Burns, and J. Tschopp, *The Inflammasome: A Molecular Platform Triggering Activation of Inflammatory Caspases and Processing of proIL-β.* Molecular Cell, 2002. **10**(2): p. 417-426.
78. Bauernfeind, F.G., et al., *Cutting edge: NF-kappaB activating pattern recognition and cytokine receptors license NLRP3 inflammasome activation by regulating NLRP3 expression.* J Immunol, 2009. **183**(2): p. 787-91.
79. Winer, D.A., et al., *B cells promote insulin resistance through modulation of T cells and production of pathogenic IgG antibodies.* Nat Med, 2011. **17**(5): p. 610-7.
80. Nishimura, S., et al., *CD8+ effector T cells contribute to macrophage recruitment and adipose tissue inflammation in obesity.* Nat Med, 2009. **15**(8): p. 914-20.
81. Winer, S., et al., *Normalization of obesity-associated insulin resistance through immunotherapy.* Nat Med, 2009. **15**(8): p. 921-9.
82. Famakin, B.M., *The Immune Response to Acute Focal Cerebral Ischemia and Associated Post-stroke Immunodepression: A Focused Review.* Aging Dis, 2014. **5**(5): p. 307-26.
83. Mombaerts, P., et al., *RAG-1-deficient mice have no mature B and T lymphocytes.* Cell, 1992. **68**(5): p. 869-77.
84. Ahmed, S., J. Deng, and J. Borjigin, *A new strain of rat for functional analysis of PINA.* Brain Res Mol Brain Res, 2005. **137**(1-2): p. 63-9.
85. McMillian, M.K., et al., *Nile Red binding to HepG2 cells: an improved assay for in vitro studies of hepatosteatosis.* In Vitr Mol Toxicol, 2001. **14**(3): p. 177-90.

86. Repetto, G., A. del Peso, and J.L. Zurita, *Neutral red uptake assay for the estimation of cell viability/cytotoxicity.* Nat Protoc, 2008. **3**(7): p. 1125-31.
87. Pesta, D. and E. Gnaiger, *High-resolution respirometry: OXPHOS protocols for human cells and permeabilized fibers from small biopsies of human muscle.* Methods Mol Biol, 2012. **810**: p. 25-58.
88. Schulz, S., et al., *Progressive stages of mitochondrial destruction caused by cell toxic bile salts.* Biochim Biophys Acta, 2013. **1828**(9): p. 2121-33.
89. Zischka, H., et al., *Isolation of highly pure rat liver mitochondria with the aid of zone-electrophoresis in a free flow device (ZE-FFE).* Methods Mol Biol, 2008. **424**: p. 333-48.
90. Schmitt, S., et al., *Why to compare absolute numbers of mitochondria.* Mitochondrion, 2014. **19 Pt A**: p. 113-23.
91. Schulz, S., et al., *A protocol for the parallel isolation of intact mitochondria from rat liver, kidney, heart, and brain.* Methods Mol Biol, 2015. **1295**: p. 75-86.
92. Schmitt, S., et al., *A semi-automated method for isolating functionally intact mitochondria from cultured cells and tissue biopsies.* Anal Biochem, 2013. **443**(1): p. 66-74.
93. Martin, B.R. and R.M. Denton, *Intracellular localization of enzymes in white-adipose-tissue fat-cells and permeability properties of fat-cell mitochondria. Transfer of acetyl units and reducing power between mitochondria and cytoplasm*. Vol. 117. 1970. 861-877.
94. Barrientos, A., *In vivo and in organello assessment of OXPHOS activities.* Methods, 2002. **26**(4): p. 307-16.
95. Kirby, D.M., et al., *Biochemical Assays of Respiratory Chain Complex Activity*, in *Methods in Cell Biology*. 2007, Academic Press. p. 93-119.
96. Williams, M.D., *Increased Oxidative Damage Is Correlated to Altered Mitochondrial Function in Heterozygous Manganese Superoxide Dismutase Knockout Mice.* Journal of Biological Chemistry, 1998. **273**(43): p. 28510-28515.
97. Muller, F.L., et al., *High rates of superoxide production in skeletal-muscle mitochondria respiring on both complex I- and complex II-linked substrates.* Biochem J, 2008. **409**(2): p. 491-9.
98. Prendergast, F.G., R.P. Haugland, and P.J. Callahan, *1-[4-(Trimethylamino)phenyl]-6-phenylhexa-1,3,5-triene: synthesis, fluorescence properties, and use as a fluorescence probe of lipid bilayers.* Biochemistry, 1981. **20**(26): p. 7333-8.
99. Duportail, G. and A. Weinreb, *Photochemical changes of fluorescent probes in membranes and their effect on the observed fluorescence anisotropy values.* Biochim Biophys Acta, 1983. **736**(2): p. 171-7.
100. Grebowski, J., A. Krokosz, and M. Puchala, *Membrane fluidity and activity of membrane ATPases in human erythrocytes under the influence of polyhydroxylated fullerene.* Biochimica et Biophysica Acta (BBA) - Biomembranes, 2013. **1828**(2): p. 241-248.
101. Zischka, H., et al., *Electrophoretic analysis of the mitochondrial outer membrane rupture induced by permeability transition.* Anal Chem, 2008. **80**(13): p. 5051-8.
102. Hackenbrock, C.R., *Ultrastructural bases for metabolically linked mechanical activity in mitochondria. II. Electron transport-linked ultrastructural transformations in mitochondria.* J Cell Biol, 1968. **37**(2): p. 345-69.
103. Wisniewski, J.R., et al., *Universal sample preparation method for proteome analysis.* Nat Meth, 2009. **6**(5): p. 359-362.
104. von Toerne, C., et al., *Apoe, Mbl2, and Psp plasma protein levels correlate with diabetic phenotype in NZO mice--an optimized rapid workflow for SRM-based quantification.* J Proteome Res, 2013. **12**(3): p. 1331-43.
105. Hauck, S.M., et al., *Deciphering membrane-associated molecular processes in target tissue of autoimmune uveitis by label-free quantitative mass spectrometry.* Mol Cell Proteomics, 2010. **9**(10): p. 2292-305.

106. *UniProt: a hub for protein information.* Nucleic Acids Res, 2015. **43**(Database issue): p. D204-12.
107. Kanehisa, M., et al., *KEGG as a reference resource for gene and protein annotation.* Nucleic Acids Res, 2016. **44**(D1): p. D457-62.
108. Thomas, P.D., et al., *PANTHER: a library of protein families and subfamilies indexed by function.* Genome research, 2003. **13**(9): p. 2129-2141.
109. Bradford, M.M., *A rapid and sensitive method for the quantitation of microgram quantities of protein utilizing the principle of protein-dye binding.* Anal Biochem, 1976. **72**: p. 248-54.
110. Wittig, I., H.-P. Braun, and H. Schagger, *Blue native PAGE.* Nat. Protocols, 2006. **1**(1): p. 418-428.
111. Diaz, F., A. Barrientos, and F. Fontanesi, *Evaluation of the mitochondrial respiratory chain and oxidative phosphorylation system using blue native gel electrophoresis.* Curr Protoc Hum Genet, 2009. **Chapter 19**: p. Unit19 4.
112. Towbin, H., T. Staehelin, and J. Gordon, *Electrophoretic transfer of proteins from polyacrylamide gels to nitrocellulose sheets: procedure and some applications.* Proc Natl Acad Sci U S A, 1979. **76**(9): p. 4350-4.
113. Rasband, W., *ImageJ. US National Institutes of Health, Bethesda, MD*. 1997.
114. Folch, J., M. Lees, and G.H. Sloane Stanley, *A simple method for the isolation and purification of total lipides from animal tissues.* J Biol Chem, 1957. **226**(1): p. 497-509.
115. Grebowski, J., A. Krokosz, and M. Puchala, *Membrane fluidity and activity of membrane ATPases in human erythrocytes under the influence of polyhydroxylated fullerene.* Biochim Biophys Acta, 2013. **1828**(2): p. 241-8.
116. Schagger, H. and K. Pfeiffer, *Supercomplexes in the respiratory chains of yeast and mammalian mitochondria.* EMBO J, 2000. **19**(8): p. 1777-83.
117. Pepe, S., et al., *PUFA and aging modulate cardiac mitochondrial membrane lipid composition and Ca2+ activation of PDH.* Am J Physiol, 1999. **276**(1 Pt 2): p. H149-58.
118. O'Shea, K.M., et al., *Dietary omega-3 fatty acids alter cardiac mitochondrial phospholipid composition and delay Ca2+-induced permeability transition.* J Mol Cell Cardiol, 2009. **47**(6): p. 819-27.
119. Rossol, M., et al., *Extracellular Ca2+ is a danger signal activating the NLRP3 inflammasome through G protein-coupled calcium sensing receptors.* Nat Commun, 2012. **3**: p. 1329.
120. Lee, G.S., et al., *The calcium-sensing receptor regulates the NLRP3 inflammasome through Ca2+ and cAMP.* Nature, 2012. **492**(7427): p. 123-7.
121. Liu, G., et al., *Discovery of potent, selective, orally bioavailable stearoyl-CoA desaturase 1 inhibitors.* J Med Chem, 2007. **50**(13): p. 3086-100.
122. Tu, Q.Q., et al., *Palmitic acid induces autophagy in hepatocytes via JNK2 activation.* Acta Pharmacol Sin, 2014. **35**(4): p. 504-12.
123. Seglen, P.O. and P.B. Gordon, *3-Methyladenine: specific inhibitor of autophagic/lysosomal protein degradation in isolated rat hepatocytes.* Proc Natl Acad Sci U S A, 1982. **79**(6): p. 1889-92.
124. Malaguarnera, M., et al., *L-carnitine supplementation to diet: a new tool in treatment of nonalcoholic steatohepatitis--a randomized and controlled clinical trial.* Am J Gastroenterol, 2010. **105**(6): p. 1338-45.
125. Rajasekar, P., P. Viswanathan, and C.V. Anuradha, *Renoprotective action of L-carnitine in fructose-induced metabolic syndrome.* Diabetes Obes Metab, 2008. **10**(2): p. 171-80.
126. Rajasekar, P. and C.V. Anuradha, *Fructose-induced hepatic gluconeogenesis: effect of L-carnitine.* Life Sci, 2007. **80**(13): p. 1176-83.
127. Liang, Y., et al., *The effects of oral L-carnitine treatment on blood lipid metabolism and the body fat content in the diabetic patient.* Asia Pac J Clin Nutr, 1998. **7**(2): p. 192-5.

128. Horner, S.M., et al., *Proteomic analysis of mitochondrial-associated ER membranes (MAM) during RNA virus infection reveals dynamic changes in protein and organelle trafficking.* PLoS One, 2015. **10**(3): p. e0117963.
129. Voelker, D.R., *Phosphatidylserine translocation to the mitochondrion is an ATP-dependent process in permeabilized animal cells.* Proc Natl Acad Sci U S A, 1989. **86**(24): p. 9921-5.
130. Ciapaite, J., et al., *Differential effects of short- and long-term high-fat diet feeding on hepatic fatty acid metabolism in rats.* Biochim Biophys Acta, 2011. **1811**(7-8): p. 441-51.
131. Puri, P., et al., *The plasma lipidomic signature of nonalcoholic steatohepatitis.* Hepatology, 2009. **50**(6): p. 1827-38.
132. Yamada, K., et al., *Characteristics of hepatic fatty acid compositions in patients with nonalcoholic steatohepatitis.* Liver Int, 2015. **35**(2): p. 582-90.
133. Hulver, M.W., et al., *Elevated stearoyl-CoA desaturase-1 expression in skeletal muscle contributes to abnormal fatty acid partitioning in obese humans.* Cell Metab, 2005. **2**(4): p. 251-61.
134. Flowers, M.T., *The delta9 fatty acid desaturation index as a predictor of metabolic disease.* Clin Chem, 2009. **55**(12): p. 2071-3.
135. Attie, A.D., et al., *Relationship between stearoyl-CoA desaturase activity and plasma triglycerides in human and mouse hypertriglyceridemia.* J Lipid Res, 2002. **43**(11): p. 1899-907.
136. Listenberger, L.L., et al., *Triglyceride accumulation protects against fatty acid-induced lipotoxicity.* Proc Natl Acad Sci U S A, 2003. **100**(6): p. 3077-82.
137. Inomoto, T., et al., *Changes in the distribution of the control of the mitochondrial oxidative phosphorylation in regenerating rabbit liver.* Biochimica et Biophysica Acta (BBA) - Bioenergetics, 1994. **1188**(3): p. 311-317.
138. Monteiro, J.P., et al., *Rapeseed oil-rich diet alters hepatic mitochondrial membrane lipid composition and disrupts bioenergetics.* Arch Toxicol, 2013. **87**(12): p. 2151-63.
139. Hagopian, K., et al., *Complex I-associated hydrogen peroxide production is decreased and electron transport chain enzyme activities are altered in n-3 enriched fat-1 mice.* PLoS One, 2010. **5**(9): p. e12696.
140. Petrosillo, G., et al., *Mitochondrial dysfunction in rat with nonalcoholic fatty liver Involvement of complex I, reactive oxygen species and cardiolipin.* Biochim Biophys Acta, 2007. **1767**(10): p. 1260-7.
141. Yang, S., et al., *Mitochondrial adaptations to obesity-related oxidant stress.* Arch Biochem Biophys, 2000. **378**(2): p. 259-68.
142. Ramsey, J.J., et al., *Influence of mitochondrial membrane fatty acid composition on proton leak and H2O2 production in liver.* Comparative Biochemistry and Physiology Part B: Biochemistry and Molecular Biology, 2005. **140**(1): p. 99-108.
143. Chen, Y., et al., *The influence of dietary lipid composition on liver mitochondria from mice following 1 month of calorie restriction.* Biosci Rep, 2012. **33**(1): p. 83-95.
144. Stienstra, R., et al., *The inflammasome-mediated caspase-1 activation controls adipocyte differentiation and insulin sensitivity.* Cell Metab, 2010. **12**(6): p. 593-605.
145. Lee, H.M., et al., *Upregulated NLRP3 inflammasome activation in patients with type 2 diabetes.* Diabetes, 2013. **62**(1): p. 194-204.
146. Zhou, R., et al., *A role for mitochondria in NLRP3 inflammasome activation.* Nature, 2011. **469**(7329): p. 221-225.
147. Nakahira, K., et al., *Autophagy proteins regulate innate immune responses by inhibiting the release of mitochondrial DNA mediated by the NALP3 inflammasome.* Nat Immunol, 2011. **12**(3): p. 222-230.

7. Appendix

Abbreviations

ADP	Adenosine-5’-diphosphate
ALiOS	American Lifestyle-induced Obesity Syndrome
ALT	Alanine aminotransferase
ANOVA	Analysis of variance between groups
ANT	Adenine nucleotide translocator
AST	Aspartate aminotransferase
ATP	Adenosine-5’-triphosphate
BSA	Bovine serum albumin
Ca	Calcium
CCCP	Carbonyl cyanide m-chlorophenyl hydrazine
CD-HFD	Choline-deficient high fat diet
CL	Cardiolipin
Cyt c	Cytochrome c
DAMP	Damage-associated molecular pattern
ER	Endoplasmic reticulum
ETC	Electron transport chain
FA	Fatty acid
$FADH_2$	Flavin adenine dinucleotide
FCCP	Carbonyl cyanide-ρ-(trifluoromethoxy)phenylhydrazone
H_2O_2	Hydrogen peroxide
HCC	Hepatocellular carcinoma
HFD	High fat diet
HFLC	High fat liver composition
IM	Inner mitochondrial membrane
IMS	Intermembrane space
3-MA	3-Methyladenine
MAM	Mitochondrial-associated membranes
MCD	Methionine choline-deficient diet
MHCII	Major histocompartibility complex II
MMP	Mitochondrial membrane potential
MOMP	Mitochondrial outer membrane rupture

MPT	Mitochondrial permeability transition
mtDNA	Mitochondrial desoxyribunucleic acid
MUFA	Monounsaturated fatty acid
N_2	Nitrogen
NADH	Nicotinamide adenine dinucleotide
NAFLD	Non-alcoholic fatty liver disease
NASH	Non-alcoholic steatohepatitis
ND	Normal diet
NEFA	Non-esterified fatty acids
NFκB	nuclear factor kappa-light-chain-enhancer of activated B cells
O_2	Oxygen
OM	Outer mitochondrial membrane
PC	Phosphatidylcholine
PCC	Pump controlled cell rupture system
PE	Phosphatidylethanolamine
PEP	Phosphoenolpyruvate
Pi	Inorganic phosphate
PK	Pyruvate kinase
PUFA	Polyunsaturated fatty acid
RFU	Relative fluorescence units
ROS	Reactive oxygen species
RT	Room temperature
SFA	Saturated fatty acid
SLFC	Standard liver fatty acid composition
TG	Triglyceride
VDAC	Voltage-dependent anion channel
VLDL	Very low density lipoprotein
WD	Western diet

List of figures and tables

List of figures and tables

Publications

C. Einer, S. Hohenester, R. Wimmer, L. Wottke, R. Artmann, S. Schulz, C. Gosmann, M. Seifert, A. Simmons, C. Leitzinger, C. Eberhagen, S. Schmitt, S. M. Hauck, C. von Toerne, M. Jastroch, E. Walheim, C. Rust, A. L. Gerbes, B. Popper, D. Mayr, M. Schnurr, A. M. Vollmar, G. Denk, H. Zischka. "*Mitochondrial adaptation counterbalances steatosis in mice"*.
Manuscript in revision

M. J. Wolf, A. Adili, K. Piotrowitz, Z. Abdullah, Y. Boege, K. Stemmer, M. Ringelhan, N. Simonavicius, M. Egger, D. Wohlleber, A. Lorentzen, C. Einer, S. Schulz, T. Clavel, U. Protzer, C. Thiele, H. Zischka, H. Moch, M. Tschop, A. V. Tumanov, D. Haller, K. Unger, M. Karin, M. Kopf, P. Knolle, A. Weber and M. Heikenwalder (2014). "*Metabolic activation of intrahepatic CD8+ T cells and NKT cells causes nonalcoholic steatohepatitis and liver cancer via cross-talk with hepatocytes."* Cancer Cell 26(4): 549-*564.*

S. Schulz, J. Lichtmannegger, S. Schmitt, C. Leitzinger, C. Eberhagen, C. Einer, J. Kerth, M. Aichler and H. Zischka (2015). "*A protocol for the parallel isolation of intact mitochondria from rat liver, kidney, heart, and brain."* Methods Mol Biol 1295: 75-*86.*

V. Chubanov, S. Ferioli, A. Wisnowsky, D. G. Simmons, C. Leitzinger, C. Einer, W. Jonas, Y. Shymkiv, H. Bartsch, A. Braun, B. Akdogan, L. Mittermeier, L. Sytik, F. Torben, V. Jurinovic, E. van der Vorst, C. Weber, Ö. A. Yildirim, K. Sotlar, A. Schürmann, S. Zierler, H. Zischka, A. G. Ryazanov, T. Gudermann. "*Epithelial magnesium transport by TRPM6 is essential for prenatal development and adult survival."* eLife (accepted)

C. Leitzinger, C. Einer, J. Lichtmannegger, S. Borchard, C. Eberhagen, T. Rieder, B. Popper, F. Neff, C. von Toerne, A. A. DiSpirito, N. Bandow, B. S. Baral, S. Hohenester and H. Zischka. *"Western diet aggravates liver damage in a Wilson disease rat model"*. Manuscript in preparation.

Poster/Abstracts

C. Einer, R. Wimmer, C. Rust, A. L. Gerbes, G. Denk, H. Zischka, S. Hohenester. "*Mitochondrial adaptation to high caloric challenge protects against fatty acid-induced hepatotoxicity but promotes liver steatosis in NASH."* EASL, The International Liver Congress, 2016, Barcelona, *Spain.*

S. Hohenester, C. Einer, R. Wimmer, J. Nagel, F. P. Reiter, S. Schulz, C. Rust, A. L. Gerbes, H. Zischka, G. Denk. "*Progression of non-alcoholic fatty liver disease towards steatohepatitis is differentially mediated by inflammasome-induced downstream pathways IL-1 and IL-18."* EASL, The International Liver Congress, 2016, Barcelona, *Spain.*

S. Hohenester, C. Einer, R. Wimmer, J. Nagel, F. P. Reiter, C. Rust, A. L. Gerbes, H. Zischka, G. Denk. *"Der Inflammasome-induzierte IL-18 Signalweg fördert den Progress der Nicht-alkoholischen Fettleber zur Fettleberhepatitis"*. 71. Jahrestagung der Deutschen Gesellschaft für Gastroenterologie, Verdauungs- und Stoffwechselkrankheiten (DGVS), 2016, Hamburg, Deutschland

S. Schmitt, C. Einer, C. Eberhagen, C. von Toerne, S. M. Hauck, H. Zischka. *"Mitochondria: A potential target in hepatocellular carcinoma"*. European Bioenergetics Conference, 2016, Riva Del Garda, Italy

Ackowledgements

Zu aller erst möchte ich mich bei PD Dr. Hans Zischka bedanken, dass ich die Möglichkeit bekommen habe in seiner Arbeitsgruppe zu promovieren. Danke für die sehr gute fachliche Betreuung und Unterstützung sowie für die hilfreichen Diskussionen, die mir die Möglichkeit gaben mich auch persönlich weiter zu entwickeln.

Zudem möchte ich mich ganz herzlich bei Frau Prof. Dr. A. Vollmar bedanken, dass Sie sich bereit erklärt haben als Gutachterin meiner Arbeit zur Verfügung zu stehen und dass Sie stets mit großem Interesse und hilfreichen Anmerkungen den Fortgang der Dissertation verfolgt haben.

Des weiteren möchte ich mich bei PD Dr. G. Denk und Dr. S. Hohenester für die gute fachliche Betreuung und Unterstützung während meiner Promotionszeit bedanken. Vielen Dank, dass Sie zur Koordination und Betreuung des Projektes sowie zum Gelingen beigetragen haben.

Ein herzliches Dankeschön gilt auch den weiteren Mitgliedern der Prüfungskommission: Prof. Dr. F. Bracher, Prof. Dr. M. Biel und Prof. Dr. C. Wahl-Schott. Danke, dass Sie sich die Zeit genommen haben diese Arbeit zu bewerten.

Ein großes Dankeschön geht an alle Kollegen der AG Zischka und AG Denk: Christin L., Sabine S., Sabine M., Sabine B., Carola E., Joseph L., Yashar K., Tamara R., Ralf W., Lena W. und Renate Artmann. Danke, dass ich bei allen technischen Fragen immer zu euch kommen konnte, dass ihr mir stets mit Rat und Tat zur Seite standet und mir auch fürs Schreiben den Rücken frei gehalten habt. Bedanken möchte ich mich weiterhin bei Alisha S., Michael S. und Christian G., dass ihr als Bachelor Studenten mein Projekt unterstützt und bereichert habt.

Für die hilfreiche und kooperative Zusammenarbeit möchte ich mich außerdem bei Prof. Dr. M. Heikenwälder, Dr. J. Bauer., Dr. K. Hofmann, Dr. S.M. Hauck, Dr. C. von Törne, Dr. U. Ohmayer, Prof. Dr. D. Mayr., Dr. B. Popper, Prof. Dr. T. Gudermann, Dr. V. Chubanov, Dr. M. Jastroch und Ellen Wahlheim bedanken.

Ein herzliches Dankeschön gilt auch meiner Familie und meinen Freunden, die mich stets unterstützt und motiviert haben und danke Torsten, dass du dich bereit erklärt hast diese Arbeit vorab zu lesen.

Supplementary Table

Regulated proteins relative to age-matched ND control identified by mass spectrometry and determined as regulated if p-value <0.05, coefficient of variation (CV) < 33% or average fold change of raw and normalized abundance < 0.67 or >1.5.

6 weeks							
			determined as regulated based on:				
Protein	Protein description	Localization	p-value	CV < 33%	fold change >1.5, <0.67 raw abundance	fold change >1.5, <0.67 normalized abundance	Pathway
ACOT13	acyl-CoA thioesterase 13	mitochondrion			1.75	1.77	lipid degradation
ALDOB	aldolase B, fructose-bisphosphate	cytoplasm		√		1.64	miscellaneous
ATP5D	ATP synthase, H+ transporting, mitochondrial F1 complex, delta subunit	mitochondrion		√	1.88	2.44	oxidative phosphorylation
BHMT	betaine-homocysteine methyltransferase	cytoplasm		√		1.79	amino acid metabolism
CALR	calreticulin	ER			1.62	1.84	ER stress
CANX	calnexin	ER			1.65	2.05	ER stress
CYP2A12	cytochrome P450, family 2, subfamily a, polypeptide 12	ER			2.70	2.94	steroid metabolism
EEF1A	eukaryotic translation elongation factor 1 alpha 1	nucleus/ER			1.91	2.29	translation
ELOVL2	elongation of very long chain fatty acids	ER			2.41	2.87	lipid synthesis
FMO5	flavin containing monooxygenase 5	ER			1.79	2.60	amino acid metabolism
GM10036	predicted gene 10036	unknown			5.69	8.38	translation
GM5619	predicted gene 5619	unknown			2.68	3.26	translation
HADHB	hydroxyacyl-Coenzyme A dehydrogenase/3-ketoacyl-Coenzyme A thiolase/enoyl-Coenzyme A hydratase (trifunctional protein), beta subunit	mitochondrion	0.037			1.21	ß-oxidation/ amino acid metabolism
HMGCS2	3-hydroxy-3-methylglutaryl-Coenzyme A synthase 2	mitochondrion		√		1.56	lipid synthesis
HSP90B1	heat shock protein 90, beta (Grp94), member 1	ER			1.88	2.08	ER stress
HSPA5	heat shock protein 5	ER			1.74	1.80	ER stress
METTL7a1	methyltransferase like 7A1	ER			1.69	2.15	miscellaneous

Supplementary Table

Regulated proteins relative to age-matched ND control identified by mass spectrometry and determined as regulated if p-value <0.05, coefficient of variation (CV) < 33% or average fold change of raw and normalized abundance < 0.67 or >1.5.

6 weeks			determined as regulated based on:				
Protein	**Protein description**	**Localization**	**p-value**	**CV < 33%**	**fold change >1.5, <0.67** raw abundance	normalized abundance	**Pathway**
MRPL10	mitochondrial ribosomal protein L10	mitochondrion		√		1.55	translation
MRPL43	mitochondrial ribosomal protein L43	mitochondrion			2.62	3.40	translation
MRPS23	mitochondrial ribosomal protein S23	mitochondrion			1.64	2.07	translation
MTTP	microsomal triglyceride transfer protein	ER			1.92	3.06	lipid transport
OTUB1	OTU domain, ubiquitin aldehyde binding 1	cytoplasm			1.66	1.69	protein degradation
P4HB	prolyl 4-hydroxylase, beta polypeptide	ER	0.027	√	1.87	2.59	ER stress
PDIA6	protein disulfide isomerase associated 6	ER	0.024	√	1.92	2.56	ER stress
PEX14	peroxisomal biogenesis factor 14	peroxisome			1.95	2.91	autophagy
PGRMC1	progesterone receptor membrane component 1	ER	0.034	√	1.55	2.30	autophagy
RPLP0	ribosomal protein, large, P0	ribosome/ER			1.58	1.85	translation
RPLP2	ribosomal protein, large P2	ribosome/ER			2.90	3.02	translation
RPN2	ribophorin II	ribosome/ER			1.87	1.99	translation
RPS3	ribosomal protein S3	ribosome/ER			3.59	4.42	miscellaneous
SLC27A5	olute carrier family 27 (fatty acid transporter), member 5	ER			1.59	1.73	lipid transport
SOD1	superoxide dismutase 1, soluble	cytoplasm		√		1.54	antioxidative
SURF4	surfeit gene 4	ER/Golgi			2.61	2.09	miscellaneous
TECR	trans-2,3-enoyl-CoA reductase	ER			2.15	3.19	lipid synthesis
TMEM205	transmembrane protein 205	membrane			2.16	2.32	miscellaneous
UGT1A1	UDP glucuronosyltransferase 1 family, polypeptide A1	ER			1.66	2.07	miscellaneous
VKORC1	vitamin K epoxide reductase complex, subunit 1	ER			4.00	4.08	miscellaneous
ACOX2	acyl-Coenzyme A oxidase 2, branched chain	peroxisome			0.55	0.60	ß-oxidation
CREG1	cellular repressor of E1A-stimulated genes 1	unknown			0.24	0.28	autophagy

Supplementary Table

Regulated proteins relative to age-matched ND control identified by mass spectrometry and determined as regulated if p-value <0.05, coefficient of variation (CV) < 33% or average fold change of raw and normalized abundance < 0.67 or >1.5.

6 weeks

Protein	Protein description	Localization	determined as regulated based on: p-value	CV < 33%	fold change >1.5, <0.67 raw abundance	fold change >1.5, <0.67 normalized abundance	Pathway
CTSB	cathepsin B	lysosome		√	0.39	0.44	lysosomal degradation
DHRS1	dehydrogenase/reductase (SDR family) member 1	mitochondrion			0.53	0.61	steroid metabolism
ETHE1	ethylmalonic encephalopathy 1	mitochondrion			0.47	0.52	amino acid metabolism
GPX1	glutathione peroxidase 1	cytoplasm		√		0.67	antioxidative
LGMN	legumain	lysosome			0.42	0.37	lysosomal degradation
LIPA	lysosomal acid lipase A	lysosome			0.22	0.23	lipid degradation
LYPLA1	lysophospholipase 1	cytoplasm			0.62	0.66	lipid degradation
MCU	mitochondrial calcium uniporter	mitochondrion			0.48	0.57	miscellaneous
NAGS	N-acetylglutamate synthase	mitochondrion			0.38	0.40	amino acid metabolism
NIT1	nitrilase 1	mitochondrion		√		0.61	apoptosis
PHYH	phytanoyl-CoA hydroxylase	peroxisome			0.47	0.50	lipid degradation
SCPEP1	serine carboxypeptidase 1	unknown			0.25	0.31	protein degradation
STRA6	stimulated by retinoic acid gene 6	membrane			0.42	0.59	retinol metabolism
TPP1	tripeptidyl peptidase I	lysosome			0.47	0.55	lysosomal degradation

Supplementary Table

Regulated proteins relative to age-matched ND control identified by mass spectrometry and determined as regulated if p-value <0.05, coefficient of variation (CV) < 33% or average fold change of raw and normalized abundance < 0.67 or >1.5.

12 weeks

Protein	Protein description	Localization	determined as regulated based on: p-value	CV < 33%	fold change >1.5, <0.67 raw abundance	fold change >1.5, <0.67 normalized abundance	Pathway
1110001J03 Rik	RIKEN cDNA 1110001J03 gene, FMC1 (mitochondrial complex I homolog)	unknown			1.62	1.89	miscellaneous
DAP3	death associated protein 3	mitochondrion	0.042	V		2.33	apoptosis
ECHS1	enoyl Coenzyme A hydratase, short chain, 1,	mitochondrion	0.030			1.17	lipid degradation
ECI2	enoyl-Coenzyme A delta isomerase 2	mitochondrion	0.031			1.05	lipid degradation
H2-Q10	histocompatibility 2, Q region locus 10	membrane			2.04	2.59	miscellaneous
HSPE1	heat shock protein 1 (chaperonin 10)	mitochondrion	0.024			1.15	miscellaneous
MCAT	malonyl CoA:ACP acyltransferase	mitochondrion			1.60	1.83	lipid transport
MT-CO3	mitochondrially encoded cytochrome c oxidase III	mitochondrion			1.78	1.75	oxidative phosphorylation
RPL26	ribosomal protein L26	ER			2.05	1.82	translation
RPL9	ribosomal protein L9	ribosome		V		1.53	translation
SELO	selenoprotein O	unknown			1.83	1.77	miscellaneous
ATL2	atlastin GTPase 2	ER			0.39	0.67	miscellaneous
BNIP3	BCL2/adenovirus E1B interacting protein 3	mitochondrion			0.45	0.61	autophagy
CREG1	cellular repressor of E1A-stimulated genes 1	unknown			0.45	0.59	autophagy
CTSB	cathepsin B	lysosome			0.49	0.60	lysosomal degradation
CYP2A5	cytochrome P450, family 2, subfamily a, polypeptide 5	unknown			0.27	0.48	retinol metabolism
CYP2D9	cytochrome P450, family 2, subfamily d, polypeptide 9	ER			0.28	0.52	retinol metabolism
CYP3A16	cytochrome P450, family 3, subfamily a, polypeptide 16	ER			0.31	0.56	steroid metabolism

Regulated proteins relative to age-matched ND control identified by mass spectrometry and determined as regulated if p-value <0.05, coefficient of variation (CV) < 33% or average fold change of raw and normalized abundance < 0.67 or >1.5.

12 weeks							
			determined as regulated based on:				
Protein	Protein description	Localization	p-value	CV < 33%	fold change >1.5, <0.67 raw abundance	fold change >1.5, <0.67 normalized abundance	Pathway
DHRS1	dehydrogenase/reductase (SDR family) member 1	mitochondrion			0.56	0.62	steroid metabolism
FMO1	flavin containing monooxygenase 1	ER			0.13	0.31	amino acid metabolism
GAA	glucosidase, alpha, acid	lysosome			0.35	0.49	lysosomal degradation
GM2A	GM2 ganglioside activator protein	lysosome			0.32	0.47	lysosomal degradation
GNMT	glycine N-methyltransferase	cytoplasm			0.30	0.42	amino acid metabolism
GSTA3	glutathione S-transferase, alpha 3	cytoplasm			0.50	0.59	antioxidative
GSTM1	glutathione S-transferase, mu 1	cytoplasm			0.33	0.29	antioxidative
GSTZ1	glutathione transferase zeta 1	cytoplasm	0.044	V	0.61	0.63	antioxidative
ISCU	IscU iron-sulfur cluster scaffold homolog	mitochondrion			0.52	0.63	miscellaneous
MRRF	mitochondrial ribosome recycling factor	mitochondrion			0.66	0.65	translation
MT-ND4	mitochondrially encoded NADH dehydrogenase 4	mitochondrion			0.43	0.43	oxidative phosphorylation
NAGS	N-acetylglutamate synthase	mitochondrion			0.49	0.65	amino acid metabolism
PEX14	peroxisomal biogenesis factor 14	peroxisome			0.44	0.48	autophagy
PTGES2	prostaglandin E synthase 2	cytoplasm/Golgi			0.54	0.58	miscellaneous
QDPR	quinoid dihydropteridine reductase	mitochondrion			0.30	0.30	amino acid metabolism
RNASET2B	ribonuclease T2B	ER			0.47	0.60	translation
STRA6	stimulated by retinoic acid gene 6	membrane			0.15	0.23	retinol metabolism
TMEM256	transmembrane protein 256	membrane		V		0.51	miscellaneous

Supplementary Table

Regulated proteins relative to age-matched ND control identified by mass spectrometry and determined as regulated if p-value <0.05, coefficient of variation (CV) < 33% or average fold change of raw and normalized abundance < 0.67 or >1.5.

Protein	Protein description	Localization	determined as regulated based on: p-value	CV < 33%	fold change >1.5, <0.67 raw abundance	fold change >1.5, <0.67 normalized abundance	Pathway
12 weeks							
TTR	transthyretin	unknown			0.48	0.58	retinol metabolism
UQCR11	ubiquinol-cytochrome c reductase, complex III subunit XI	mitochondrion			0.63	0.56	oxidative phosphorylation
24 weeks							
ACOT2	acyl-CoA thioesterase 2	mitochondrion			1.92	2.05	lipid degradation
AMT	aminomethyltransferase	mitochondrion			1.57	1.60	amino acid metabolism
ATL2	atlastin GTPase 2	ER			2.83	7.35	miscellaneous
BDH1	3-hydroxybutyrate dehydrogenase, type 1	mitochondrion		√		1.58	miscellaneous
CYP2D9	cytochrome P450, family 2, subfamily d, polypeptide 9	ER			1.88	1.91	lipid degradation
ECHDC2	enoyl Coenzyme A hydratase domain containing 2	mitochondrion	0.034	√		1.79	lipid synthesis
EHHADH	enoyl-Coenzyme A, hydratase/3-hydroxyacyl Coenzyme A dehydrogenase	peroxisome	0.018	√		1.82	lipid degradation
ELOVL2	elongation of very long chain fatty acids	ER			4.99	3.75	lipid synthesis
GM10036	predicted gene 10036	unknown			1.66	1.67	translation
HADHA	hydroxyacyl-Coenzyme A dehydrogenase/3-ketoacyl-Coenzyme A thiolase/enoyl-Coenzyme A hydratase (trifunctional protein), alpha subunit	mitochondrion	0.018	√		1.56	lipid degradation
HMGCS2	3-hydroxy-3-methylglutaryl-Coenzyme A synthase 2	mitochondrion	0.031	√		1.69	lipid synthesis
MCU	mitochondrial calcium uniporter	mitochondrion			1.48	1.63	miscellaneous
MRPS30	mitochondrial ribosomal protein S30	mitochondrion		√	1.45	2.14	translation

Supplementary Table

Regulated proteins relative to age-matched ND control identified by mass spectrometry and determined as regulated if p-value <0.05, coefficient of variation (CV) < 33% or average fold change of raw and normalized abundance < 0.67 or >1.5.

24 weeks							
			determined as regulated based on:				
Protein	Protein description	Localization	p-value	CV < 33%	fold change >1.5, <0.67 raw abundance	fold change >1.5, <0.67 normalized abundance	Pathway
MTHFS	5, 10-methenyltetrahydrofolate synthetase	cytoplasm			1.96	2.51	miscellaneous
MT-ND5	mitochondrially encoded NADH dehydrogenase 5	mitochondrion			1.90	1.69	oxidative phosphorylation
NDUFA11	NADH dehydrogenase (ubiquinone) 1 alpha subcomplex 11	membrane		V		1.73	oxidative phosphorylation
NIT1	nitrilase 1	mitochondrion		V	1.40	1.90	apoptosis
NNT	nicotinamide nucleotide transhydrogenase	mitochondrion	0.005	V		1.89	miscellaneous
P4HB	prolyl 4-hydroxylase, beta polypeptide	ER	0.037	V		2.14	antioxidative
PMPCA	peptidase (mitochondrial processing) alpha	mitochondrion			1.64	2.02	protein degradation
RPL9	ribosomal protein L9	ribosome		V		1.55	translation
SCD1	stearoyl-Coenzyme A desaturase 1	ER			1.56	1.69	lipid synthesis
SCP2	sterol carrier protein 2	mitochondrion		V		1.79	lipid transport
SSR4	signal sequence receptor, delta	ER			1.15	1.64	miscellaneous
STRA6	stimulated by retinoic acid gene 6	membrane			1.88	3.32	retinol metabolism
SURF4	surfeit gene 4	ER/Golgi			1.38	3.72	miscellaneous
UGT2B36	UDP glucuronosyltransferase 2 family, polypeptide B36	unknown	0.029		1.54	3.33	steroid metabolism
ALDH1B1	aldehyde dehydrogenase 1 family, member B1	mitochondrion		V		0.62	steroid metabolism
CTSB	cathepsin B	lysosome			0.43	0.46	lysosomal degradation
CYP2A5	cytochrome P450, family 2, subfamily a, polypeptide 5	unknown	0.041		0.28	0.29	retinol metabolism
CYP3A16	cytochrome P450, family 3, subfamily a, polypeptide 16	ER			0.14	0.25	steroid metabolism

Supplementary Table

Regulated proteins relative to age-matched ND control identified by mass spectrometry and determined as regulated if p-value <0.05, coefficient of variation (CV) < 33% or average fold change of raw and normalized abundance < 0.67 or >1.5.

24 weeks

Protein	Protein description	Localization	determined as regulated based on:				Pathway
			p-value	CV < 33%	fold change >1.5, <0.67 raw abundance	fold change >1.5, <0.67 normalized abundance	
ETHE1	ethylmalonic encephalopathy 1	mitochondrion			0.42	0.35	amino acid metabolism
FBXO16	F-box protein 16	unknown	0.019		0.39	0.44	protein degradation
GAA	glucosidase, alpha, acid	lysosome			0.38	0.58	lysosomal degradation
GNMT	glycine N-methyltransferase	cytoplasm			0.23	0.30	amino acid metabolism
LIPA	lysosomal acid lipase A	lysosome			0.29	0.32	lipid degradation
MUP10	major urinary protein 10	unknown			0.42	0.57	miscellaneous
OTC	ornithine transcarbamylase	mitochondrion	0.025			0.73	miscellaneous
PHYH	phytanoyl-CoA hydroxylase	peroxisome			0.41	0.41	lipid degradation
SARDH	sarcosine dehydrogenase	mitochondrion	0.047	V		0.66	amino acid metabolism
SCPEP1	serine carboxypeptidase 1	unknown			0.40	0.56	protein degradation
SARDH	sarcosine dehydrogenase	mitochondrion	0.047	V		0.66	amino acid metabolism
SCPEP1	serine carboxypeptidase 1	unknown			0.40	0.56	protein degradation